UC Irvine

UC Irvine Electronic Theses and Dissertations

Title

OpenFOAM simulations of impinging coflow flames, including chemi-ionization and electric field

Permalink

https://escholarship.org/uc/item/9bc396vc

Author

Ricchiuti, Valentina L. A.

Publication Date

2016

Peer reviewed|Thesis/dissertation

eScholarship.org Powered by the California Digital Library
University of California

UNIVERSITY OF CALIFORNIA,
IRVINE

OpenFOAM simulations of impinging coflow flames, including chemi-ionization and electric fields

THESIS

submitted in partial satisfaction of the requirements
for the degree of

MASTER OF SCIENCE

in Mechanical and Aerospace Engineering

by

Valentina Ricchiuti

Thesis Committee:
Professor Derek Dunn-Rankin
Professor William Sirignano
Professor Manuel Gamero

2016

© 2016 Valentina Ricchiuti

DEDICATION

To my parents...
Thank you for making me what I am
Thank you for believing in me

TABLE OF CONTENTS

LIST OF FIGURES

LIST OF TABLES

ACKNOWLEDGMENTS

First of all I would like to thank my parents Rosa and Carlo, who always supported and stood with me, even from far away; I should not have arrived this far without them.

I would like to thank also my boyfriend Fede, who gave me the strength to ride out many hard times and shared with me unforgettable happiness moments.

Special thanks also to my advisor Prof. Derek Dunn-Rankin, who gave me the opportunity to study at UCI; to Professor William Sirignano and to Professor Manuel Gamero, who provided me important insights in the field of combustion and electric propulsion respectively.

Finally I would like to thank all the friends I met during my stay at UCI; thank you for this unique experience.

ABSTRACT OF THE THESIS

OpenFOAM simulations of impinging coflow flames, including chemi-ionization and electric fields

By

Valentina Ricchiuti

Master of Science in Mechanical and Aerospace Engineering

University of California, Irvine, 2016

Professor Derek Dunn-Rankin, Advisor

Electric fields can have several effects on the behavior of hydrocarbon flames: they may affect flame shape, burning velocity, temperature profile, speed of propagation, lift-off distance, species diffusion, stabilization, and extinction. The reason is that combustion of hydrocarbon fuels involves a chemi-ionization process, which generates electrically charged species, namely ions and electrons; external manipulation of these chemi-ions can potentially produce two major effects on the flame: (1) alteration of the chemical kinetics and (2) generation of a body force. The former arises because the chemistry of the system is affected by the redistribution of charges due to their mobility and to the direction of the applied electric field; the latter includes physical effects: ion wind and Ohmic heating. The applied electric field makes charged species acquire momentum, which is then lost during collisions with neutral molecules; these multiple collisions have two consequences. Chemi-ions gain a drift velocity, which depends on their mobility, that is what makes them travel toward the respective oppositely charged electrode; while neutral molecules gain a small net velocity in the same direction (known as ion wind effect), which produces a net force whose contribution is included in the momentum equation. The Ohmic heating represents the work done by electrostatic forces; it includes both the work done by the electric field on the charged species (by pushing them toward the electrode of opposite charge) and the work done by the

chemi-ions themselves (because they have also a diffusion velocity).

The aim of this thesis is to better understand, through numerical simulations, the effects of chemi-ionization and electric fields on a non-premixed coflow flame that impinges on a metallic plate; this configuration is very useful in order to investigate both how electric fields can be used to reduce carbon monoxide emissions and how they affect the heat flux on a solid surface. In order to analyze how chemi-ionization and electric fields influence the fluid dynamics and the chemistry of a flame in this configuration, numerical simulations have been performed using OpenFOAM. The validation of the numerical model has been performed by comparing numerical results to experimental result; these comparisons show that, taking into account some simplifying assumptions (e.g., axialsymmetric geometry, absence of radiation heat losses, unitary Lewis and Schmidt number) introduced in the model, results agree well with literature findings.

Chapter 1

Introduction

1.1 Motivations

The effects of electric fields on hydrocarbon flames have captured the attention of scientists for many years; there are many reasons to investigate the interactions between electric fields and the combustion process. It has been widely accepted that the chemi-ionization process is the main source for the creation of charged species in flames [2],[3],[4]; however, ions and electrons do not contribute substantially to the heat release, since they are rapidly consumed in the flame through ion-electron recombination reactions. But when an external electric field is applied, ions rapidly gain a drift velocity which reduces the recombination rate and increases the flow of charges through the applied potential gradient [5]. The earliest research mainly focused on identifying the relation between diffusion and concentration of charged species in methane or acetylene flames [6], [7]; subsequently, it has been found that electric fields strongly influence flame speed and heat transfer [8]. Experiments have proven that a relation exists between strong electric fields and the flame stand-off distance [9]; this behavior has been studied numerically in order to understand its effect on the flame stabilization [4].

A major problem related to hydrocarbon flames combustion is the generation of pollutants; recent studies have shown that electric fields can be used to suppress soot [9]. Moreover, because chemi-ionization generates many free charges in the reaction zone, and because some of the gas products are conductors of electricity, there exists the possibility that flame propagation can be mainly driven by the application of a potential difference instead of convection [10]; this condition becomes important particularly in the absence of gravity, where natural convection does not exist, so it cannot drive the heat transfer from the flame to the ambiance [11].

It is evident that electric fields influence the entire life of a flame, from ignition (they can enhance spark ignition) until extinction (their effects on the flame stability impact the blow-off distance [12]); in order to use electric fields to control flames, it is crucial to understand the effects that they induce on the combustion process.

1.2 Objectives

Combustion of hydrocarbons is arguably among the most important reactions to the human race; it has been the main source of energy for thousands of years. Since previous studies have proven that electric fields affect flame properties and behavior, it is important to understand not only how charged species appear in the flame, but also what role they play in the flame. In this way, it will be possible to manipulate electric fields in order to control and enhance the combustion of hydrocarbon flames.

The aim of this thesis is to analyze, through numerical simulations, the effects of chemi-ionization and electric fields (implemented by incorporating the solution to Poisson's equation) on the fluid dynamics and the chemistry of a non-premixed coflow flame impinging a plate; in order to do that, the study has been divided into three parts:

1. identify the behavior of the flame using neutral chemical reaction mechanisms (three-steps mechanism for the formation of methane [13] and a reduced mechanism based on GRI-Mech [14]) when the Poisson's equation is implemented in the numerical solver

2. identify the behavior of the flame using an ion mechanism [15] without implementing Poisson's equation in the numerical solver to incorporate electric field effects

3. identify the behavior of the flame using an ion mechanism when Poisson's equation is implemented in the numerical solver.

This procedure allows to understand that chemi-ionization is the real process through which electric fields affect flame properties: if charged species are not included in the reaction mechanism, there is no coupling between Poisson's equation and the conservations equations (mass, momentum, energy, species), so the applied potential difference will be constant in time. If the charged species are included in the kinetic mechanism instead, coupling will occur because of charge accumulation; ion wind effects and Ohmic heating will influence momentum and energy conservation respectively.

Chapter 2

Impinging coflow flames

2.1 Configuration

Even though the geometry of impinging jet flames is quite simple, the corresponding flame configuration is strongly influenced by the nozzle exit velocity and by the distance between nozzle and plate [1]. Some typical reacting patterns are illustrated in Figure 2.1:

a) ring flame: it is established when the flow has a high radial velocity close to the plate, so the flame can be ignited at the edge of the impinging jet

b) conical flame: when the plate is far enough from the burner and the flow axial velocity close to the plate is low, the flame can propagate back to the nozzle and stabilize on the nozzle rim

c) disc flame: when the axial velocity of the flow increases, the flame detaches from the nozzle to form a disc flame

d) envelope flame: if the mixture is fuel rich, a self-propagating flame is established (close to the stagnation point) only where the mixture becomes lean enough

e) cool central core flame: if the mixture is very fuel rich, a diffusion flame is generated; the cool central core is created because the distance between burner and plate is so small that the reacting zone cannot propagate back to the symmetry axis.

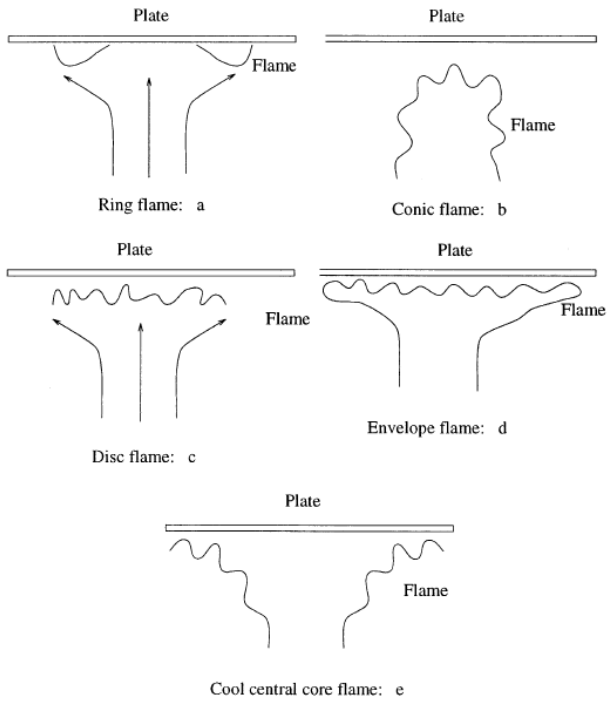

Figure 2.1: Typical reacting patterns for impinging jet flames [1]

2.2 Physical properties

Impinging flames represent a very efficient way to heat solid surfaces [16], [17]; this occurs because of the high heat transfer rate associated with some high temperature combustion products being brought into close proximity of the plate surface. The only disadvantage is that the local heat flux can be non uniform. In the laminar regime, the heat transfer mechanism to the plate is mainly governed by convection; radiation can be neglected since hot gases have very low emissivity. In addition to convection however, there can be another mechanism responsible for the increase of heat transfer [16]; it is known as thermochemical

heat release and is related to the presence of radicals (OH, H, O) in the flame. When hot gases impinge on the solid surface, the very reactive radical species will immediately recombine exothermically, and this will result in an increase in the local heat transfer. Recent studies have shown, however, that the recombination occurs relatively far from the surface (when the surface is cool) so the heat transfer remains dominated by convection.

Recent studies have shown that flame jets and hot isothermal jets have very similar aerodynamics properties [18]: flow zones generated during the evolution of the jet, stagnation point and radial velocity gradient; this is why impinging jet flames have been modeled as hot inert jets [19]. As shown in Figure 2.2, four different zones can be identified in an axi-symmetric laminar coflow flame impinging on a flat plate: the flame jet region, the free jet region, the stagnation region and the wall jet region. In the flame jet region, chemical reactions ignite the flow exiting the burner, which undergoes a sudden expansion; the ignited mixture then travels towards the free jet region, that is not influenced by the presence of the plate. As the mixture moves, it enters the impingement region (or stagnation region): here, the axial velocity decreases while the radial component increases, giving rise to an increase in pressure; this region is strongly influenced by the distance between the plate and the burner. As the flow direction changes from axial to radial, a viscous boundary layer develops near the flat plate; finally, in the wall jet region the flow moves radially over the plate while decelerating.

It can be noticed that the only difference between impinging jet flames and hot isothermal gases is that chemical reactions will occur also in the stagnation region and in the wall jet region; the recombination of radicals contained in these region can generate an additional heat release, which in turn will affect the temperature gradients.

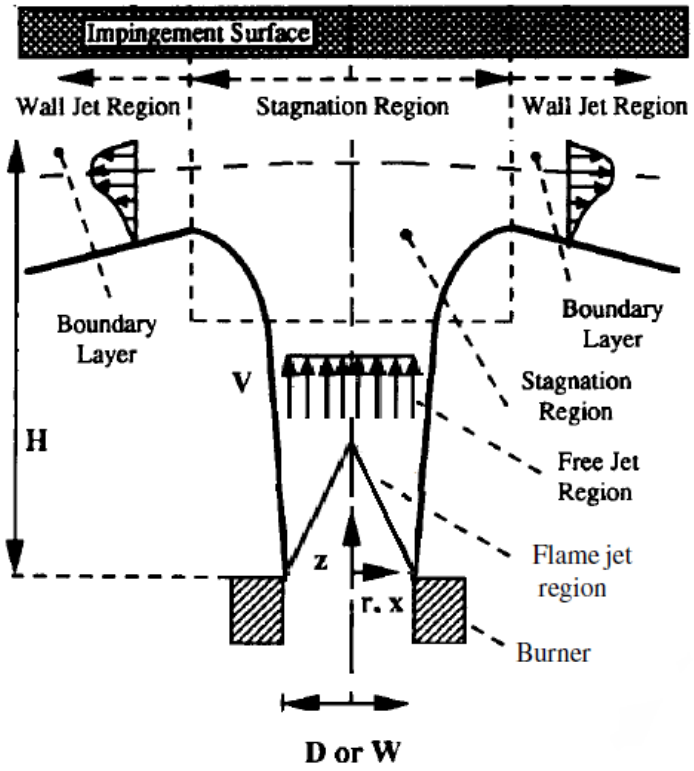

Figure 2.2: Flow regions in an impinging jet flame

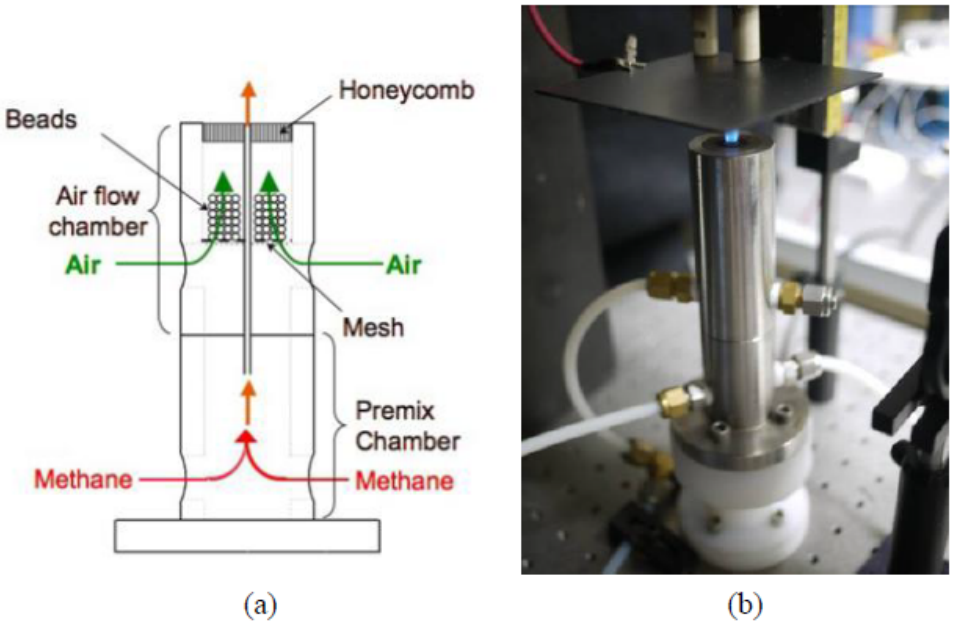

Figure 2.3: a) Schematic representation of the coflow burner. b) the UCI coflow burner

2.3 Experimental setup

Figure 2.3 shows the UCI experimental apparatus used to analyze the behavior of impinging jet flames (subjected or not to an external electric field) [20]. It consists of a stainless steel coflow burner with a $4cm$ outer diameter and a stainless steel impinging plate which can move along the vertical axis. Inside the burner, fuel is injected in the inner ring ($d_{in} = 2mm$) while air is provided in the outer ring ($d_{out} = 2.5cm$); an internal honeycomb mesh produces a uniform flow at the exit area. The plate is a $10x10cm^2$ surface with a $3mm$ thickness. The configuration with the plate above the burner is ideal to identify the effect of the ion wind on the bulk flow; in a downward configuration instead, either bouyancy or ion wind could be responsible for driving the flame on the burner surface. Further details of the burner, its configuration, and examples of flames appear in [20].

Chapter 3

Numerical model

3.1 OpenFOAM: a free open-source package for CFD

OpenFOAM (Open Field Operation And Manipulation) is a free, open-source package that can solve problems related to many different areas, ranging from engineering to finance [21]; it is written in *C++* so it has all the advantages of an objected-oriented language. The most important capabilities of an object-oriented language are:

- encapsulation: group data and functions (i.e, operations supported by *C++*) together as objects (or *classes*) and define interfaces to them; different classes interact through their interfaces. A class interface is all the user needs to know, in order to use the class itself

- inheritance: code can be reused between related types; it means that if a certain class (*derived class*) is based on an other class (*base class*), they use the same implementation. This feature allows a derived class to override and add methods, but those defined in the base class cannot be removed. So if there are two classes, *class b* and

class c, that have some properties in common, these can be included into a *class a* base class

- polymorphism: allow an object to have several types, and determine at runtime which function to call basing on its type; this means that a *class b* object can be used wherever the code expects a *class a* object (it is valid also for pointers and references, so it is useful to define *virtual* functions in the base class). The selection of the correct function at runtime is called dynamic dispatch.

The reasons why OpenFOAM was chosen as the numerical solver to analyze the effects of chemi-ionization and electric fields on impinging coflow flames are:

1. it is object-oriented, and this allows more rapid computations and makes the entire code more clear
2. it is an open-source package, so it is possible to access and modify internal libraries and solvers. These solvers and libraries solve for fluid dynamics, heat transfer, electromagnetism, combustion, etc...; but the user is free to modify and combine them, in order to obtain new solvers for different types of problem; being open source also means that there is a large network of user developed resources and support available
3. it can solve time-dependent and stationary problems, in both 2D and 3D.

The second point is the most important: in fact, the aim of this thesis is to build a new code that can solve for fluid dynamics, chemical kinetics and electric fields.

3.2 Governing equations

Figure 2.2 represents the typical geometric configuration of an impinging coflow flame; fuel (methane) and oxidizer (air), ejected respectively from the inner and outer coaxial cylinders of the burner, generate a diffusion flame; the flame stabilizes at a certain distance from the burner which depends on the velocity of the ejected reactants and on the plate to burner distance. For this study, the exit velocity of both methane and air is small enough to maintain a laminar flow (Schlieren imaging of the experimental flames confirm the laminar flow); in fact, the Reynolds numbers at the fuel and oxidizer inlets are, respectively: $Re_f = 27.8$, $Re_{ox} = 312.5$. The origin of the reference system has been set at the exit of the burner; since the problem is axi-symmetric, cylindrical coordinates have been used in OpenFOAM. The governing equations for mass, momentum, species, energy and electric potential for a compressible, laminar and multicomponent mixture of gases can be written in the following form [23], [29]:

$$\frac{\partial \rho}{\partial t} + \vec{\nabla} \cdot (\rho \mathbf{u}) = 0 \tag{3.1}$$

$$\frac{\partial (\rho \mathbf{u})}{\partial t} + \vec{\nabla} \cdot (\rho \mathbf{u}\mathbf{u}) = -\vec{\nabla} p + \rho \mathbf{g} - \rho \bar{q} \vec{\nabla} \Phi + \vec{\nabla} \cdot \vec{\boldsymbol{\tau}} \tag{3.2}$$

$$\frac{\partial (\rho Y_k)}{\partial t} + \vec{\nabla} \cdot (\rho Y_k (\mathbf{u} + \mathbf{v}_{D_k} + \mathbf{V}_k)) = \dot{\omega}_k \quad k = 1 : NS \tag{3.3}$$

$$\begin{aligned} \frac{\partial (\rho h_s)}{\partial t} + \vec{\nabla} \cdot (\rho \mathbf{u} h_s) = \dot{\omega}_T + \frac{Dp}{Dt} + \vec{\nabla} \cdot (\lambda \vec{\nabla} T) + \dot{Q} + \vec{\boldsymbol{\tau}} :: \vec{\nabla} \mathbf{u} + \\ \underbrace{- \vec{\nabla} \cdot \Big(\rho \sum_{k=1}^{NS} h_{s,k} Y_k (\mathbf{V}_k + \mathbf{v}_{D_k}) \Big)}_{a} \underbrace{- \rho (\vec{\nabla} \Phi) \Big[\sum_{k=1}^{NS} Y_k \frac{q_k}{W_k} N_A (\mathbf{V}_k + \mathbf{v}_{D_k}) \Big]}_{b} \end{aligned} \tag{3.4}$$

$$\nabla^2 \Phi = -\frac{\rho \bar{q}}{\epsilon_0 \epsilon_r} \tag{3.5}$$

$$\rho = \frac{p \bar{W}}{R_u T} \tag{3.6}$$

where:

- k represents a species (and NS is the total number of species)
- $\bar{q}$ is the sum of the charges of all the species:

$$\bar{q} = \sum_{k=1}^{NS} Y_k \frac{q_k}{W_k} N_A \tag{3.7}$$

  with q_k the charge (in Coulomb) and W_k the molecular weight of a species respectively; and N_A is the Avogadro number

- Φ is the electric potential
- $\mathbf{v}_{D_k}$ is the ion drift velocity:

$$\mathbf{v}_{D_k} = \frac{q_k}{|q_k|} \kappa \mathbf{E} \tag{3.8}$$

  with κ the species mobility

- $\mathbf{V}_k$ is the diffusion velocity of species k:

$$\mathbf{V}_k = -\frac{D_k}{Y_k} \vec{\nabla} Y_k \tag{3.9}$$

  and D_k is the diffusion coefficient of species k (in general: $D_k = f(D_{jk})$, where D_{jk} is the binary diffusion coefficient of species j into a jk mixture)

- $\vec{\boldsymbol{\tau}}$ is the stress tensor:

$$\tau_{ij} = \mu \Big(\frac{\partial u_i}{\partial x_j} + \frac{\partial u_j}{\partial x_i} \Big) - \frac{2}{3} \mu \frac{\partial u_l}{\partial x_l} \delta_{ij} \tag{3.10}$$

- $\dot{Q}$ represents the heat losses due to radiation

- h_s and $h_{s,k}$ are the sensible enthalpies of the mixture and of species k respectively
- $\dot{\omega}_k$ is the net production rate of species k
- $\dot{\omega}_T$ takes into account the enthalpy of formation of the species:

$$\dot{\omega}_T = -\sum_{k=1}^{NS} \Delta h^0_{f,k} \dot{\omega}_k \tag{3.11}$$

- ϵ_0 and ϵ_r are respectively the vacuum permittivity and the relative permittivity of air ($\epsilon_r = 1$)
- $\bar{W}$ is the average molecular weight of the mixture
- the perfect gas law is needed in order to close the system.

However, some simplifications can be introduced into this model:

1. viscous dissipation is negligible, since the Mach number is very small compared to one (e.g., in the flame zone $Ma \simeq 10^{-4}$)
2. radiation heat losses can be neglected since hot gases have very low emissivity (and in these small unconfined flames their radiative emission is a small fraction of the energy transport)
3. in Equation 3.4, two terms can be neglected: (1) $\underbrace{\quad}_{a}$ represents the contribution of the sensible enthalpy of each species which, in the presence of combustion heat release, does not have a remarkable effect on the energy balance; and (2) the $\underbrace{\quad}_{b}$ term represents the Ohmic losses, which include the contribution of the work done by the electric field on each charge and the work done by the charges themselves since they also have a diffusion velocity (in addition to the drift velocity); it has been shown that the Ohmic losses have a minor effect on the flame behavior [9],[15],[22]

4. unitary Lewis and Schmidt number ($Le = 1$, $Sc = 1$) have been used; this is a good assumption for a perfect gas, where molecular transport is the main driving factor. In particular, since it is difficult to determine the binary diffusion coefficient of all the species involved in a reaction mechanism, as a reasonable first approximation it can be assumed that all species diffuse in air, and air is approximated to a mono-component mixture (of N_2); this has been implemented in OpenFOAM in this way: $Sc = 1 \Rightarrow D_k = \nu$ for all k species (with ν the dynamic viscosity).

Under the forementioned assumptions, the following set of simplified conservation equations has been solved in OpenFOAM:

$$\frac{\partial \rho}{\partial t} + \vec{\nabla} \cdot (\rho \mathbf{u}) = 0 \tag{3.12}$$

$$\frac{\partial (\rho \mathbf{u})}{\partial t} + \vec{\nabla} \cdot (\rho \mathbf{u}\mathbf{u}) = -\vec{\nabla} p + \rho \mathbf{g} - \rho \bar{q} \vec{\nabla} \Phi + \vec{\nabla} \cdot \vec{\boldsymbol{\tau}} \tag{3.13}$$

$$\frac{\partial (\rho Y_k)}{\partial t} + \vec{\nabla} \cdot (\rho Y_k (\mathbf{u} + \mathbf{v}_{D_k} + \mathbf{V}_k)) = \dot{\omega}_k \quad k = 1 : NS \tag{3.14}$$

$$\frac{\partial (\rho h_s)}{\partial t} + \vec{\nabla} \cdot (\rho \mathbf{u} h_s) = \dot{\omega}_T + \frac{Dp}{Dt} + \vec{\nabla} \cdot (\lambda \vec{\nabla} T) \tag{3.15}$$

$$\nabla^2 \Phi = -\frac{\rho \bar{q}}{\epsilon_0} \tag{3.16}$$

$$\rho = \frac{p \bar{W}}{R_u T} \tag{3.17}$$

It can be noticed that the electric field gives an additional contribution to the momentum (3.13) and species (3.14) equations; Equations 3.16 is known as the Poisson Equation or Gauss's Equation. Once the electric potential has been determined, the electric field can be computed as:

$$\mathbf{E} = -\vec{\nabla} \Phi \tag{3.18}$$

The separation of the drift velocity and diffusion velocity for charged species is a common procedure [23], [24] in computational fluid dynamics modeling; this because the species diffusion in multi-component mixtures allows for four distinct modes of mass diffusion:

- ordinary diffusion (V_k), which is proportional to the species concentration
- thermal diffusion, related to temperature gradients (not considered in the current model)
- pressure diffusion, related to pressure gradients (not considered in the current model)
- forced diffusion ($v_{D,k}$), resulting from the interaction between charged species and an electric field.

It is also known that if the species equations are summed up (for $k = 1 : NS$), they must give the mass conservation equation 3.12; in order to do that, the numerical solver solves for $NS - 1$ species equations (it does not solve for the inert species N_2), then it forces the total mass fraction to be equal to one by imposing: $Y_{N_2} = 1 - \sum_{k=1}^{NS-1} Y_k$. Of course this is an approximation; any variation in the inert species mass fraction causes errors in the computation of the Y_{N_2} itself. This also implies that the diffusion mass fluxes, including the ionic mass flux, do not exactly sum to zero. However, since the mass fraction of nitrogen is high in air, the small variations that Y_{N_2} can undergo do not affect the actual forcing of the unitary total mass fraction.

In order to simulate this system, a new solver that solves for the coupling of CFD, chemistry and electric field must be created in OpenFOAM; in fact, the ultimate aim will be to identify how chemi-ionization and electric fields affect the behavior of the flame and so compare the numerical results with those obtained from experiments.

3.3 Solution of the numerical model

In order to run a simulation in OpenFOAM, three steps must be followed: pre-processing, run the application, post-processing; the following Paragraphs provide a short summary of this procedure.

3.3.1 Geometry of the problem

Figures 3.1 shows a schematic model of the experimental setup geometry of the coflow impinging on a square plate; the plate itself acts as the negative electrode, while the burner is the positive electrode. A negative potential and a zero potential will be assigned to the plate and to the exit area of the burner respectively.

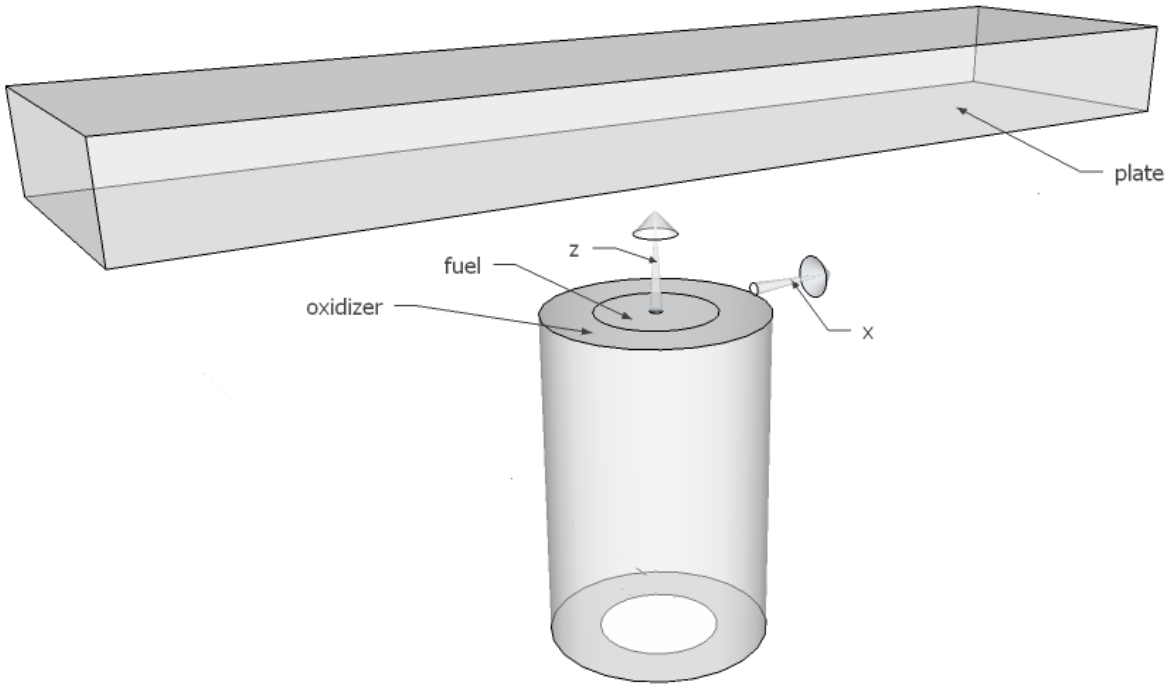

Figure 3.1: Geometry of the experimental setup of the problem

The coflow burner has been modeled as two concentric cylinders, whose upper bases corre-

spond to the exit area of the nozzle; the origin of the reference frame has been set here. Pure CH_4 (fuel) and pure air (oxidizer) are ejected respectively from the internal nozzle and the external annulus.

In OpenFOAM it is easy to deal with axially symmetric geometries; in particular, for cylinders it is sufficient to solve the problem in a wedge of small aperture (5°). In order to do that, a cylindrical plate has been considered; in this way, properties vary only along the radial coordinate x and the axial coordinate z. A large external domain must also be included to make sure that the boundaries do not affect the core combustion processes and behaviors; Figure 3.2 shows the geometrical configuration that has been built in OpenFOAM.

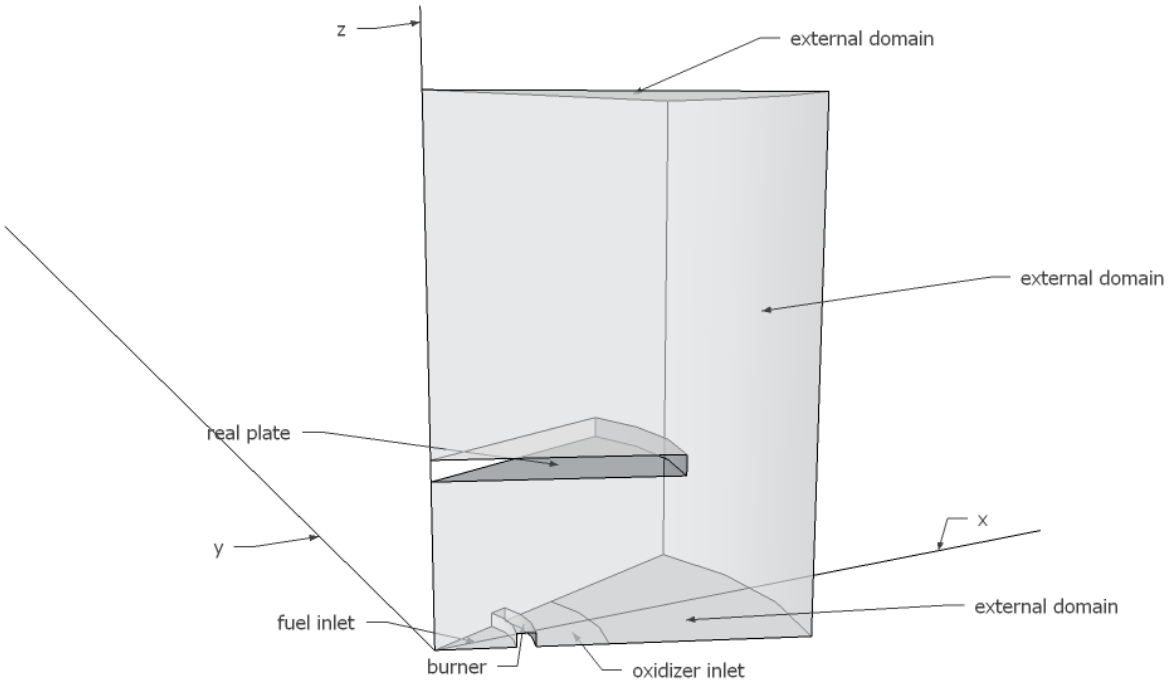

Figure 3.2: OpenFOAM model of the problem

3.3.2 Pre-processing

The stage represents the generation of a case directory; the basic structure of a case directory in OpenFOAM is shown in Figure 3.3. It must include the following folders:

- the *system* folder, which contains at least three files related to the solution procedure of the problem:
  - *controlDict* specifies the application selected to solve the problem, initial and final time, time step, etc...
  - *fvSchemes* lists the discretization schemes
  - *fvSolution* lists the equations solvers, tolerances and other control parameters
- the *constant* folder, which contains:
  - the *polymesh* folder, that includes files related to the generation of the mesh
  - files that specify some physical properties (for example, transport properties)
- the *time directories* are folders written by the solver at each time step; they contain the boundary conditions of all the parameters involved in the conservation equations; the user specifies the initial boundary conditions inside the *0* time directory. Boundary conditions must be specified on every patch that composes the mesh
- the *kinetic* folder must also be included whenever a combustion problem is considered; here, the user specifies reaction mechanism, thermophysical properties transport properties.

In the pre-processing phase, the first step consists in the generation of the mesh, through the *blockMesh* utility; Figure 3.4 shows the mesh built for the considered problem. A graded

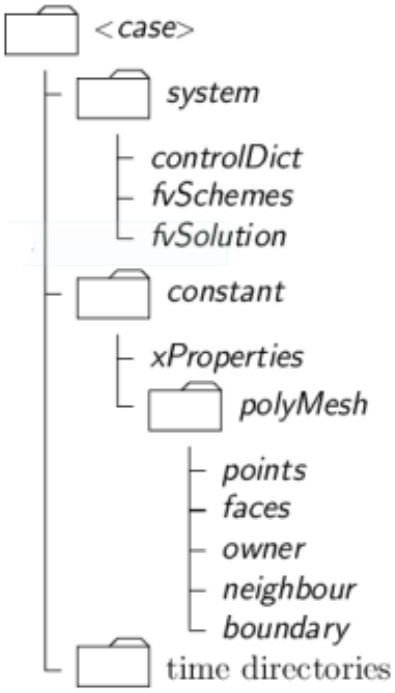

Figure 3.3: Structure of a case directory

mesh has been used, in order to increase the number of cells in the regions of large gradients (such as the flame zone and the corners of the plate) and to reduce them where the solution is smoother; this allows more accurate results and reduced computational time. The dimensions of coflow burner and plate are listed in Table 3.1. The second step specifies the initial conditions and boundary conditions, that are listed in Table 3.1. The third steps consists in choosing the reaction mechanism; for this case study, four different mechanisms have been considered, as shown in Appendix A. Finally, discretization schemes and solvers control must be selected; the former include the numerical schemes associated with the operators (Laplacians, gradients, time derivatives, etc...) that appear in the conservation equations, the latter specifies the equation solvers, algorithms, and tolerances.

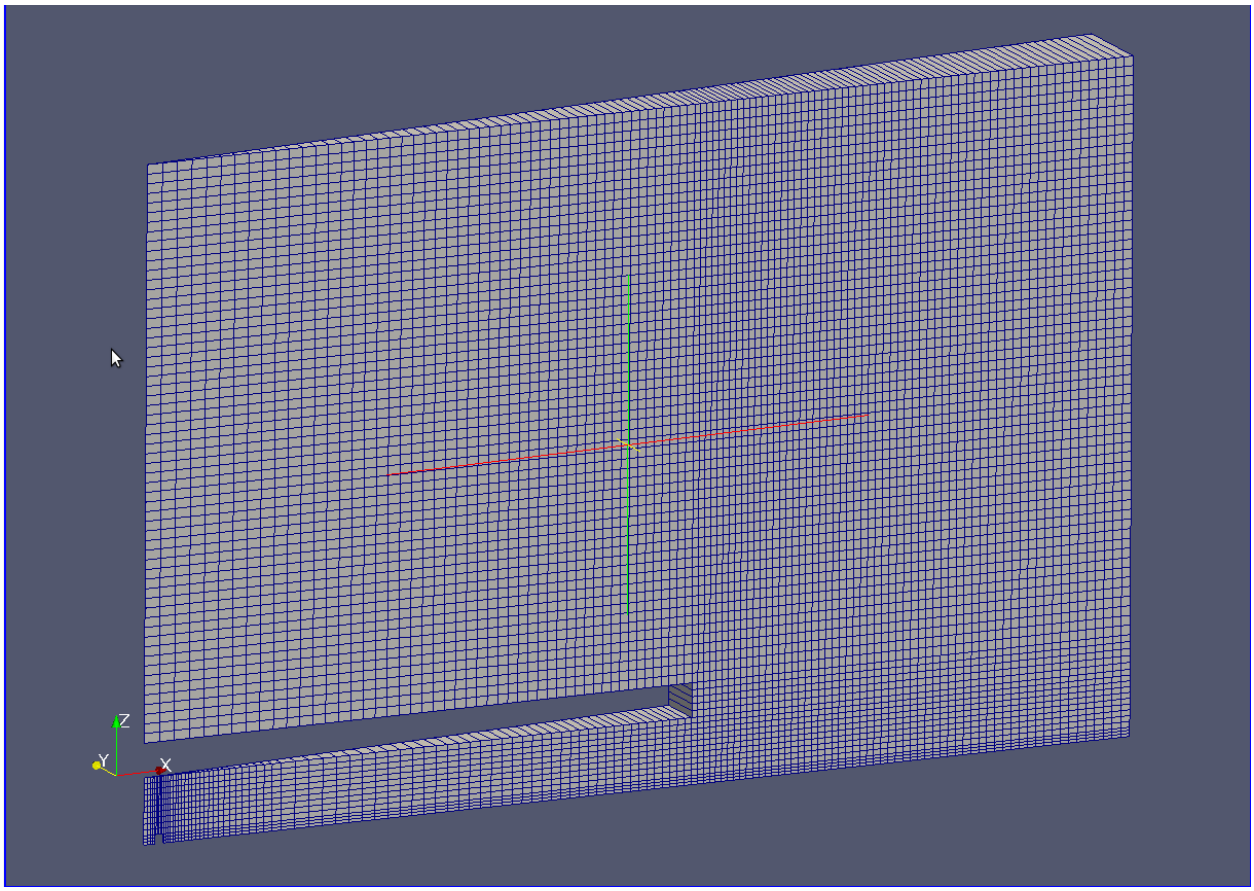

Figure 3.4: Mesh generated by OpenFOAM

Property	Symbol	Value	Unit
Pressure	p	1	atm
Fuel nozzle diameter	d_f	0.002	m
Oxidizer nozzle diameter	d_{ox}	0.025	m
Nozzles-plate distance	L	0.0058	m
Plate diameter	d_{plate}	0.10	m
Fuel and oxidizer inlet T	T_{in}	300	K
Plate initial T	$T_{in,plate}$	473	K
Oxidizer inlet mass fraction	Y_{O_2}	0.2395	–
	Y_{N_2}	0.76	–
	Y_{CO_2}	0.0005	–
Fuel inlet mass fraction	Y_{CH_4}	1	–
Fuel inlet velocity	$u_{f,in}$	0.2	$\frac{m}{s}$
Oxidizer inlet velocity	$u_{ox,in}$	0.2	$\frac{m}{s}$

Table 3.1: Geometrical properties and initial conditions

3.3.3 Running the application

In this phase, the user launches the simulation by specifying the selected application; in the present work, three different applications have been used:

a) laminarSMOKE: a solver for multi-dimensional laminar flames with detailed gas-phase kinetic mechanism [25]

b) reactingFOAM: the OpenFOAM solver for reacting flows [26]

c) a user-implemented solver that can solve for fluid dynamics, chemical kinetics and electric fields.

3.3.4 Post-processing

In this phase, the results written by OpenFOAM in the *time* directory can be visualized using a graphical interface; in this work, all the plots have been obtained using the open-source visualization application ParaView and then imported into TecPlot for more sophisticated visualization.

Chapter 4

Chemical kinetics

This Chapter provides a description of the chemi-ionization process and of the different reaction mechanisms that have been explored and used.

4.1 The chemi-ionization process

In a combustion process, there are many mechanisms that can be responsible for the formation of ions: particles collision, electron attachment, electron transfer, molecules excitation, thermal ionization and chemi-ionization. For hydrocarbon flames, it has been accepted that chemi-ionization is the most relevant process that leads to the formation of charged species [9],[27],[28]; the first step of this process consists in the chemical interaction between two neutral molecules, which generates both a positive and a negative charge:

$$A + B \rightarrow C^{+}D + e^{-} \tag{4.1}$$

$$A + B \rightarrow C^{+}D^{-} \tag{4.2}$$

In hydrocarbon flames, it has been shown that the major ions are generated by reactions involving the CH molecule [29]; in particular, for methane-air flames the initiating step is the following radical-radical reaction [30]:

$$CH + O \rightarrow HCO^+ + e^- \tag{4.3}$$

which then leads to the formation of H_3O^+, the most important ion in near stoichiometric combustion:

$$HCO^+ + H_2O \rightarrow CO + H_3O^+ \tag{4.4}$$

So, for hydrocarbon flames H_3O^+ is the ion that is present in higher concentrations (at least two orders of magnitude more than all the other ions); and it is the only ion seen to survive outside the flame reaction zone when influenced by a strong electric field. Among all the other ions, the second most important is HCO^+, because even if its concentrations are three orders of magnitude lower than that of hydronium, it is a key element for the formation of hydronium itself.

4.2 Reaction mechanisms

Four different reaction mechanisms have been used in this study:

1. detailed chemical kinetics including ions: this mechanism is based on *GRI-Mech 3.0* [31] for the neutral reactions and on the mechanism of Prager et al. for the ion reactions [32]; the complete set of reactions is included in Appendix A.1. This is a very detailed mechanism, which includes: 6 elements (O, H, N, C, Ar, E), 45 species and 260 reac-

tions (219 neutral reactions and 41 reactions including charged species). The neutral mechanism has been slightly modified since the species formed by molecular nitrogen have not been included; this is a reasonable simplification because these species do not affect the flame properties in terms of heat release

2. three-step mechanism for methane formation [13]: this is a very basic neutral mechanism which includes 4 elements (C, O, H, N), six species and three reactions; this is the first mechanism run with the new user-defined solver. The complete set of reactions is listed in Appendix A.2

3. reduced neutral mechanism based on GRI 1.2 [14]: this reduced mechanism includes 5 elements (O, H, C, N, Ar), 19 species and 84 reactions; this mechanism does not include molecules formed by molecular nitrogen nor higher order hydrocarbons. The complete set of reactions is included in Appendix A.3

4. reduced ions mechanism [15]: this mechanism includes 5 elements (O, H, C, N, E), 20 species (including three charged species: H_3O^+, HCO^+, e^-) and 31 reactions; the complete set of reactions is included in Appendix A.4. This mechanism was developed using the simplest reduction concept of combining what looked to be the most important ion reactions with the most important related neutral molecule reactions in combustion. It is a mechanism that has not been validated in other systems so it represents more of an exploration of the level of computation that might be feasible for the entire electrically activated flame system.

Chapter 5

Results for impinging coflow flames

The results of OpenFOAM simulations for impinging methane/air coflow flames are reported in this Chapter; simulations have been performed using different reaction mechanisms and different numerical solvers. Initial and boundary conditions are listed in Table 3.1; the simulation time has been set to $2s$, at which time the flame has reached steady state conditions. So, all the Figures of this section show results obtained at $t = 2s$; in addition, all the values presented in the following Figures are in SI units.

5.1 Preliminary study for detailed chemical kinetics without electric field

This sections shows the results obtained using the *laminarSMOKE* solver [25]: it solves for multi-dimensional, laminar reactive flows with detailed gas-phase reaction mechanisms; the reason why this solver can handle very large kinetic mechanisms (with up to 200 species and 6800 reactions) is that it applies the operator-splitting method to the governing equations. It is known that one of the issues related to the numerical modeling of combustion problems

is the implementation of detailed kinetic mechanisms [33]; this happens because of the large number of species involved, the stiffness of the governing equations and the presence of high gradients in the flame region. The operator-splitting method not only splits each equation into sub-equations that are easier to solve, but also separates the chemical reaction process (the stiff component of the problem) from the transport processes (the non-stiff component); this approach helps to avoid expensive matrix operations and saves computational time.

For this simulation:

- the detailed reaction mechanism based on $GRI-Mech3.0$ and Prager et al. has been used (see Appendix A.1)
- the Poisson Equation has not been implemented (it is not included in the $laminarSMOKE$ solver), so the effects of the electric field have not been considered.

Figures 5.1-5.7 present the results obtained with OpenFOAM for this first simulation: they show the profiles of temperature, velocity, density, and the most important species; since the major changes occur in the flame zone, for the species, only this portion of the original mesh has been considered.

Figures 5.3 and 5.4 show that the flame moves with a positive radial velocity below the plate, negative radial velocity above it and positive axial velocity close to its right corner. Figures 5.1 and 5.2 show the temperature profile: the reaction zone is located close to the burner, where the ignition spark is located. As a consequence, formation of species mainly occurs in this zone, as represented in Figures 5.5, 5.6 and 5.7. It is interesting to compare the profiles of CO and OH: OH is mainly produced at the right side of the burner (the negative mass fraction is attributed to numerical errors, probably due to the discretization schemes used to solve the time derivatives), while CO is produced close to the burner, then it moves up towards the plate and then goes a bit backward (along the positive radial direction) along the

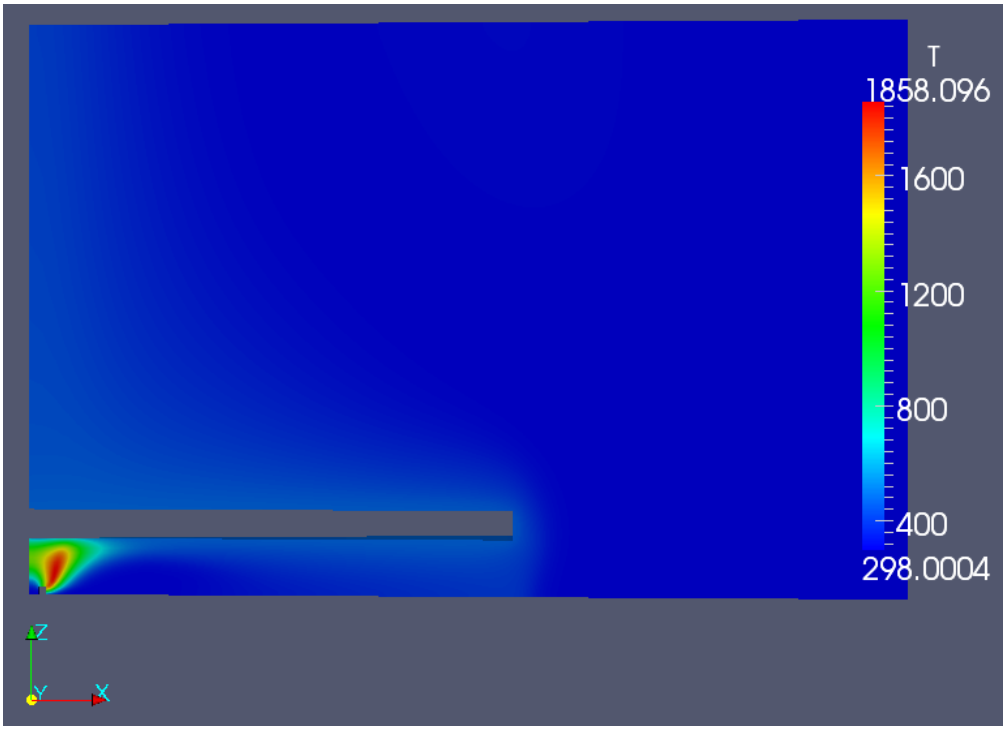

Figure 5.1: Temperature profile [K]

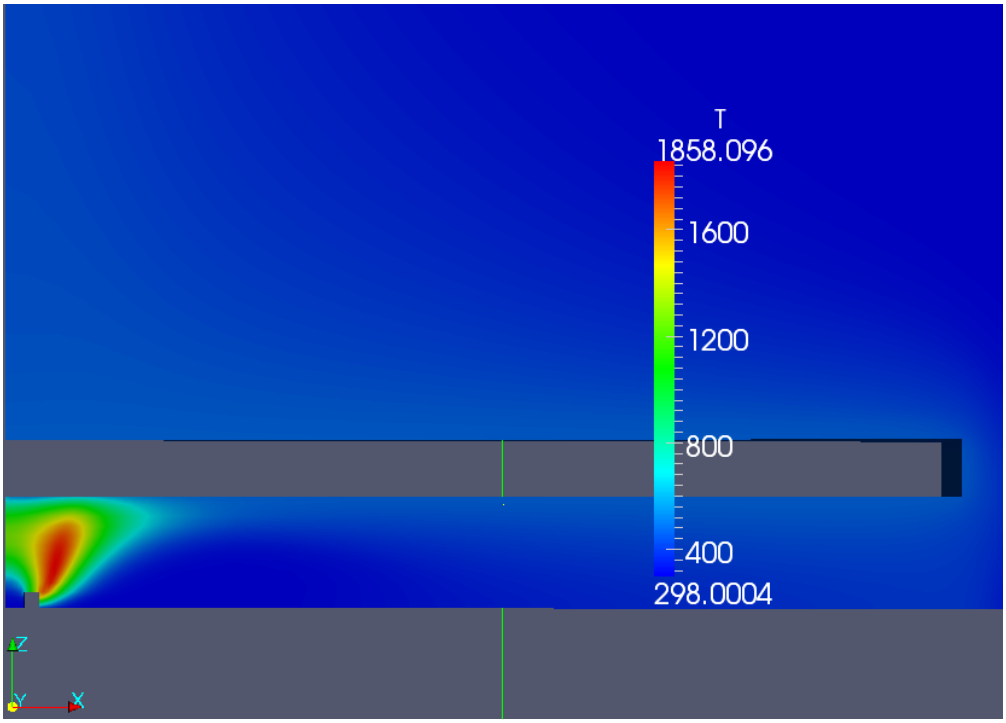

Figure 5.2: Zoom of the temperature profile [K]

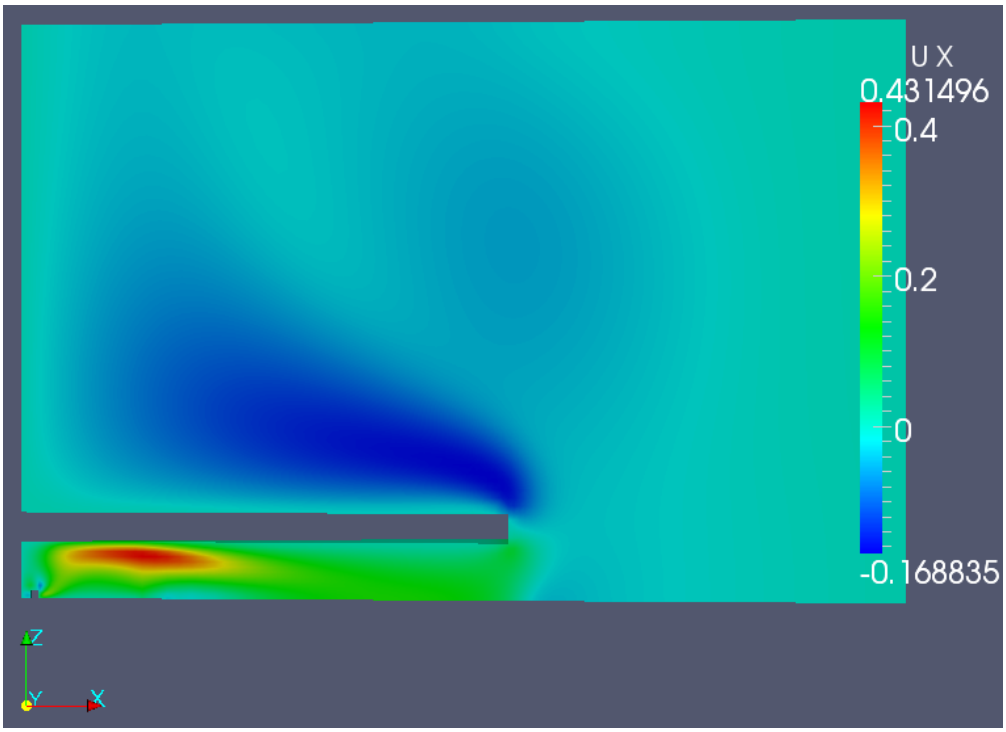

Figure 5.3: Radial velocity profile [m/s]

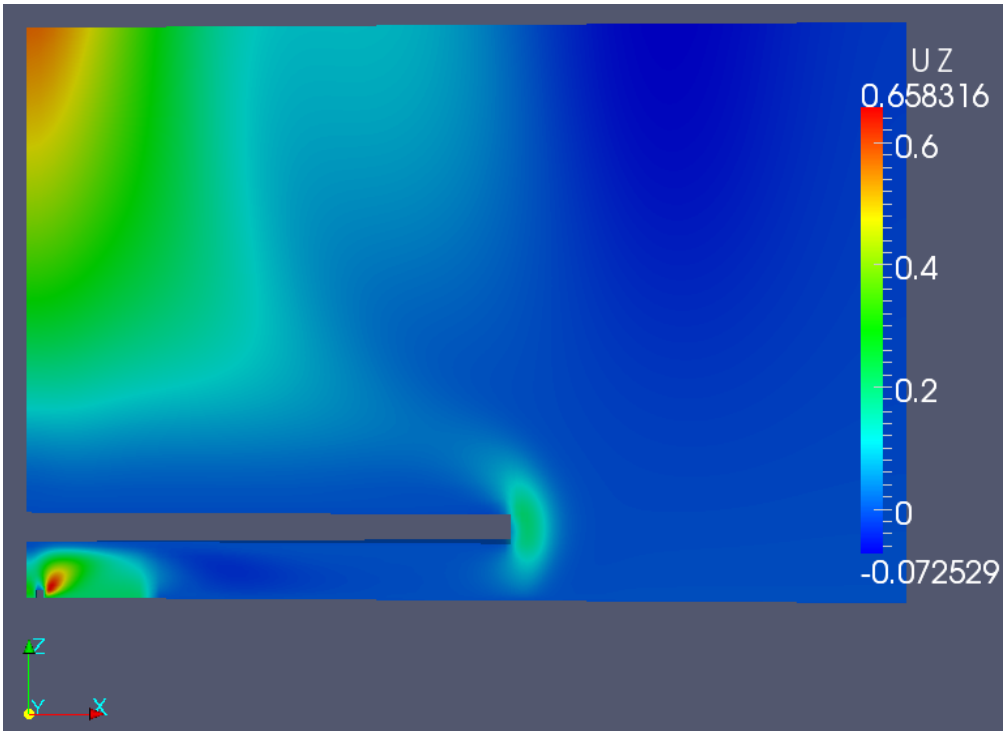

Figure 5.4: Axial velocity profile [m/s]

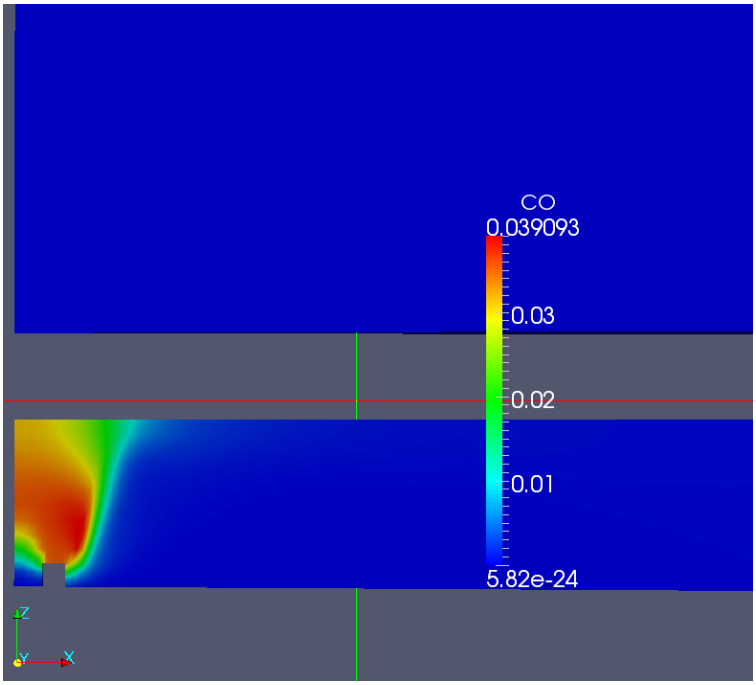

(a) CO profile

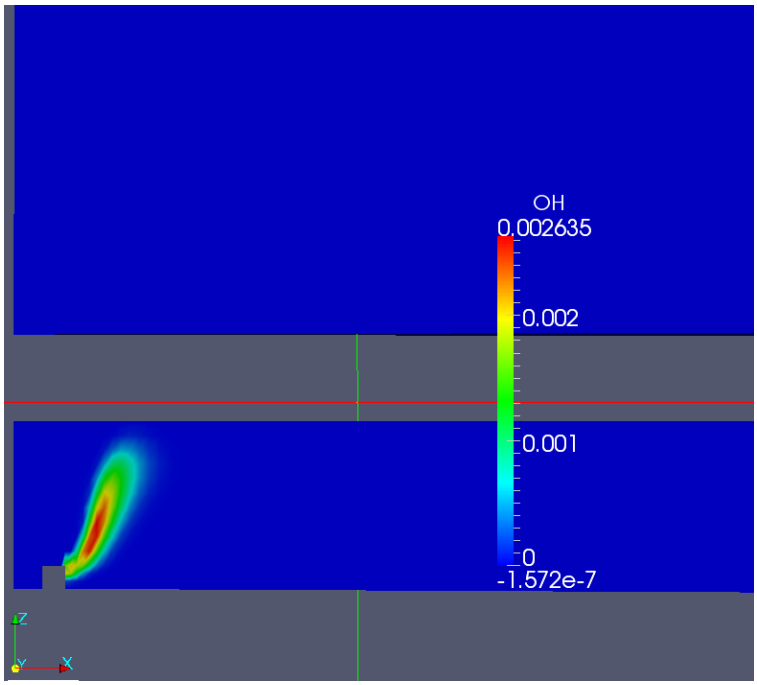

(b) OH profile

Figure 5.5: CO and OH mass fraction profiles

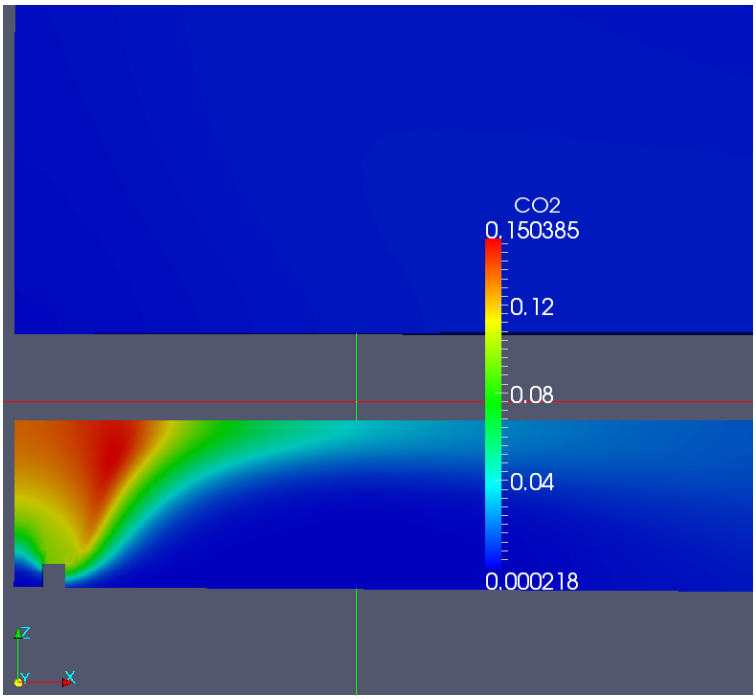

(a) CO_2 profile

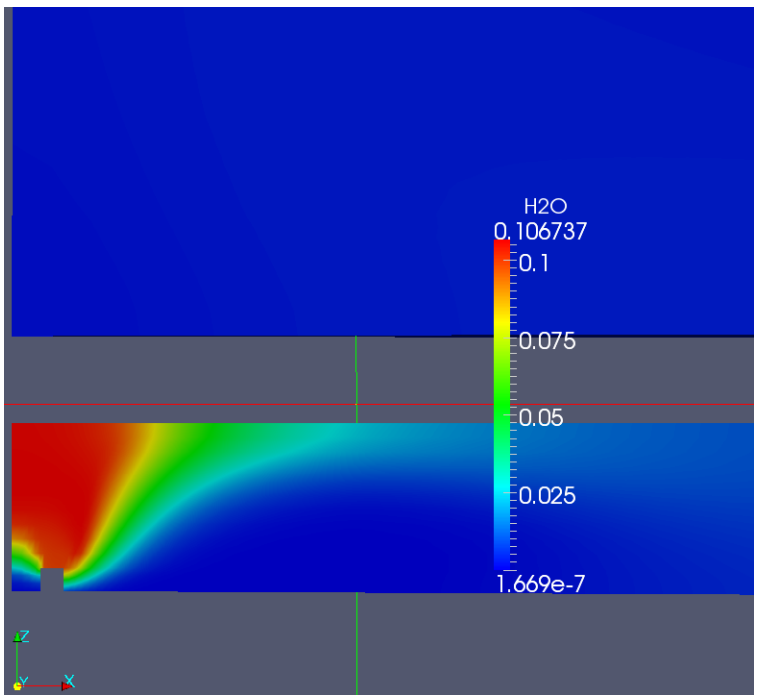

(b) H_2O profile

Figure 5.6: CO_2 and H_2O mass fraction profiles

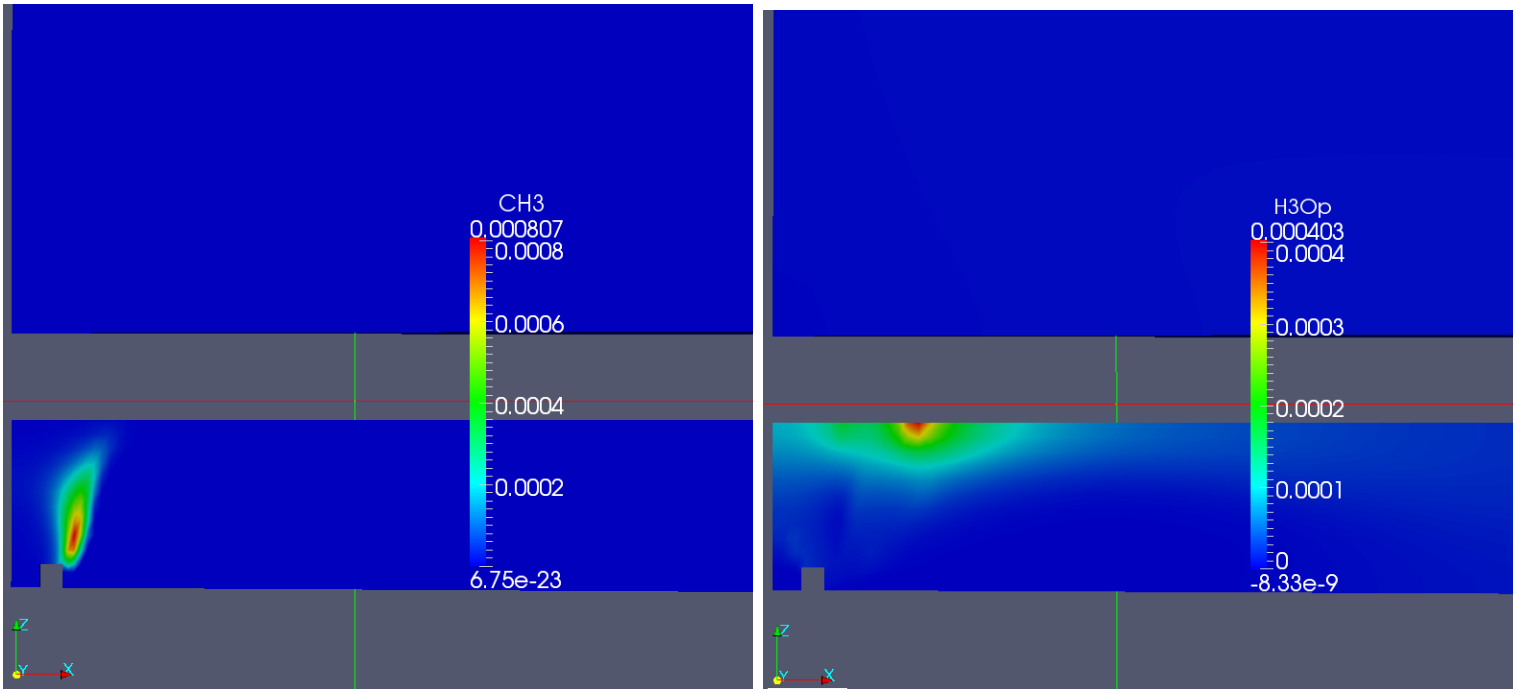

(a) CH_3 profile

(b) H_3O^+ profile

Figure 5.7: CH_3 and H_3O^+ mass fraction profiles

plate edge. So the regions where CO and OH respectively sit do not overlap; this means that OH is not able to consume the produced CO, as observed in the experimental results [20]. However, it can be noticed from Figure 5.7b that this solver is not capable of representing well kinetic mechanisms that include charged species; in fact, not only the predicted mass fraction of H_3O^+ is too high (usually, it is in the order of 10^{-9}), but also there is no reason why these ions should move up to the plate if no electric field is applied. This suggests that a different solver must be used in order to solve for reaction mechanisms that include ions and electrons; in addition, since detailed kinetic mechanisms require high computational time (even if they use the operator-splitting method), reduced mechanisms have been used in the following simulations.

5.2 3-step methane mechanism with electric field

This section shows the results obtained using a skeletal reaction mechanism (which can be found in Appendix A.2) with applied electric field and no charged species; since the mechanism involves only 3 reactions and 6 species, some results are not very accurate. However, the choice of a very simple mechanism was necessary for two reasons: first, to understand if the numerical model of the electric field was correct; second, to save computational time. The absence of charged species does not allow to test completely the accuracy of the model, because there is no source term in the Poisson Equation (that becomes a Laplace's Equation) and there are not the coupling terms related to the electric potential in the momentum and species equation; but the results obtained show that, even with these limitations, simulations match the expected outcome: since the Poisson Equation is decoupled from either the momentum equation (because the $\bar{q}$ term in equation 3.13 is null) and the species Equation (since the $\mathbf{v}_{D_k}$ term of Equation 3.14 is null), the electric potential (and so the electric field) is constant in time. The following Figures show the results obtained with OpenFOAM for this second simulation.

Figure 5.8 and 5.9 show that the peak temperature is overestimated by about 6%, since from experiments it is supposed to be around $1800K$; this can be explained by the fact that the skeletal mechanism includes only three reactions, so many important endothermic reactions (such as formation of radicals) are not taken into account. Because the Poisson Equation is decoupled, the imposed electric field does not affect the temperature behavior. The components of the electric field and the electric potential are shown in Figures 5.12, 5.13 and 5.14 respectively: a negative potential of $-1000V$ has been assigned to the plate, and a zero potential to the coflow burner (i.e., to either the fuel inlet, oxidizer inlet and the burner walls of Figure 3.2); as expected, the electric potential gradually decreases moving far from the plate. No charge accumulation occurs in the flame zone, so the high gradients of the electric field occur only at the corners of the plate and at the corners of the burner

walls. Figures 5.15 and 5.16 represent the species profiles: the mass fraction of CO is underestimated somewhat, but the other results globally agree with those obtained from experiments.

However, even if this skeletal mechanism allowed to test part of the numerical model of the electric field, a more detailed reaction mechanism is needed in order to describe the flame properties in a more accurate way, and in particular reactions that produce ion species must be included.

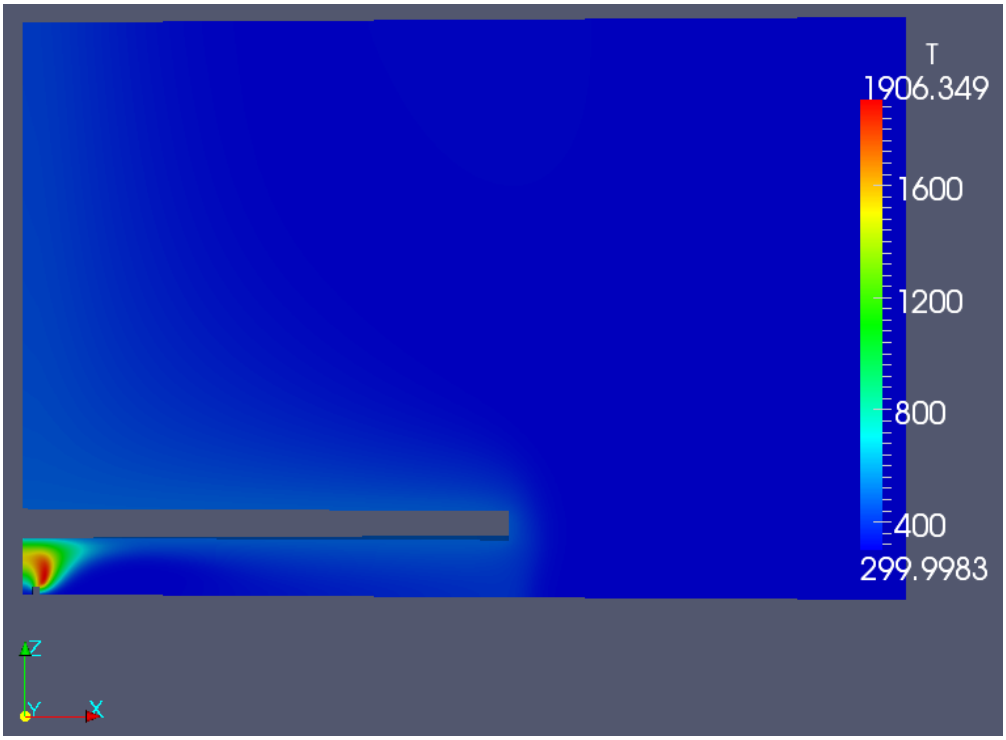

Figure 5.8: Temperature profile [K]

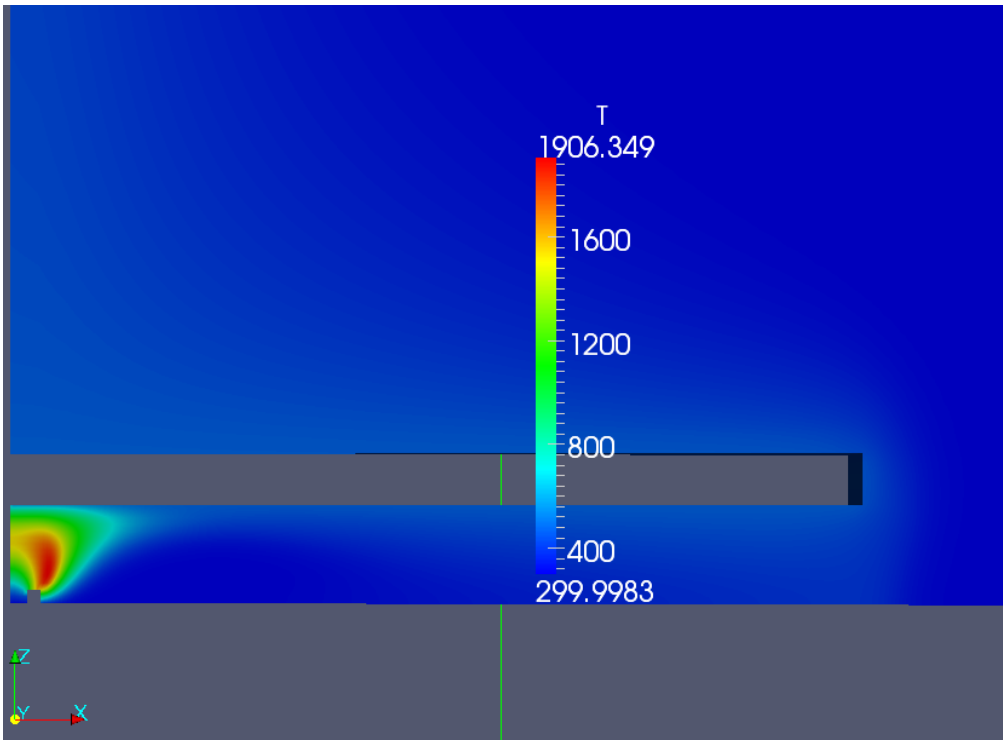

Figure 5.9: Zoom of the temperature profile [K]

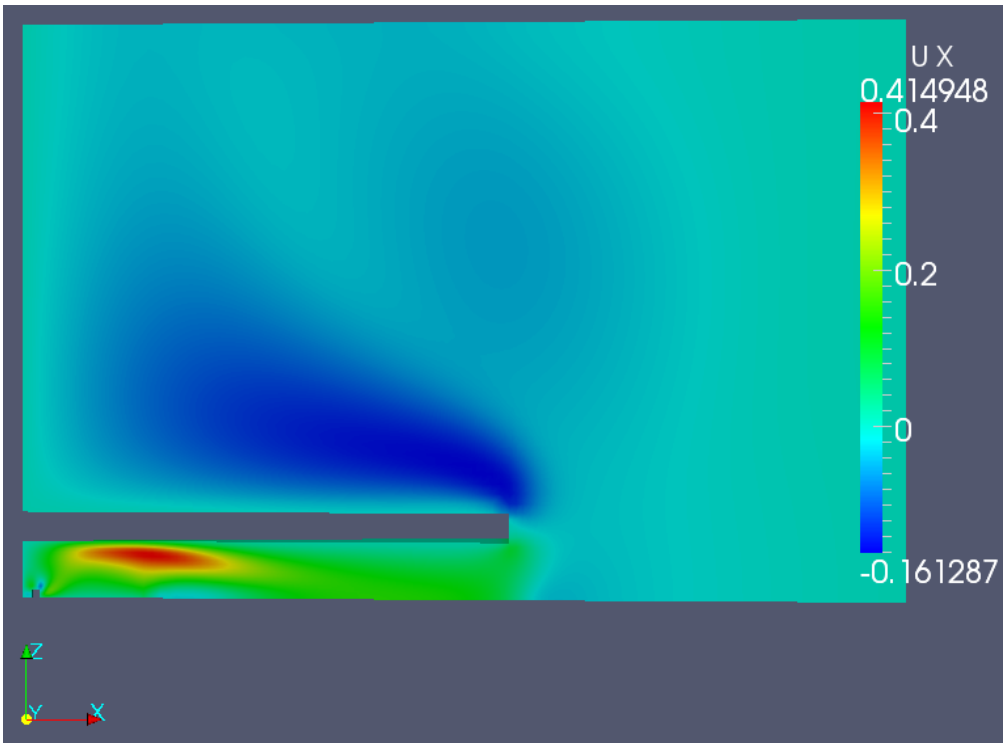

Figure 5.10: Radial velocity profile [m/s]

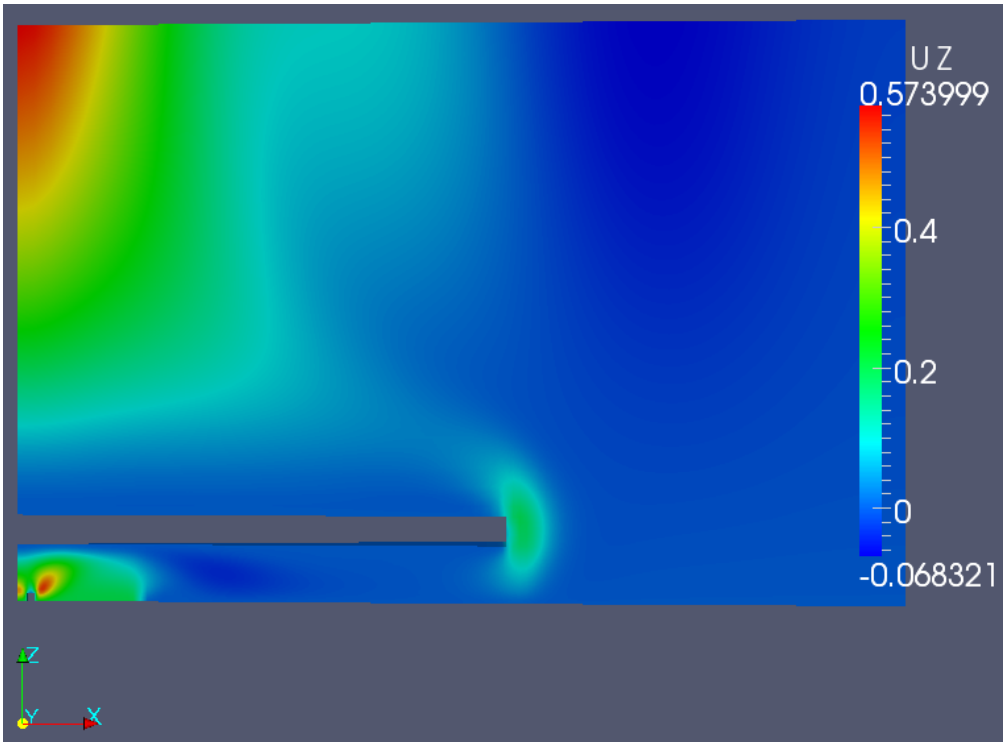

Figure 5.11: Axial velocity profile [m/s]

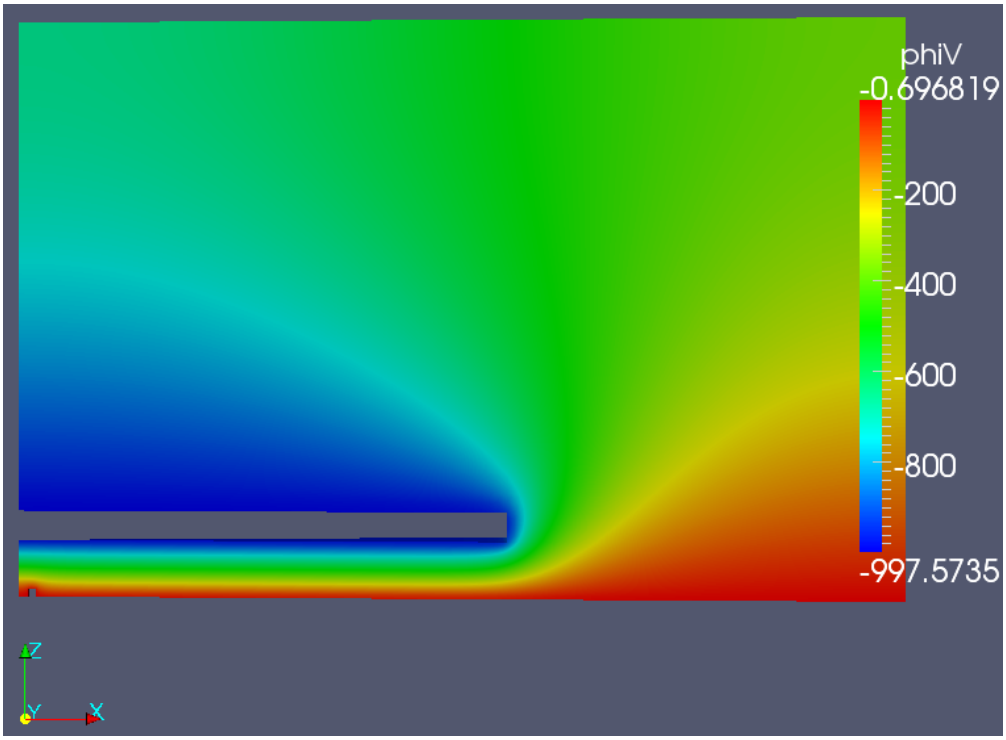

Figure 5.12: Electric potential profile [V]

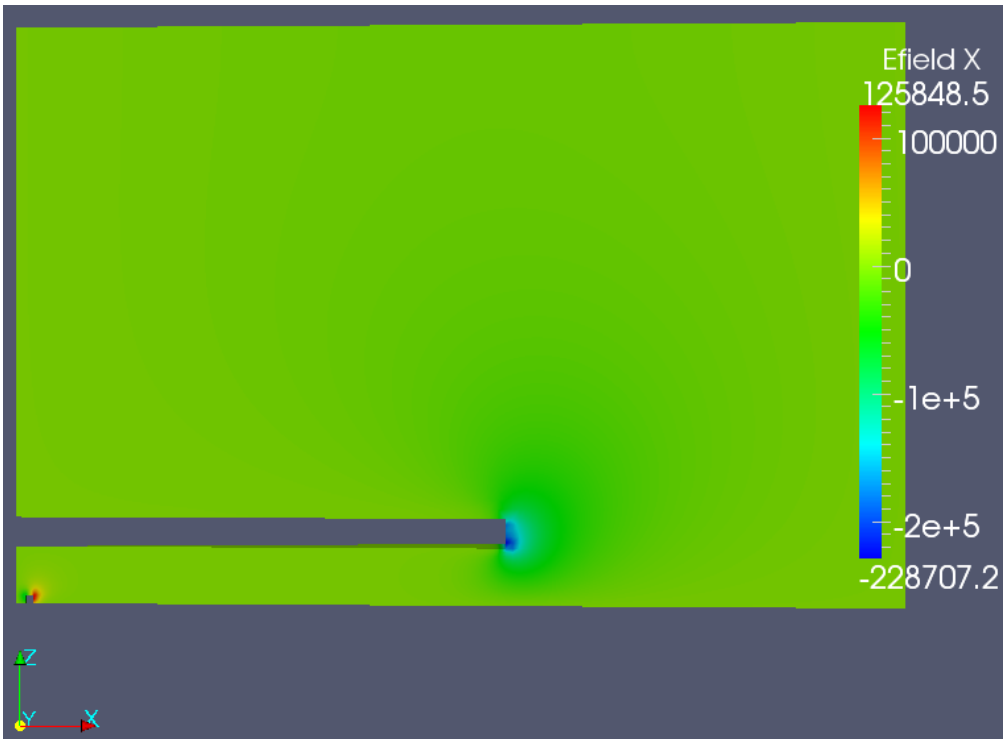

Figure 5.13: Radial electric field profile [V/m]

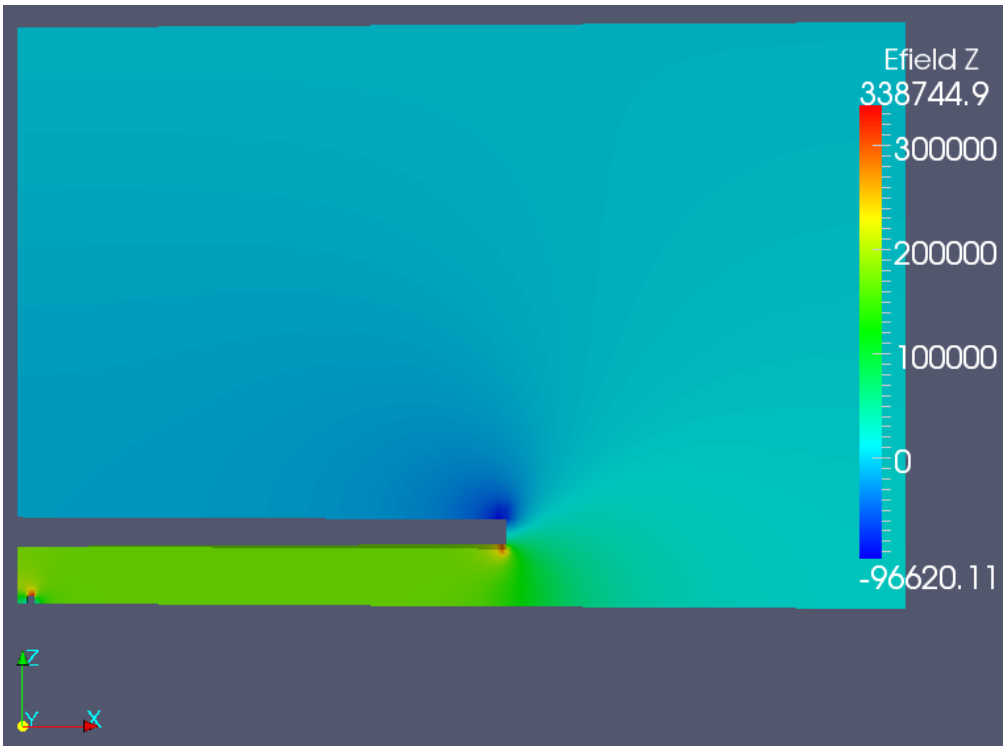

Figure 5.14: Axial electric field profile [V/m]

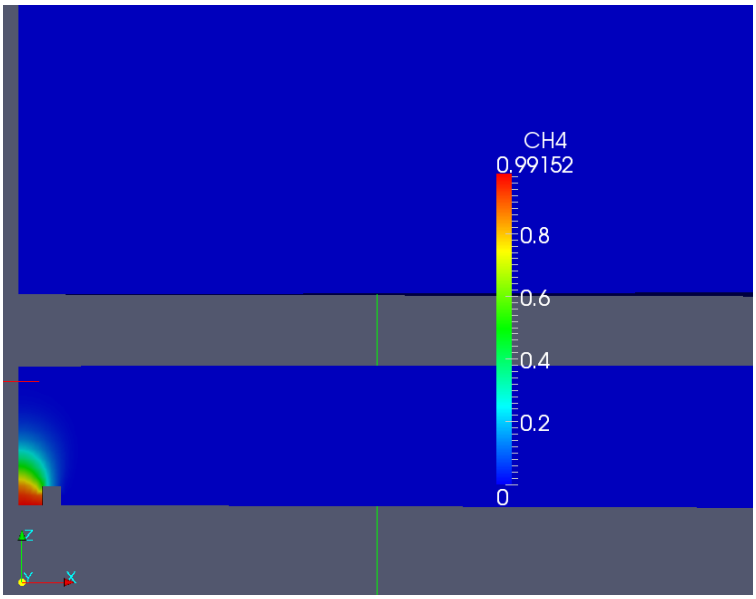

(a) CH_4 profile

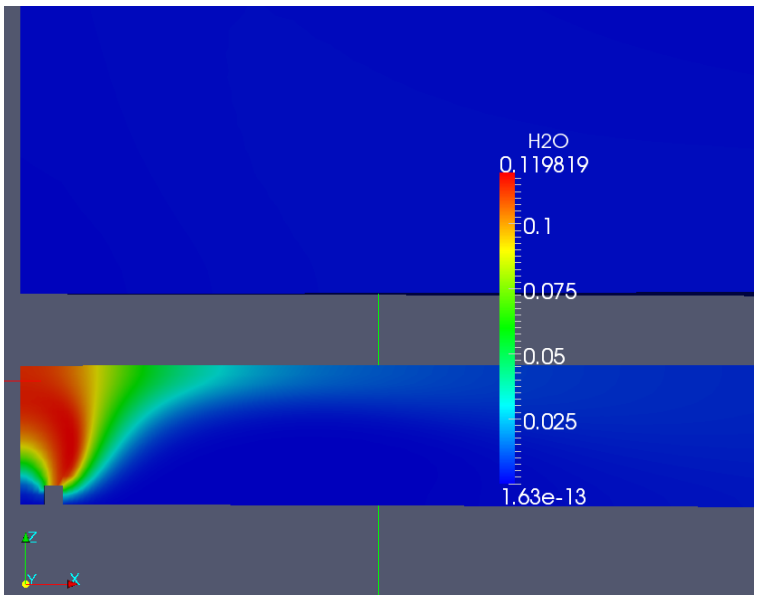

(b) H_2O profile

Figure 5.15: CH_4 and H_2O mass fraction profiles

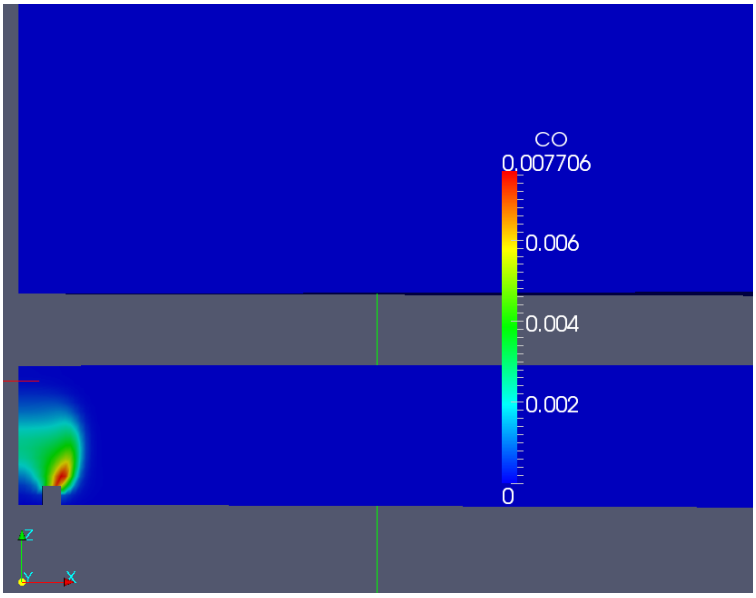

(a) CO profile

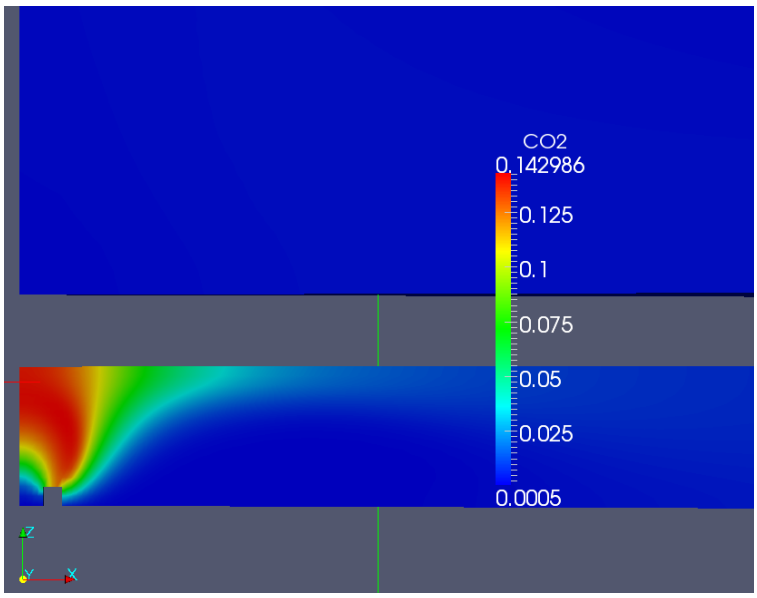

(b) CO_2 profile

Figure 5.16: CO and CO_2 mass fraction profiles

5.3 Reduced mechanism with electric field

In this section, a reduced mechanism based on $GRI - Mech1.2$ has been implemented; this mechanism does not include charged species, so as for the skeletal mechanism of the previous section the Poisson Equation is decoupled from the momentum and species conservation Equations. The reactions involved can be found in Appendix A.3. The following Figures represent the results obtained with OpenFOAM for this third simulation.

Figures 5.17 and 5.18 show that now there is only less than 3% underestimation of the peak temperature; it means that even if this is a reduced mechanism, it is able to capture the flame behavior in a very accurate way. Figures 5.21, 5.22 and 5.23 show the electric potential and electric field components respectively: as for the previous simulation, a negative potential of $-1000V$ has been assigned to the plate, and a zero potential to the coflow burner; again, since there is not charge accumulation in the flame zone the electric potential gradually decreases moving far from the plate and high gradients of the electric field occur only at the corners of the plate and at the corners of the burner walls. Figures 5.24, 5.25 and 5.26 represent the profile of the most important species; by comparing CO and OH profiles, it can be noticed that OH is mainly produced at the right side of the burner, while CO is produced close to the burner, then it moves up towards the plate edge. Since the regions where CO and OH respectively sit do not overlap, it means that OH is not able to consume the produced CO, as observed in the experimental results [20]. Figure 5.26 show the profile of two species that will be important for the chemi-ionization process; in fact, the reaction between these two species will generate the CH radicals that subsequently will react with the O radical to form HCO^+ and e^-.

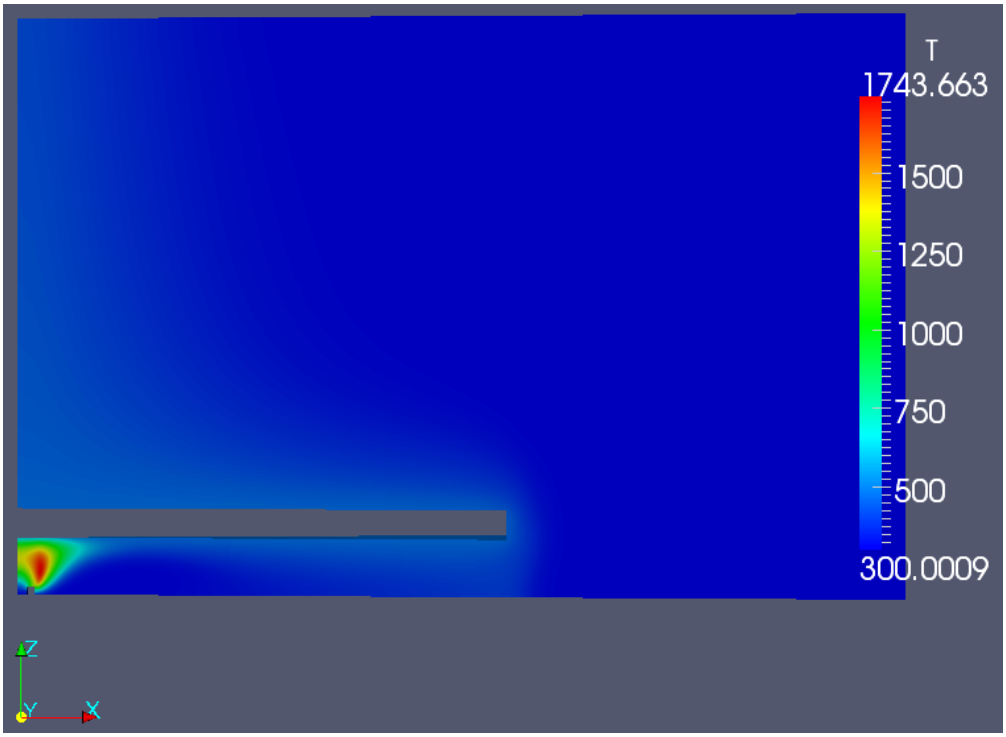

Figure 5.17: Temperature profile [K]

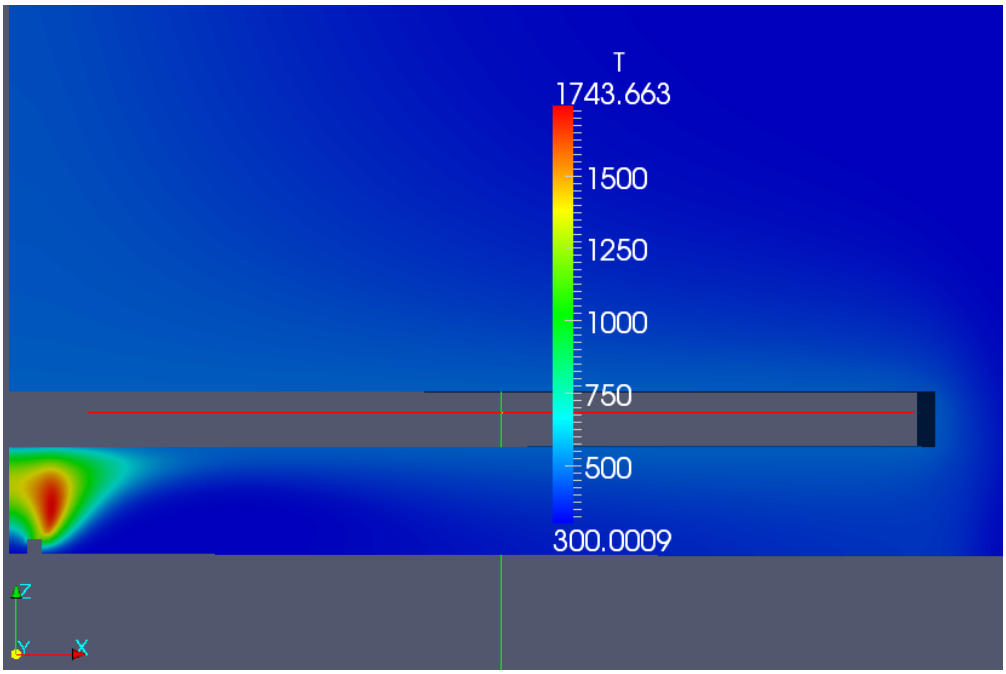

Figure 5.18: Zoom of the temperature profile [K]

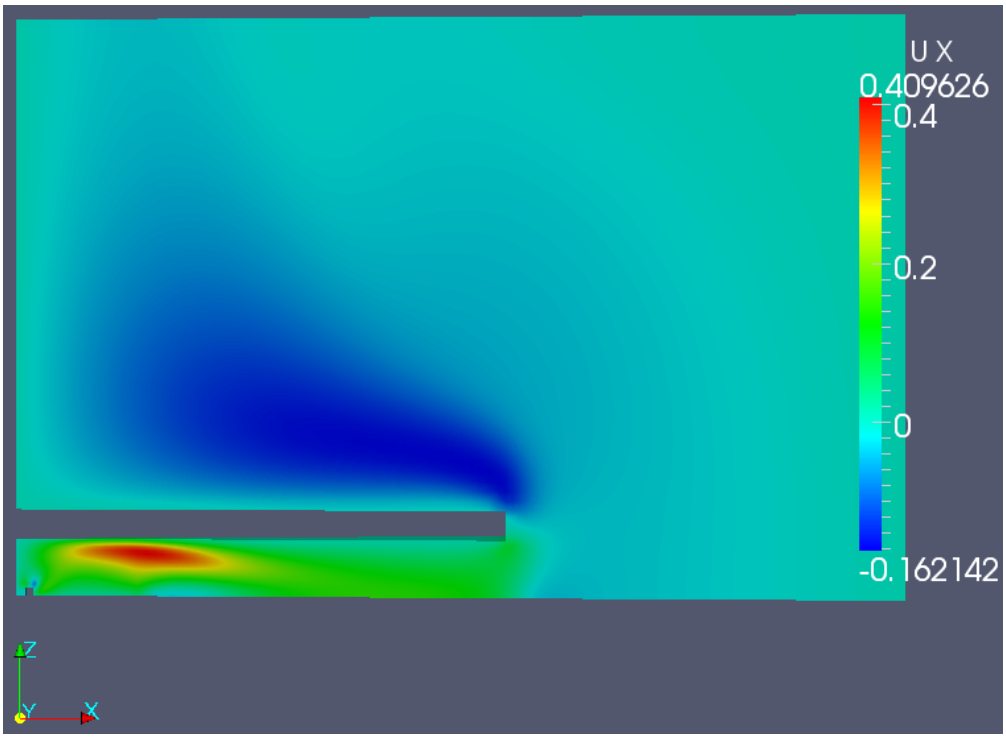

Figure 5.19: Radial velocity profile [m/s]

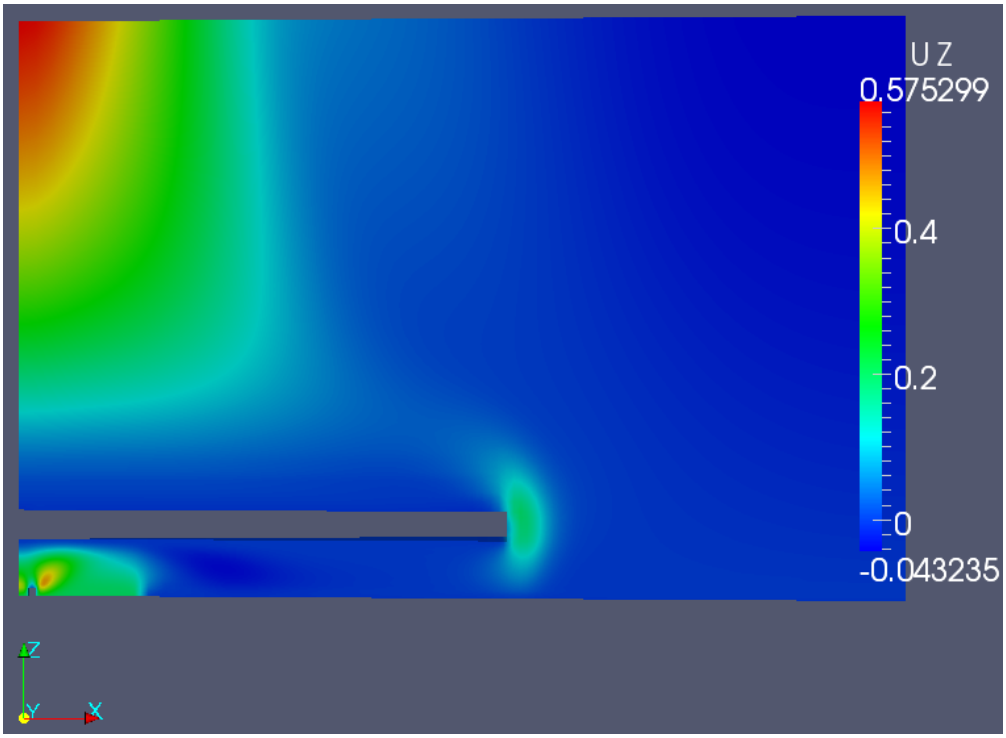

Figure 5.20: Axial velocity profile [m/s]

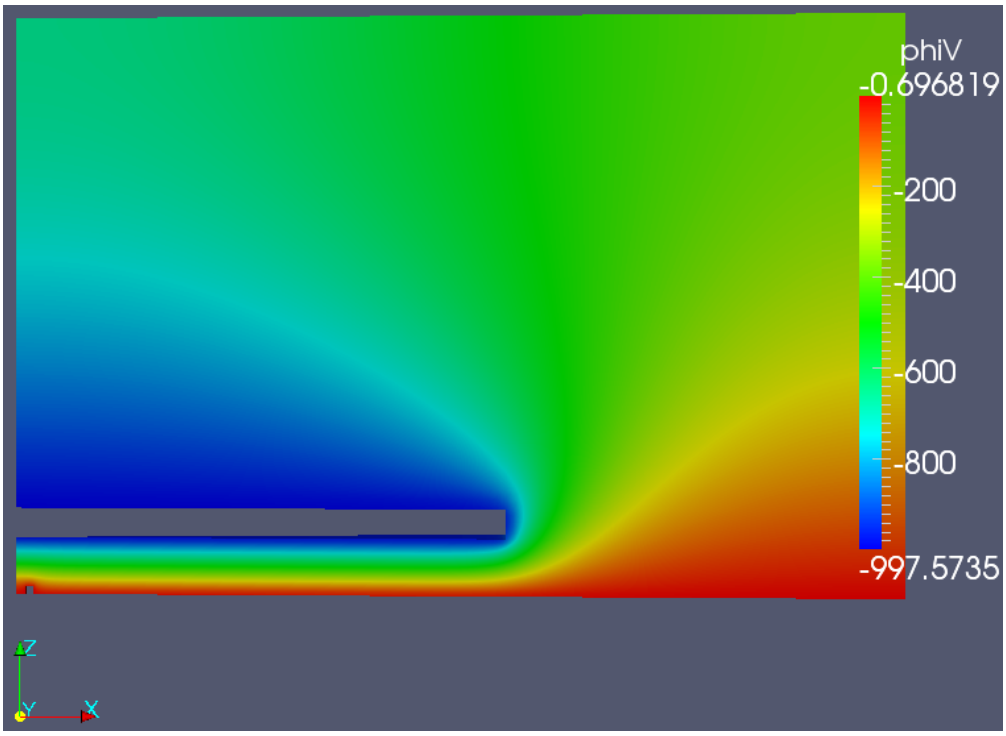

Figure 5.21: Electric potential profile [V]

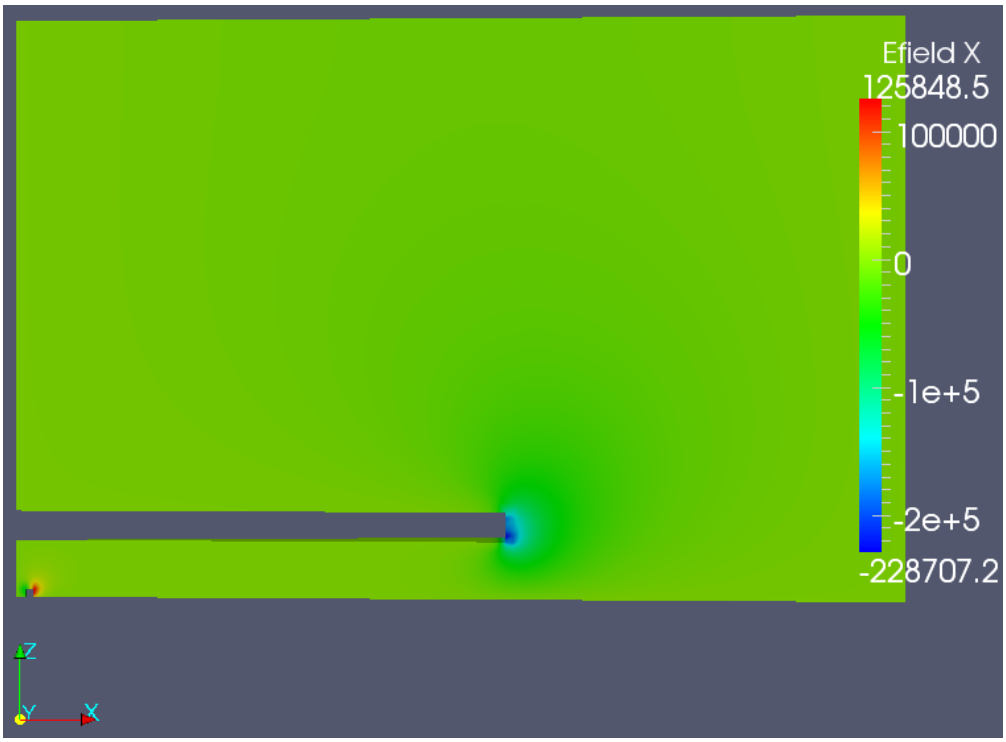

Figure 5.22: Radial electric field profile [V/m]

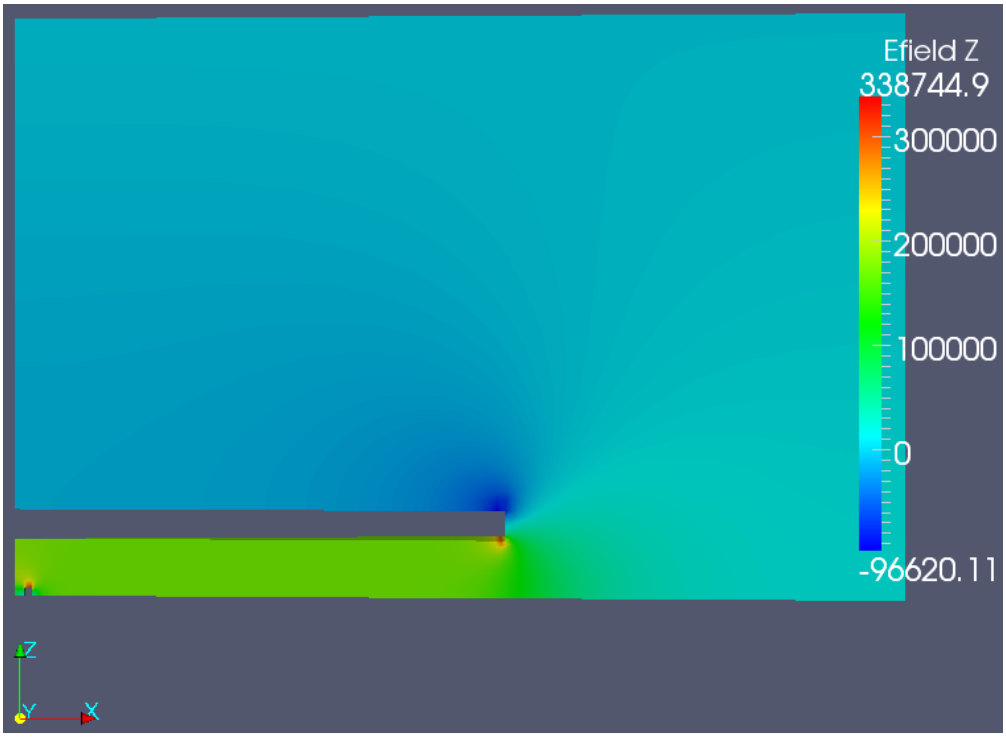

Figure 5.23: Axial electric field profile [V/m]

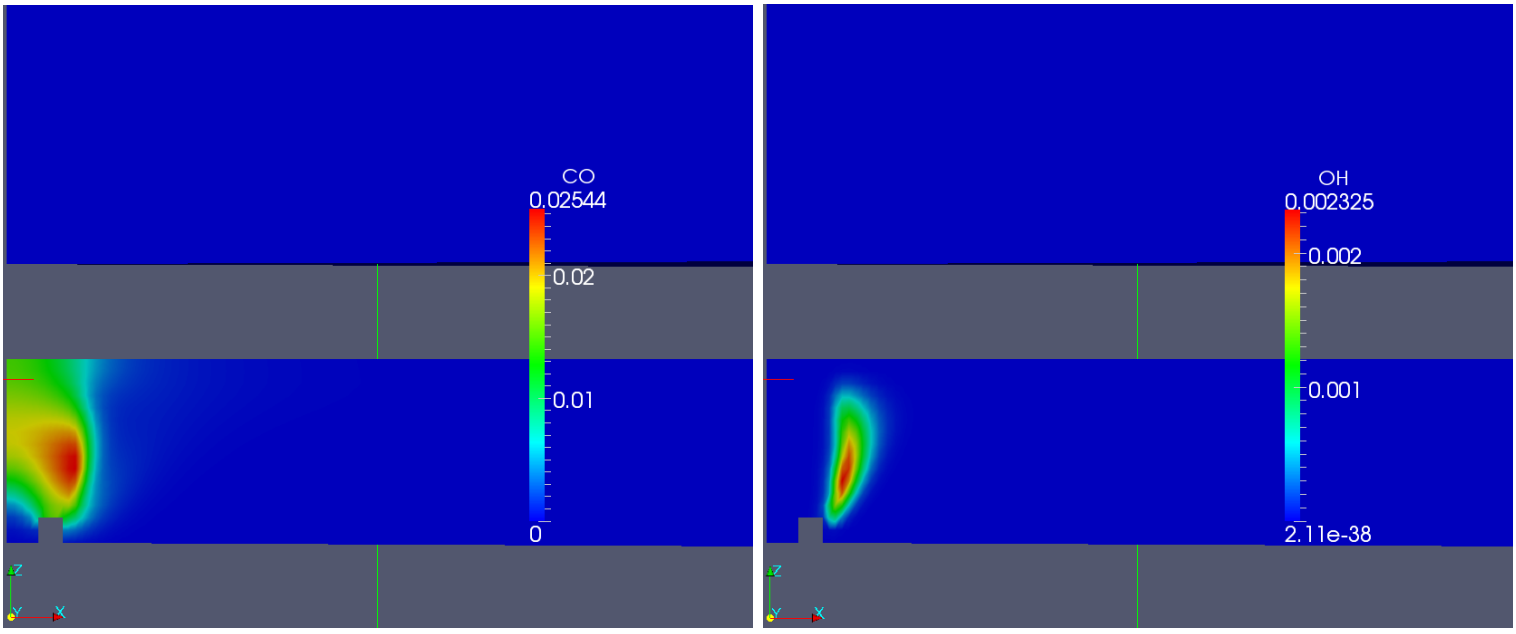

(a) *CO* profile (b) *OH* profile

Figure 5.24: *CO* and *OH* mass fraction profiles

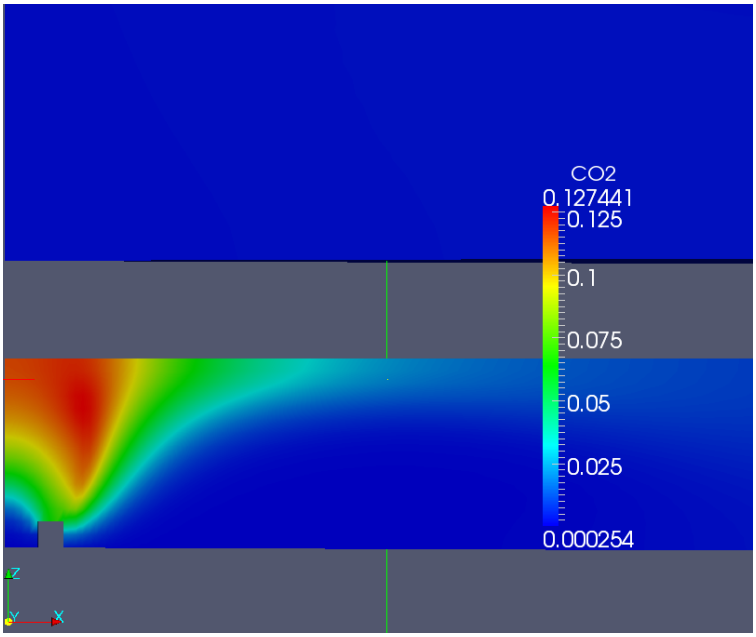

(a) CO_2 profile

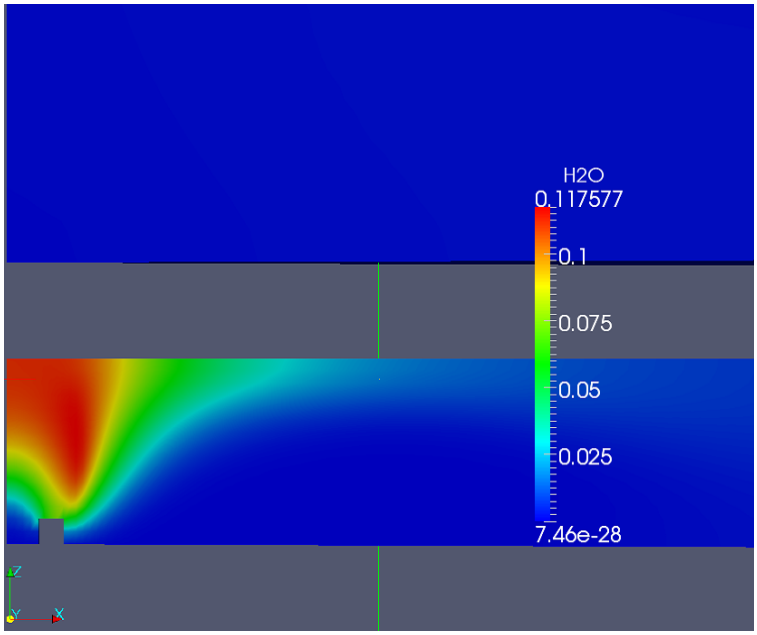

(b) H_2O profile

Figure 5.25: CO_2 and H_2O mass fraction profiles

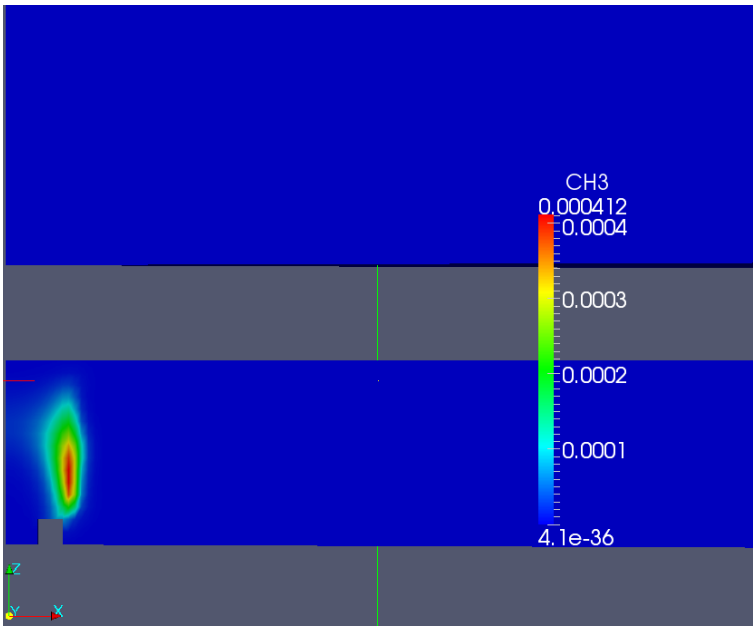

(a) CH_3 profile

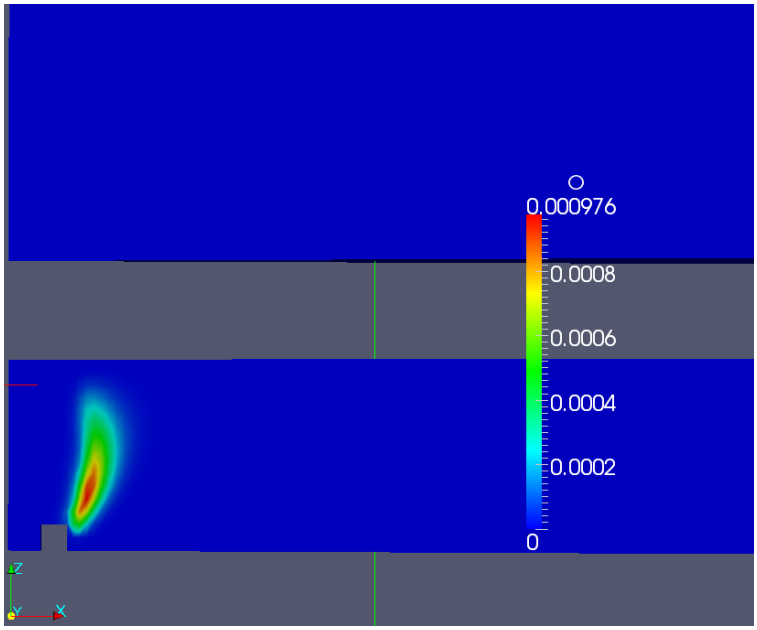

(b) O profile

Figure 5.26: CH_3 and O mass fractions profiles

5.4 Reduced ions mechanism with no electric field

This section presents the results obtained using a reduced ions mechanism with no electric field applied; it means that the Poisson Equation and the coupling terms in momentum and species conservations Equations have not been modeled. The complete set of reactions is reported in Appendix A.4. This simulation uses the OpenFOAM built-in solver for reacting flows, called *reactingFoam* [34]; the only modification introduced in the solver is the addition of the model of a spark, which has been placed at the top of the burner walls. The effect of the spark has been simulated by doubling the value of the enthalpy in few cells located above the burner for a very short time ($\Delta t = 0.05s$). Figures 5.27-5.35 show the results obtained from OpenFOAM for this fourth simulation.

Figures 5.27-5.30 show the profiles of temperature and velocity components: these results are very similar to those obtained with the previous simulation, and this indicates that the user-defined solver works pretty well. The mass fractions of the species instead are different because a different kinetic mechanism has been used; it is important to notice that even here the profiles of CO and OH do not overlap, since this is a typical characteristic of impinging coflow flames. In particular, Figures 5.33, 5.34 and 5.35 show the profiles of either neutral species directly related to the chemi-ionization process and charges species: the reaction between CH_3 and O is a precursor of the chemi-ionization process, since it produces the CH radical; this species indeed will react with O to create HCO^+ and e^-, and HCO^+ in turn will produce H_3O^+. Finally, the charged species will recombine to produce neutral species, namely H_2O and H. The results obtained for charged species agree with those found in literature [35]: the mass fraction of H_3O^+ is usually around $10^{-8} - 10^{-9}$, and that of HCO^+ is about three orders of magnitude less than that of hydronium.

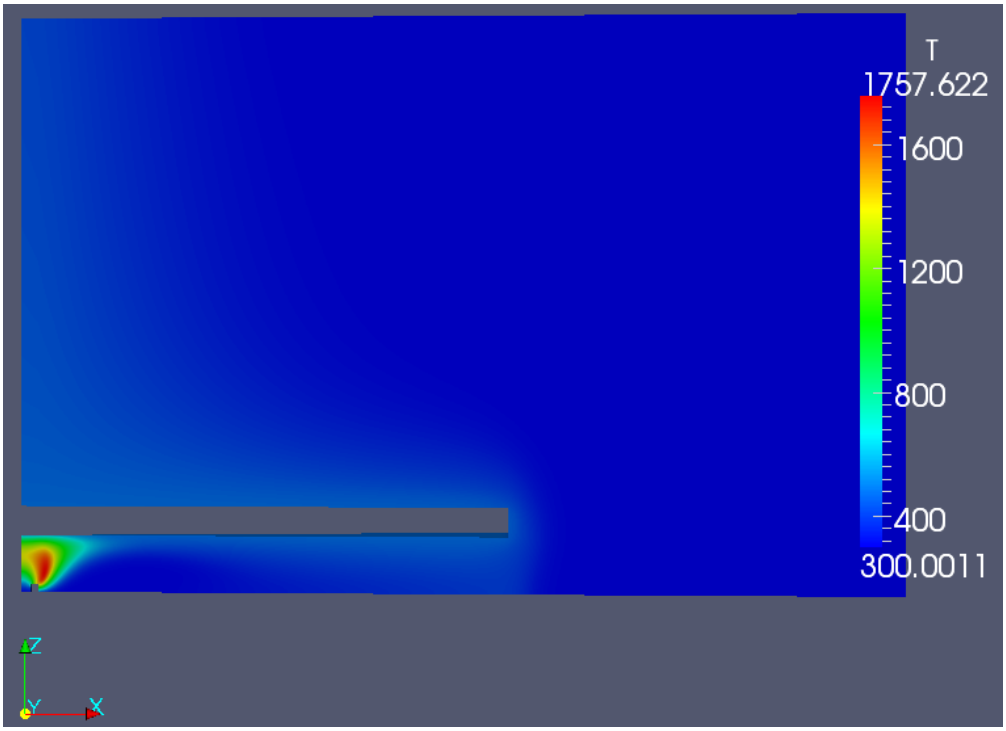

Figure 5.27: Temperature profile [K]

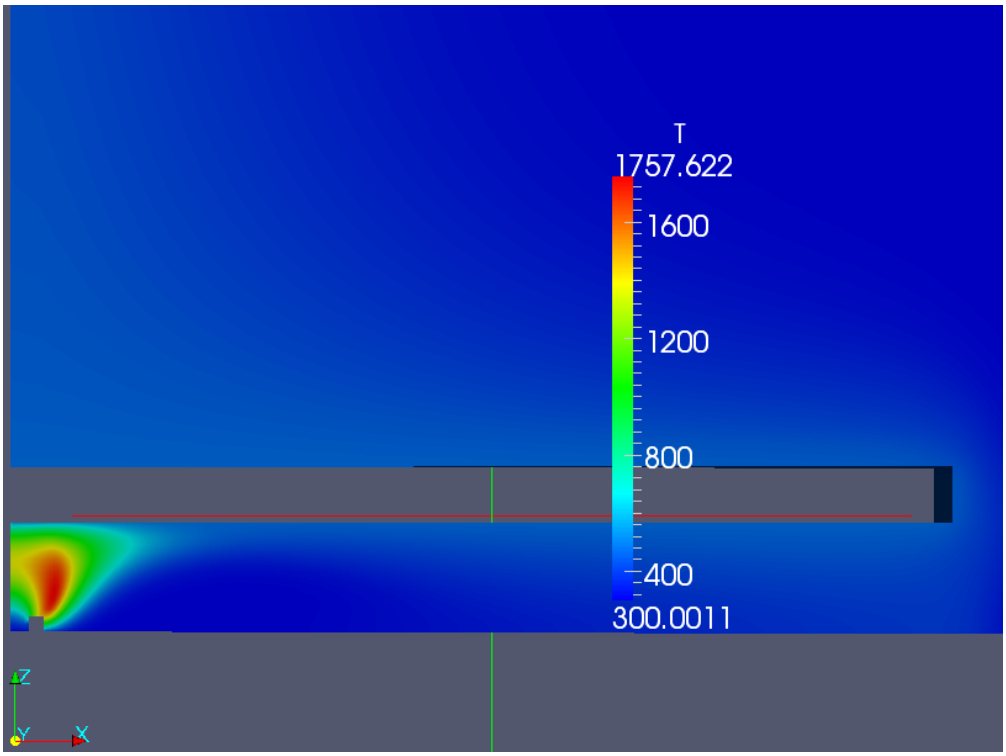

Figure 5.28: Zoom of the temperature profile [K]

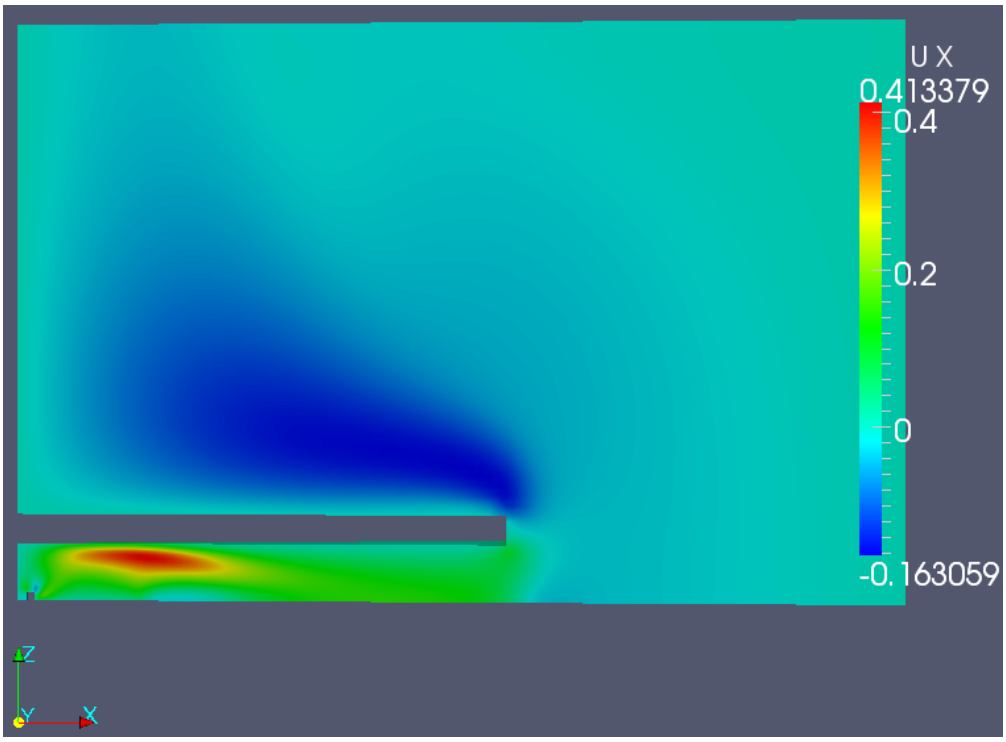

Figure 5.29: Radial velocity profile [m/s]

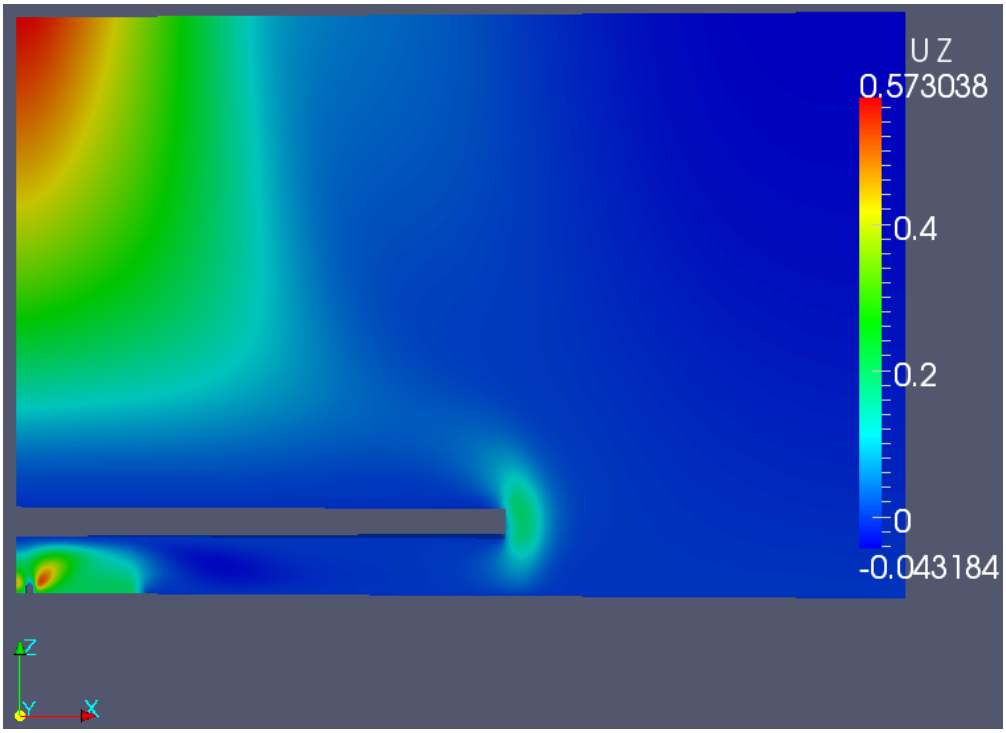

Figure 5.30: Axial velocity profile [m/s]

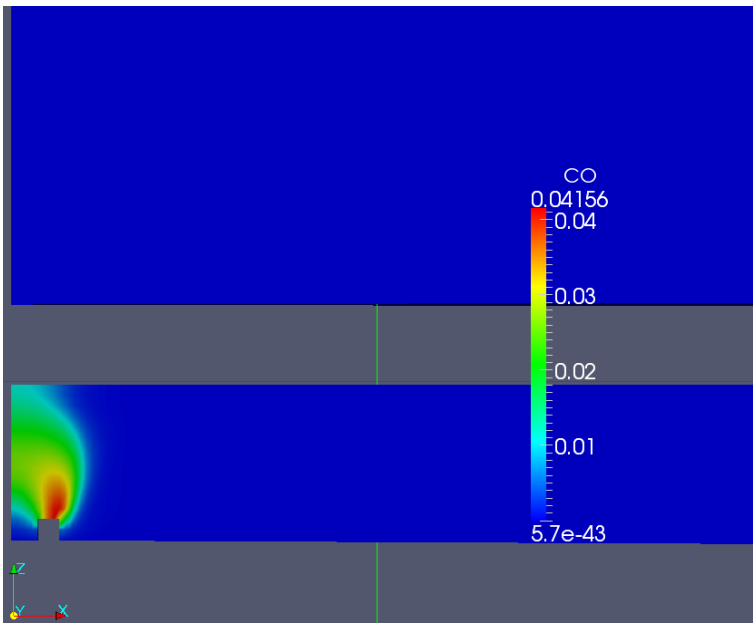

(a) CO profile

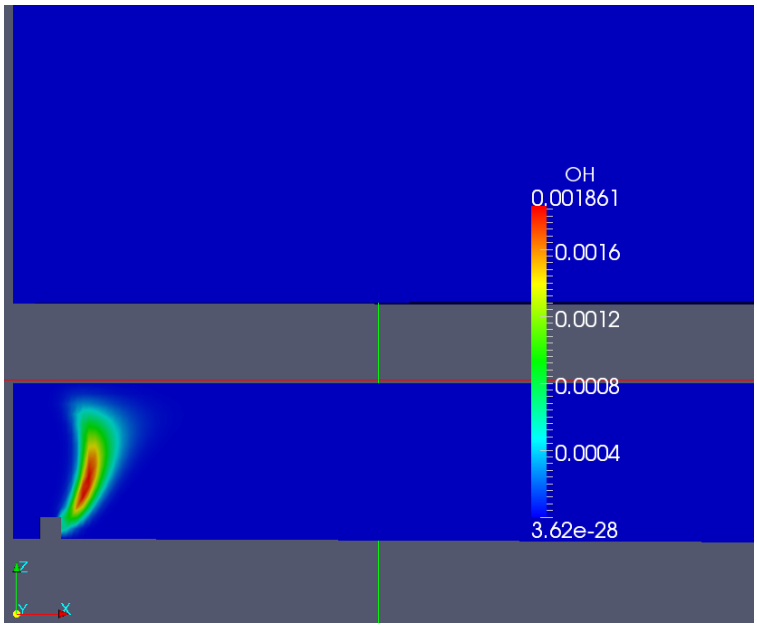

(b) OH profile

Figure 5.31: CO and OH mass fraction profiles

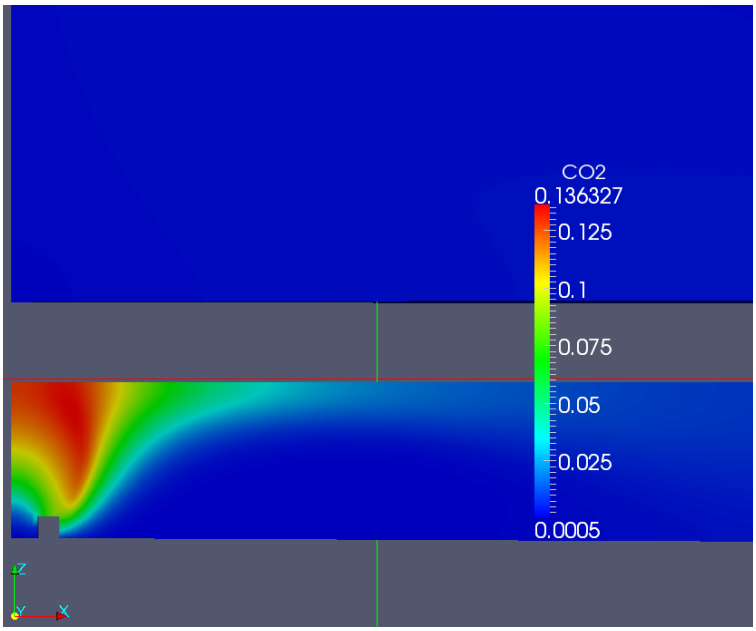

(a) CO_2 profile

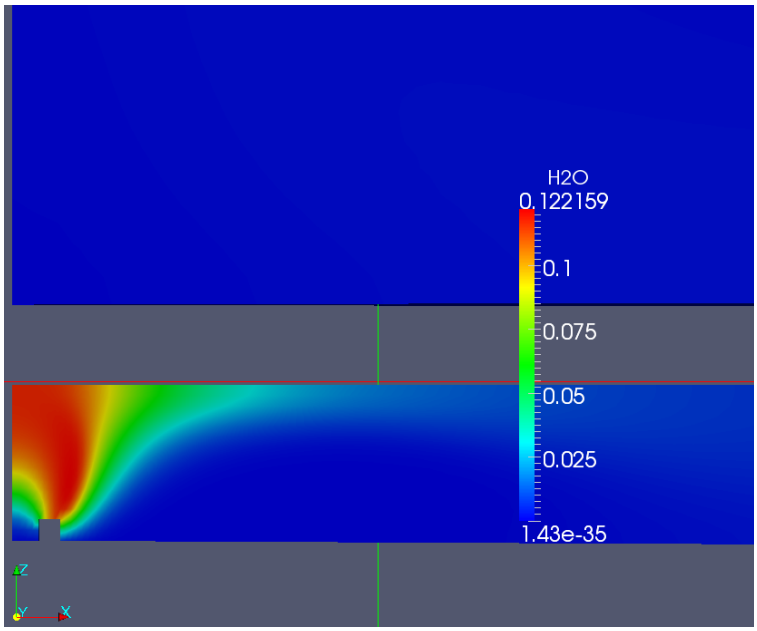

(b) H_2O profile

Figure 5.32: CO_2 and H_2O mass fraction profiles

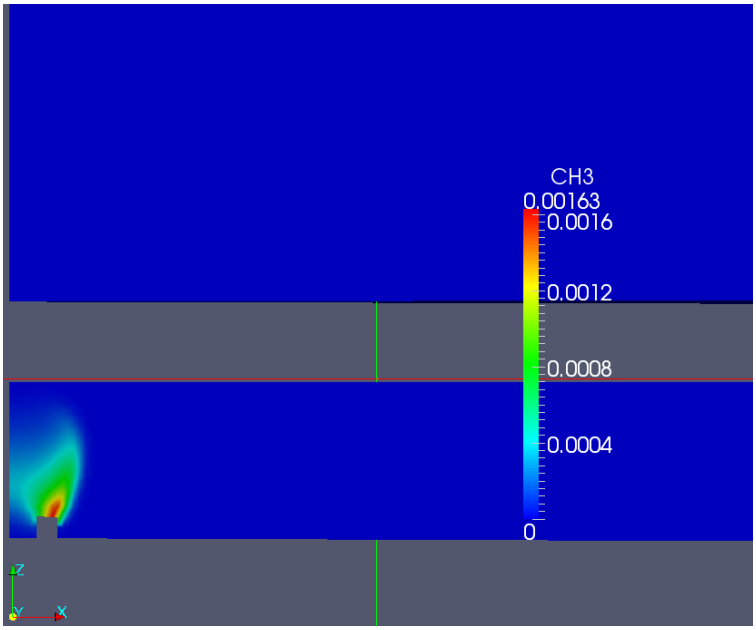

(a) CH_3 profile

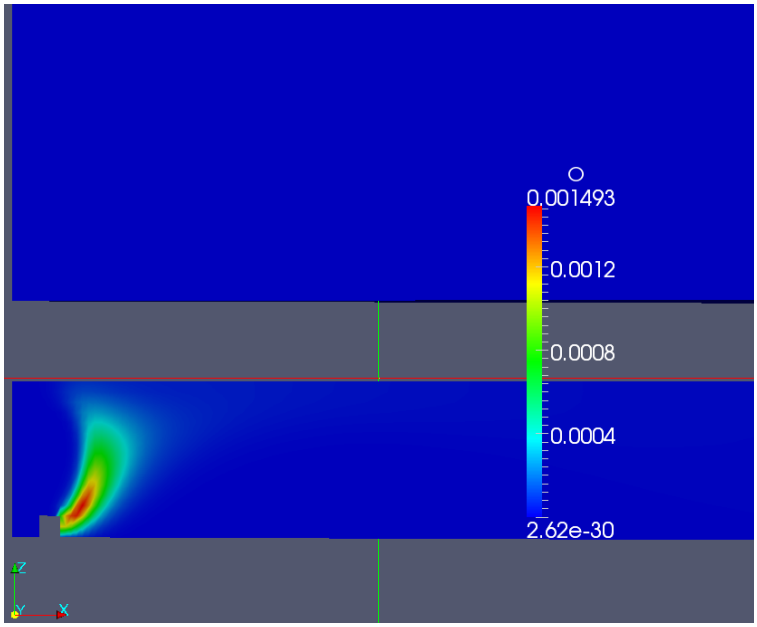

(b) O profile

Figure 5.33: CH_3 and O mass fraction profiles

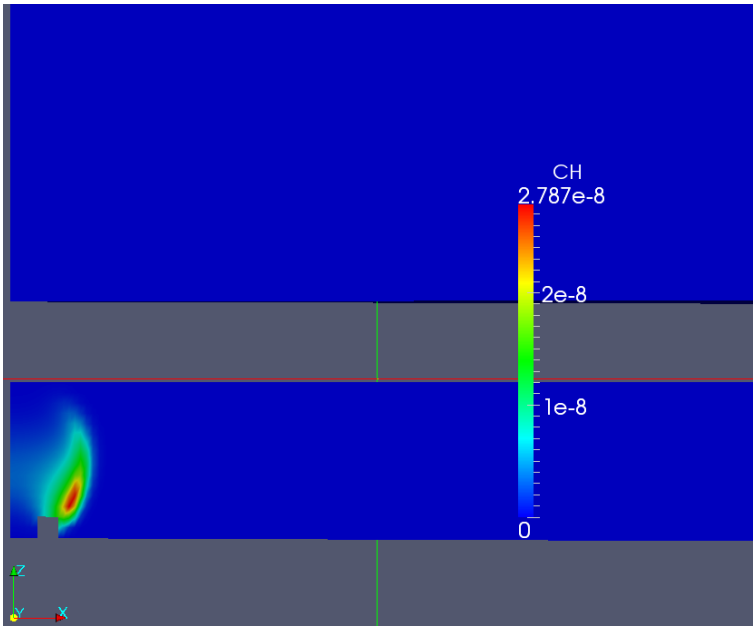

(a) CH profile

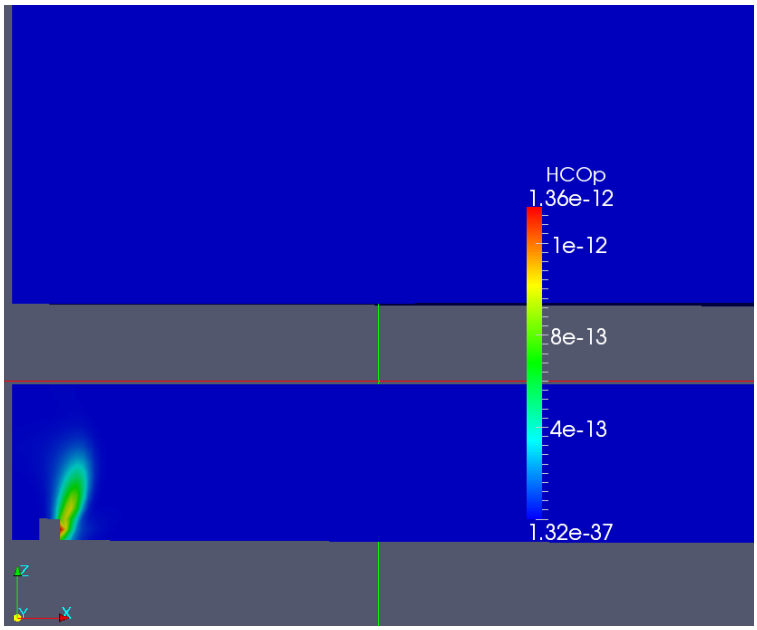

(b) HCO^+ profile

Figure 5.34: CH and HCO^+ mass fraction profiles

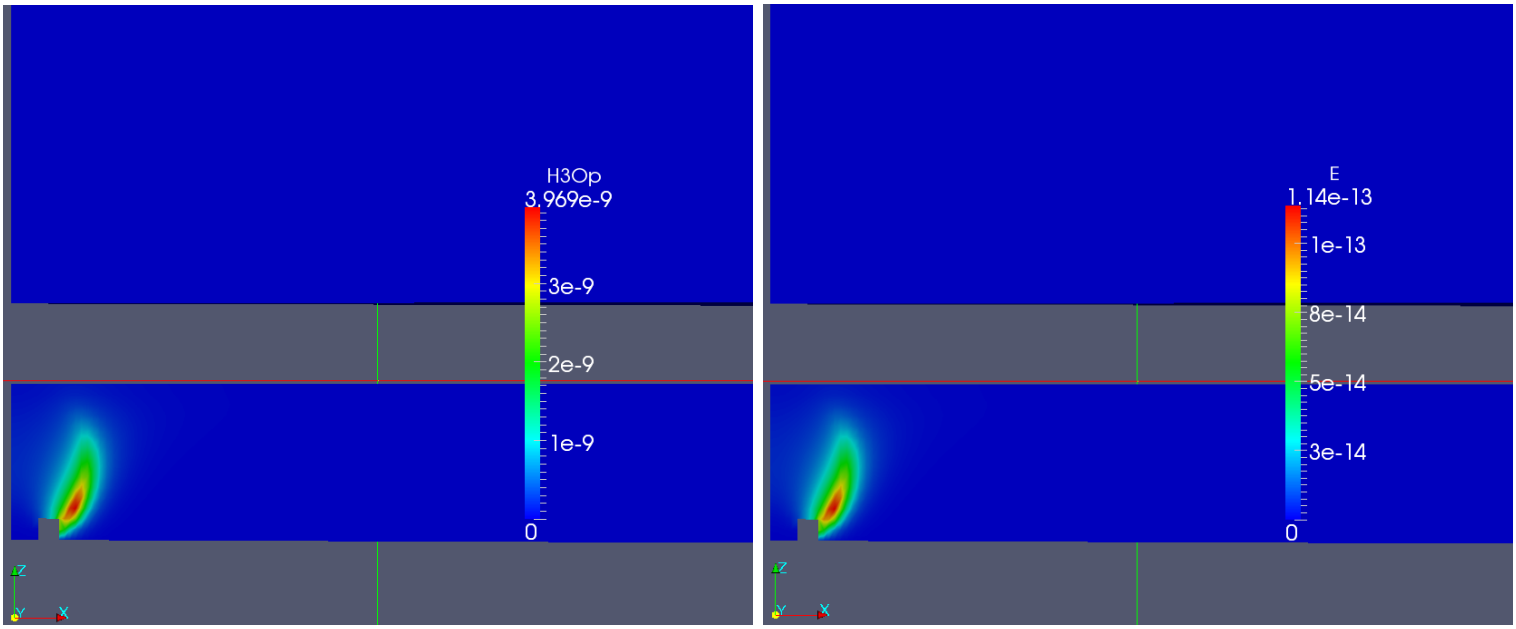

(a) H_3O^+ profile (b) e^- profile

Figure 5.35: H_3O^+ and e^- mass fraction profiles

5.5 Reduced ions mechanism with self-induced electric field

In this simulation, the user-defined solver which implements the Poisson Equation and the coupling terms in the species and momentum Equation has been used; as a first step however, a zero potential has been set on the plate and the burner walls. This means that the electric field is generated only through charge accumulation in the reaction zone. This simulation has been created using the steady state results of the previous one: it means that when the solver starts evaluating the Poisson Equation, the source term is already different from zero. This procedure helps to avoid some complicated transient phenomena, such as ignition and generation of charges through the chemi-ionization; these processes indeed can negatively affect the code and make it unstable, since chemistry is the stiff component of the problem. Figures 5.36-5.46 show the results obtained from OpenFOAM for this fifth simulation.

The effects of the self-induced electric field can be summarized in this way:

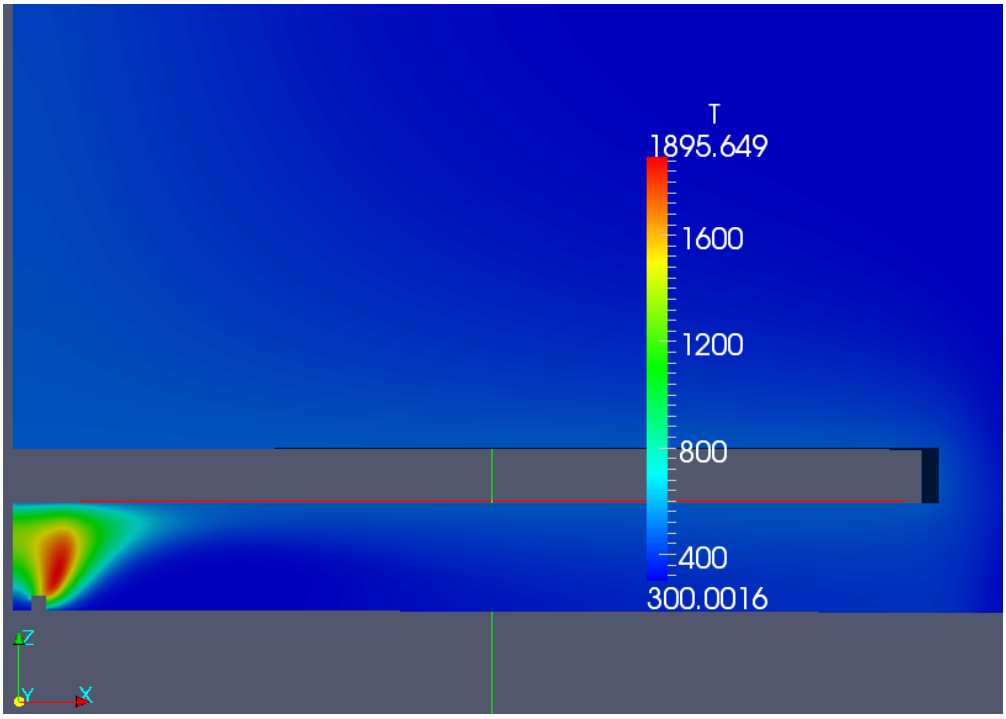

Figure 5.36: Zoom of the temperature profile [K]

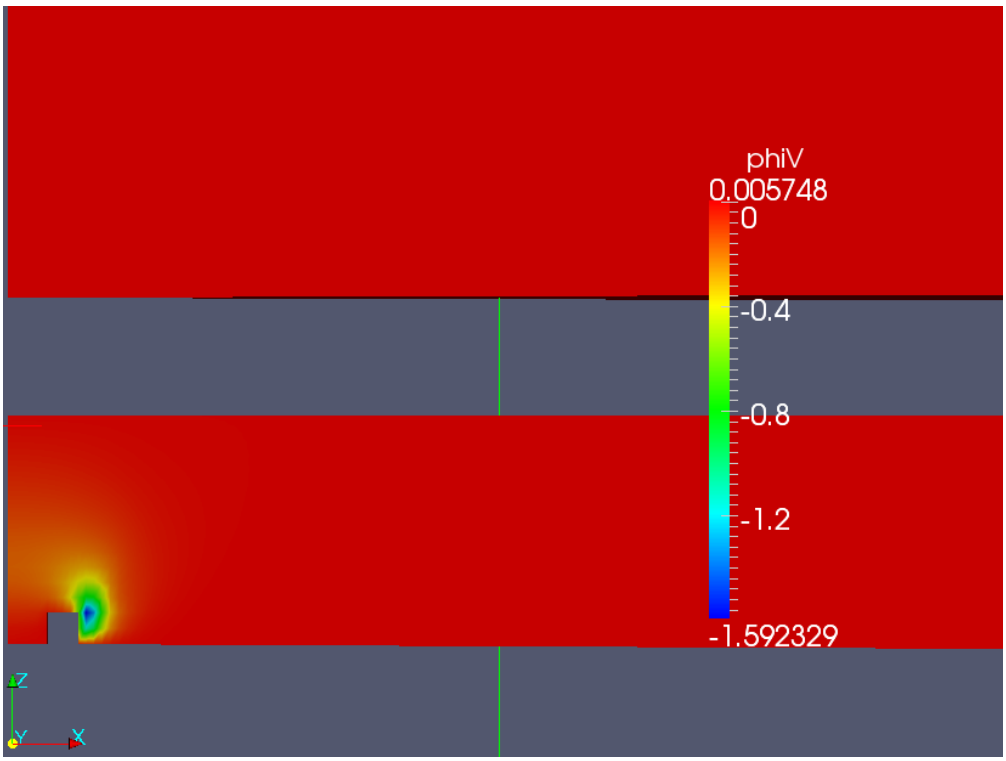

Figure 5.37: Electric potential profile [V]

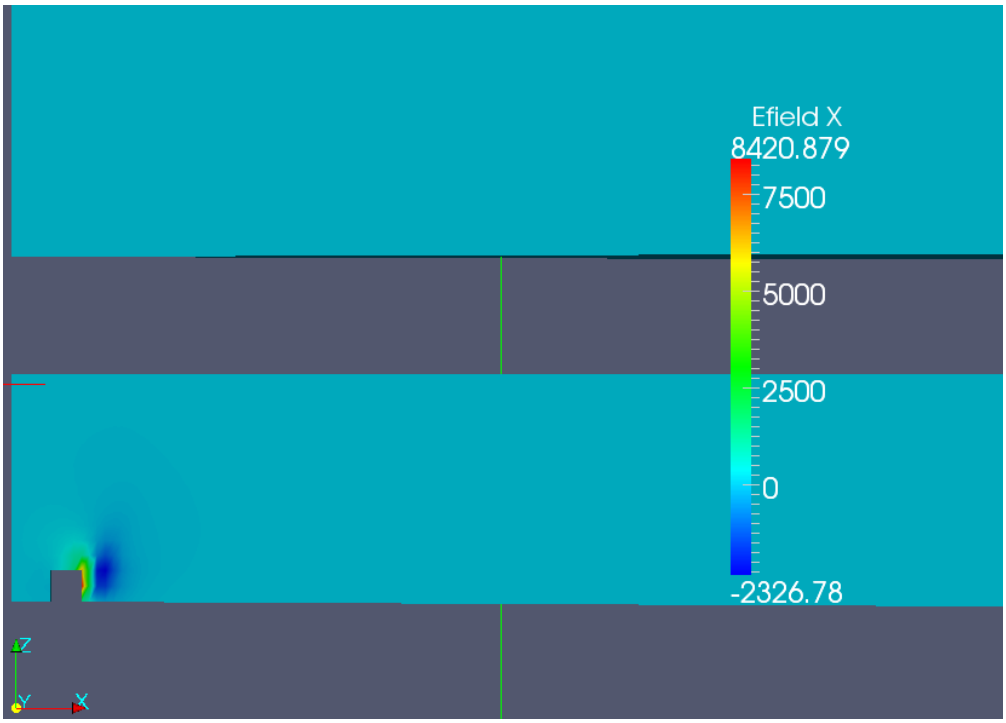

Figure 5.38: Radial electric field profile [V/m]

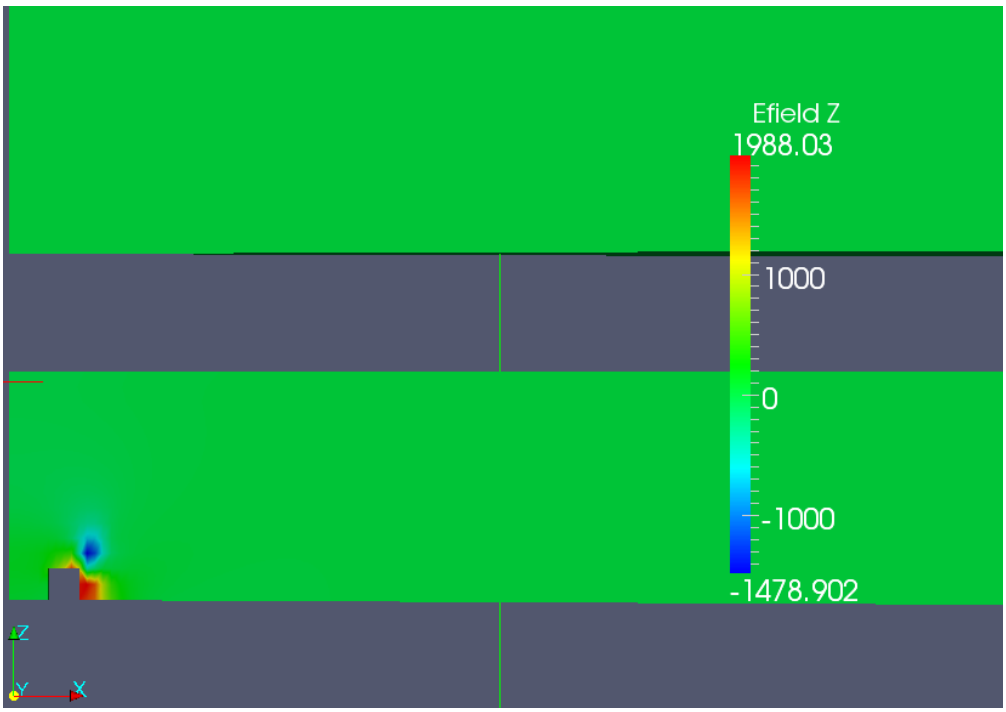

Figure 5.39: Axial electric field profile [V/m]

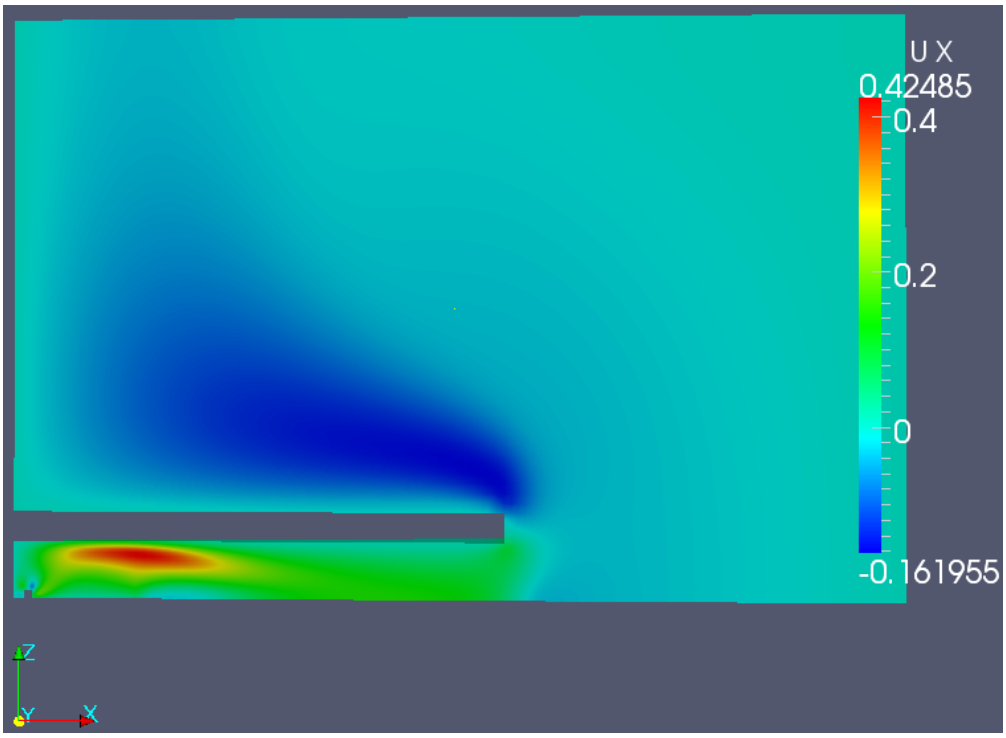

Figure 5.40: Radial velocity profile [m/s]

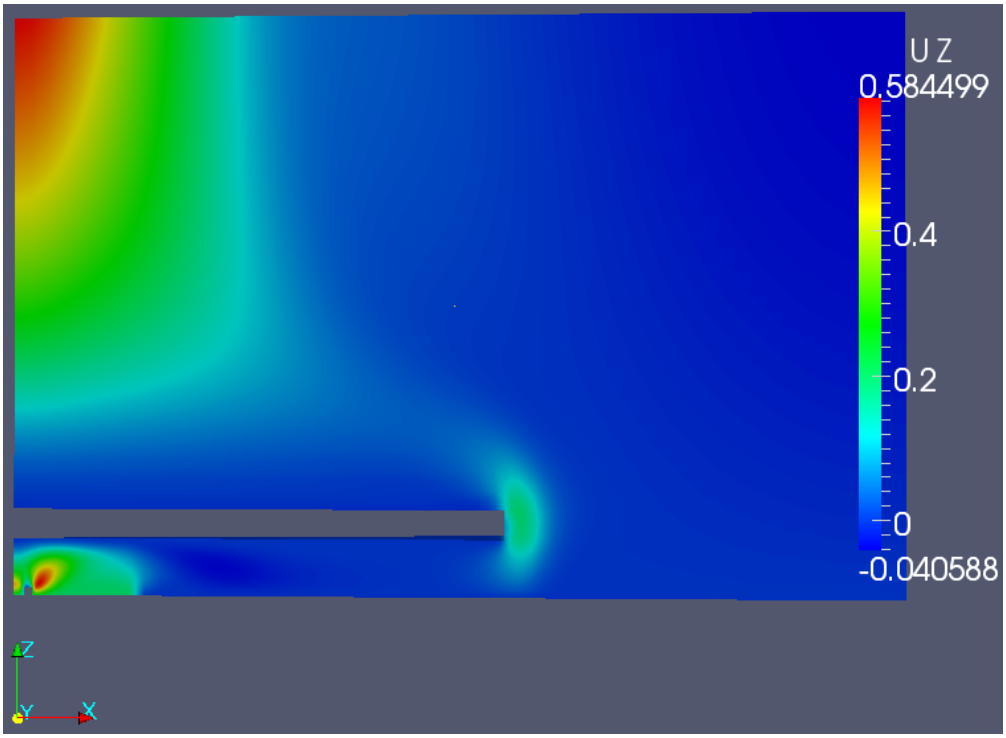

Figure 5.41: Axial velocity profile [m/s]

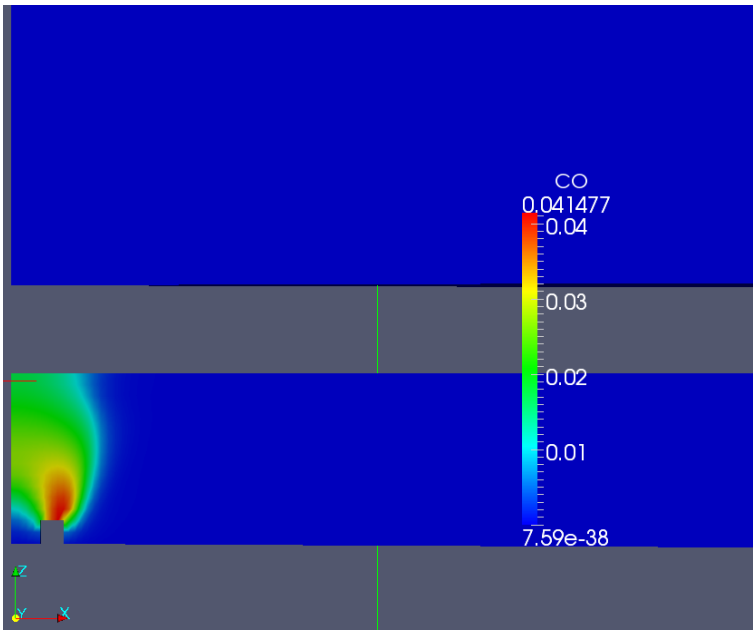

(a) CO profile

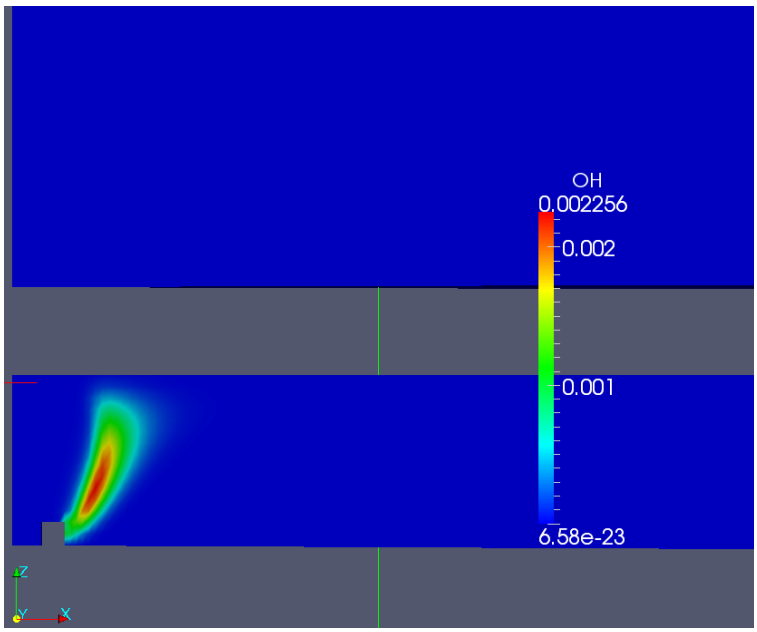

(b) OH profile

Figure 5.42: CO and OH mass fraction profiles

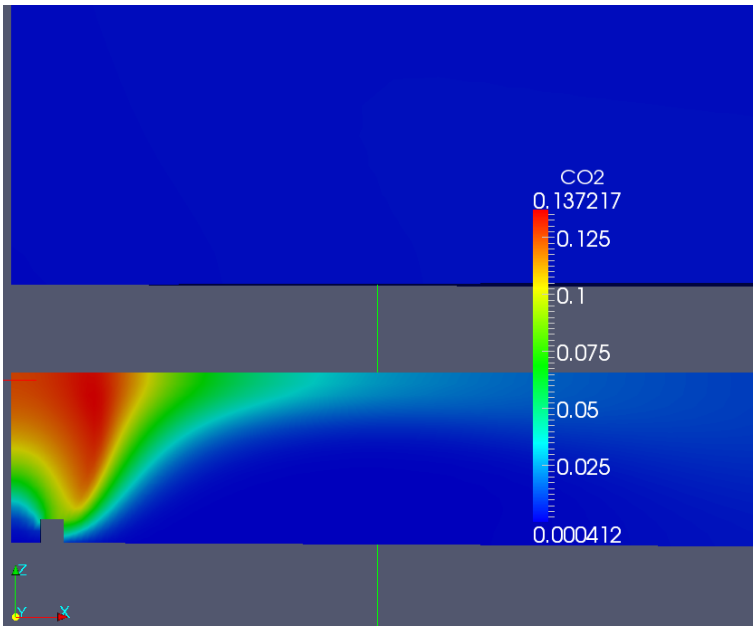

(a) CO_2 profile

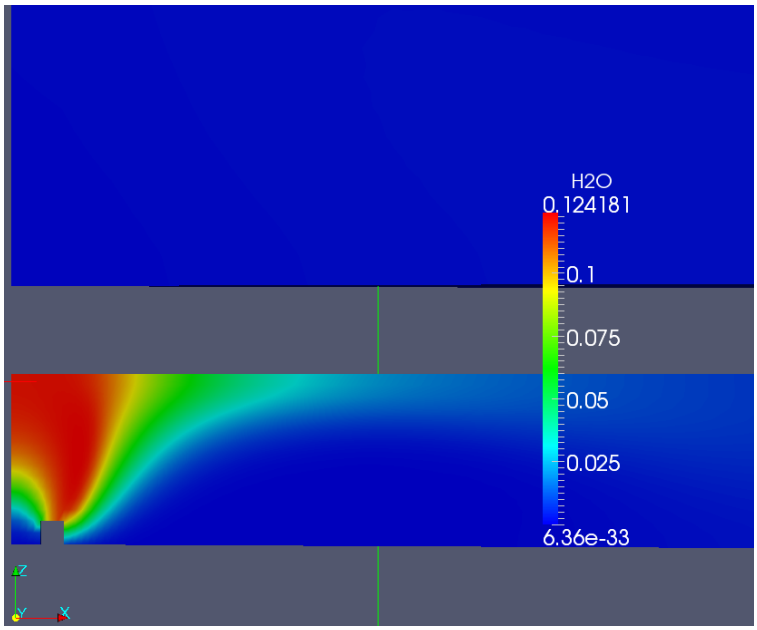

(b) H_2O profile

Figure 5.43: CO_2 and H_2O mass fraction profiles

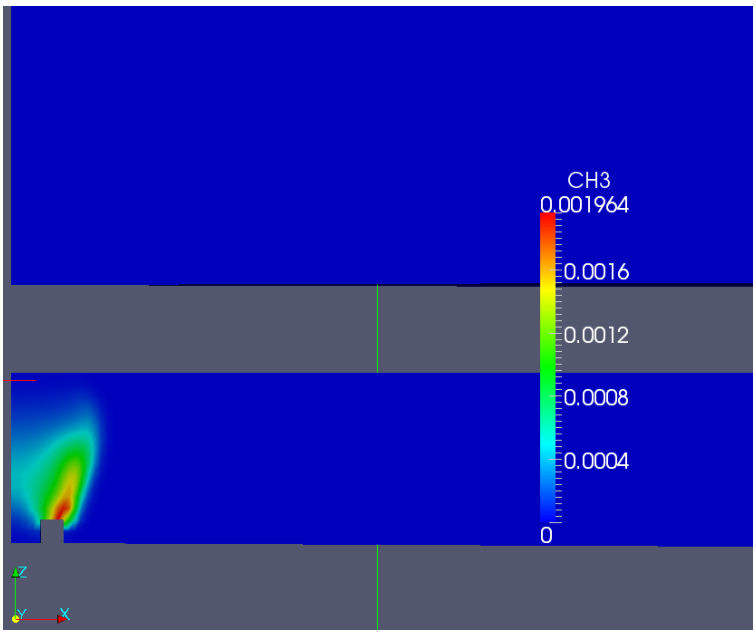

(a) CH_3 profile

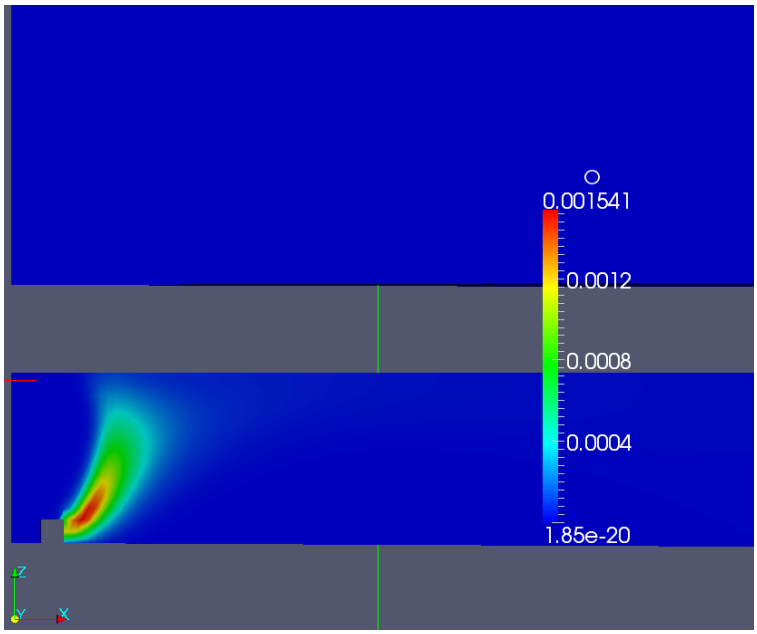

(b) O profile

Figure 5.44: CH_3 and O mass fraction profiles

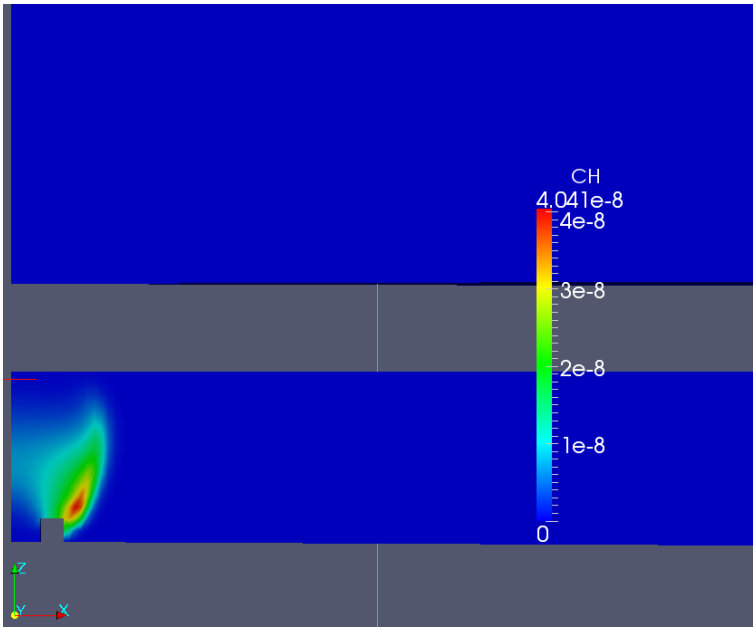

(a) CH profile

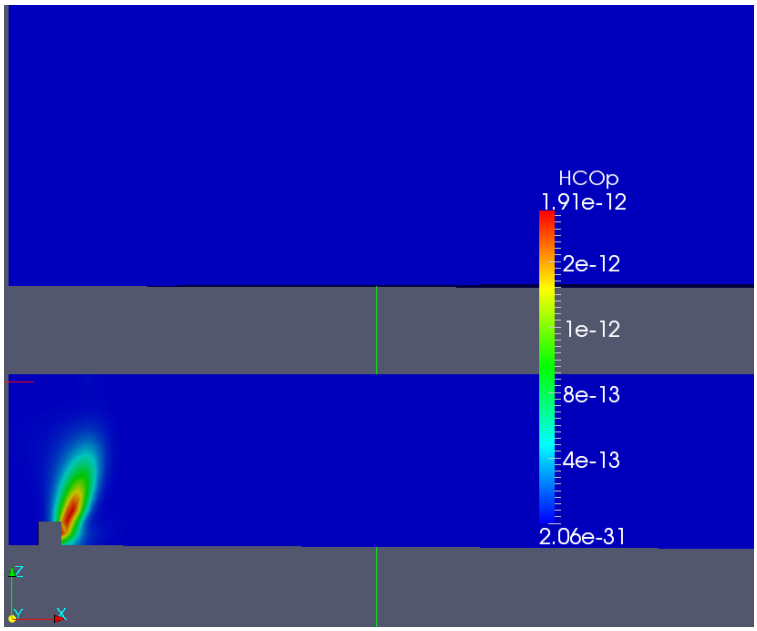

(b) HCO^+ profile

Figure 5.45: CH and HCO^+ mass fraction profiles

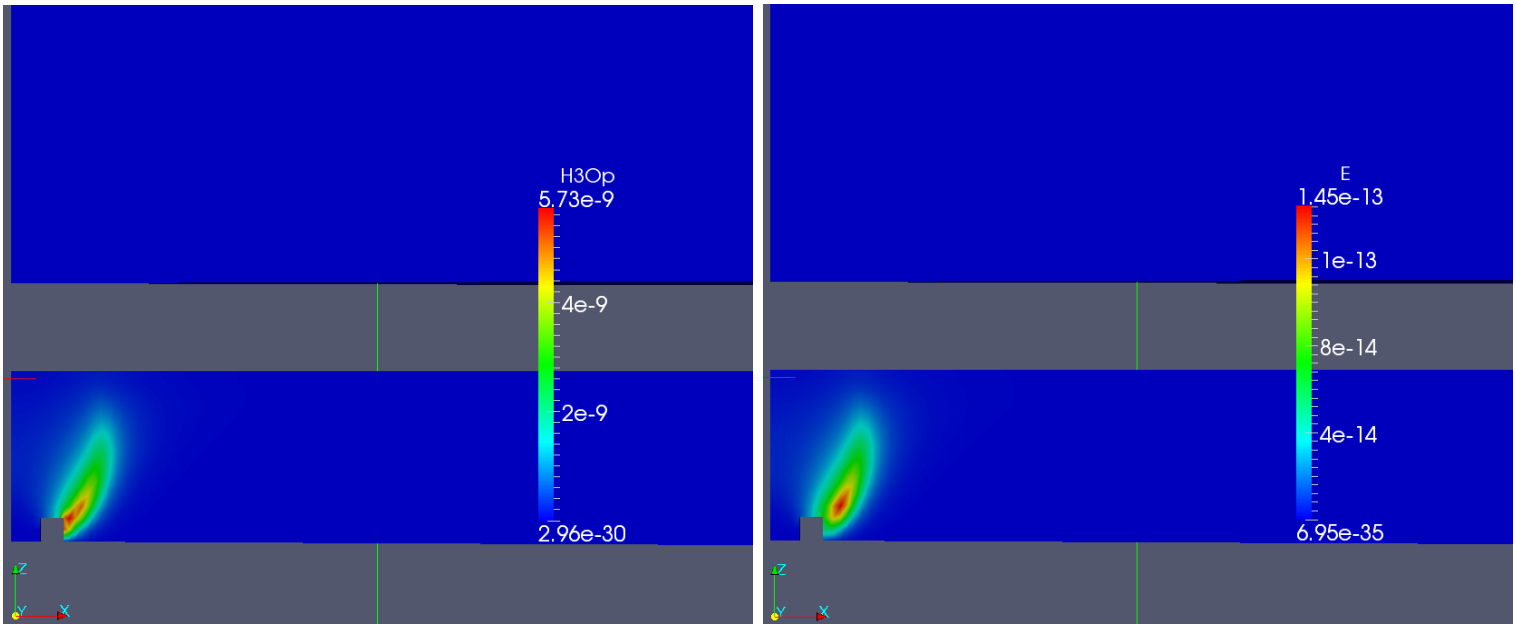

(a) H_3O^+ profile (b) e^- profile

Figure 5.46: H_3O^+ and e^- mass fraction profiles profiles

- the peak temperature increases of about 8% with respect to the previous simulation; this leads to a 5% overestimation of the experimental results
- the electric potential (and subsequently the electric field) is established only in the flame zone, because it is only here that charges are created
- the bulk velocity is slightly increased by the inclusion of the charged species in creating an electric field
- the mass fraction of CH_3 increases, and this reflects in an increase of the mass fraction of CH; this enhances the chemi-ionization process, subsequently the mass fraction of H_3O^+, HCO^+ and e^- increases too. This happens because now the solver takes into account the charge accumulation in the flame zone; this means that the weak self-induced electric field facilitates the charge generation in the flames zone. And the charges created here tend to move away from each other only because of self-repulsion, since no electric field has been applied on the plate.

The original goal of the simulation was to fully model ion formation and the effects of external electric fields on the flames from which the ions arose. Unfortunately, the combination of small concentrations of charged species and steep gradients of electric potential made the problem intractable for the desktop computer environment of OpenFOAM available. It is clear from this work that an accurate reduced mechanism for ion species (perhaps even a simpler modeling approach where ions are just sourced from the flame sheet but not kinetically modeled) will be necessary. This more comprehensive modeling effort will be taken up by future researchers. However, the impinging flame model was shown to have good comparison with experiments and so the final chapter describes the effect of plate height on the flame as a set of simulation information that can be related to experiments.

Chapter 6

Effects of the burner-to-plate distance

The results presented in the previous simulations have been obtained using a fixed burner-to-plate distance, which has been set to $5.8mm$; in this Chapter, the effects of the distance between plate and burner on the flame behavior will be analyzed.

It is known that the distance between burner and plate plays an important role in determining some flame properties such as heat release [18],[36],[37]; in laminar impinging coflow flames, convection is the main mechanism responsible for heat transfer. An other possible mechanism is the so called thermochemical heat release, which accounts for the radicals recombination in the boundary layer which develops close to the cold plate; this mechanism is quite important in oxygen-fuel flames, but for air-fuel flames its contribution is quite reduced (since the concentration of radicals is lower than in the case of pure oxygen) [38]. Basing on that, the effect of the burner-to-plate (H) distance on the heat release can be summarized in the following way:

- decreasing H: the presence of the plate close to the burner interferes with the generation of a stable flame: the strain rate increases, the flame front and the stagnation zone start interacting. This means that chemical equilibrium cannot be established

in the flame zone; in addition, species will be forced to move radially along the plate edge, enhancing the local heat transfer to the plate itself. All these phenomena will contribute to decrease the flame peak temperature, until the flame quenches

- increasing H: when the plate is far from the flame, the strain rate is low; subsequently, the mixture will reach equilibrium conditions outside the flame zone but before it reaches the stagnation zone. In addition, radicals generated in the flame zone will not spread far away, and so the heat released by recombination reactions will stay into the flame zone; and this will contribute to increase the peak temperature.

For this simulation, the reduced neutral mechanism based on $GRI-Mech1.2$ has been used, and no electric field has been implemented; the OpenFOAM built-in solver for reacting flows, *reactingFoam*, has been used (as for the third simulation of the previous Chapter, the only modification added to this solver was the model of a spark). The following Figures represent the steady state profile of temperature and mass fraction of some species for three different burner-to-plate distances: $H_1 = 5.8mm$, $H_2 = 10.8mm$, $H_3 = 15.8mm$; these results are in good agreement with those obtained from experimental results [20]. In particular, the comparison between the $10.8mm$ and $15.8mm$ distance show that by $10.8mm$ the influence of the plate on the flame is minimal, and the flame behaves similarly to a free jet flame. The comparison between $5.8mm$ and $10.8mm$ shows that the flame tip transitions from open to closed somewhere in this distance domain, which is consistent with the experimental findings. The effects of an increasing burner-to-plate distance can be summarize as follows:

a) the radial velocity U_x decreases and the axial velocity U_z increases: because the plate does not interfere with the axial velocity of the bulk, which subsequently does not have to move radially along the plate edges

b) the peak temperature increases: since species are not forced to move radially along the plate, they will tend to stay close to the flame region; subsequently, the heat released

by recombination reactions will not be spread out, but it will be confined in a narrower region close to the flame itself

c) the species profiles tend to "close" at the tip: again, the plate does not interfere with generation of species from chemical reactions, and subsequently the mass fractions profiles do not tend to open because species do not have to move radially along the plate. For simplicity, here only the mass fractions of CO and OH have been presented; those of the other species follow the same pattern. The reason why these two species have been chosen is that they are very useful during experimental measurements: because OH is usually the primary destruction partner of CO, while CO is a primary pollutant; so, they describe pretty well an important property of hydrocarbon flames.

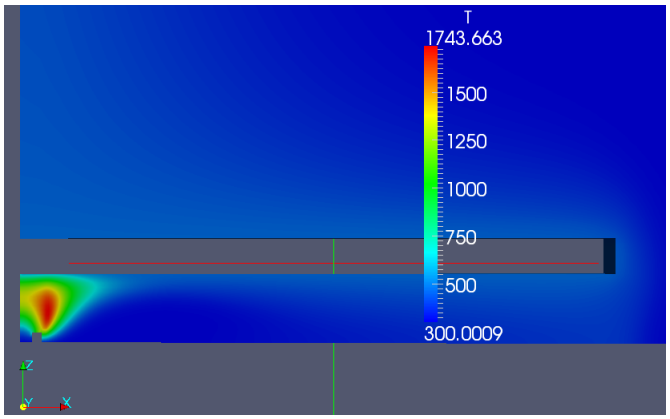

Figure 6.1: Zoom of the temperature profile [K] for $H_1 = 5.8mm$

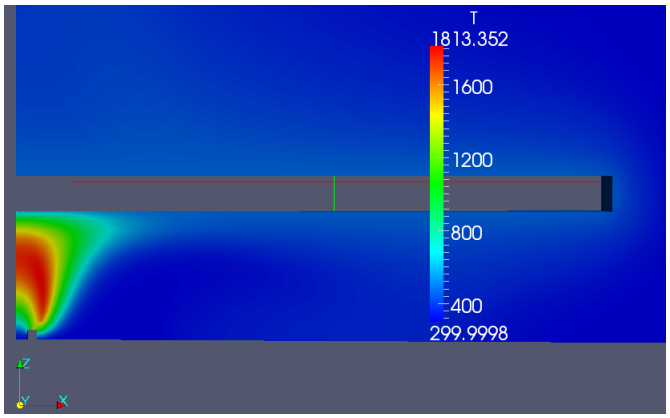

Figure 6.2: Zoom of the temperature profile [K] for $H_2 = 10.8mm$

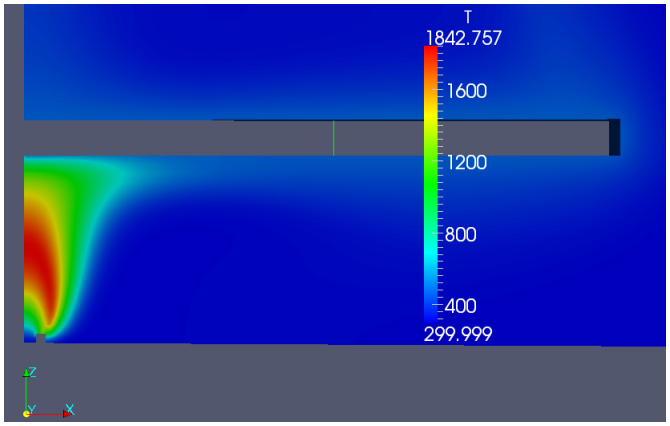

Figure 6.3: Zoom of the temperature profile [K] for $H_3 = 15.8mm$

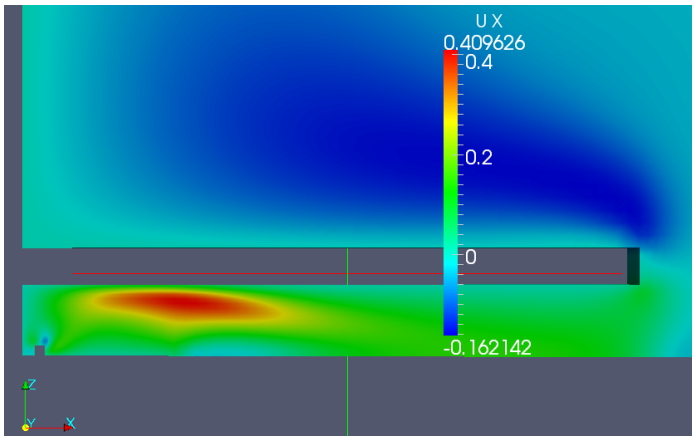

Figure 6.4: Zoom of the radial velocity profile [m/s] for $H_1 = 5.8mm$

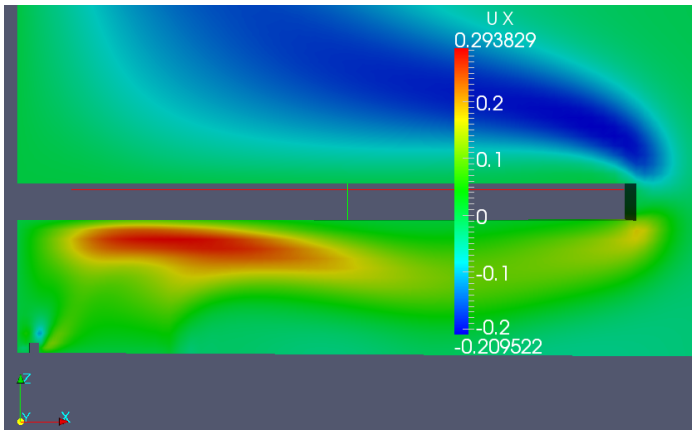

Figure 6.5: Zoom of the radial velocity profile [m/s] for $H_2 = 10.8mm$

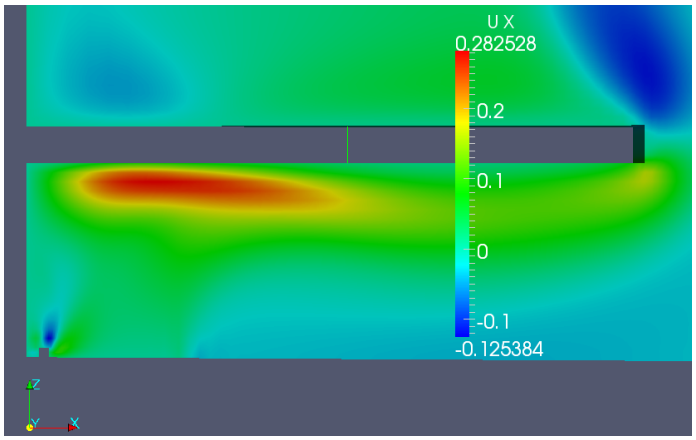

Figure 6.6: Zoom of the radial velocity profile [m/s] for $H_3 = 15.8mm$

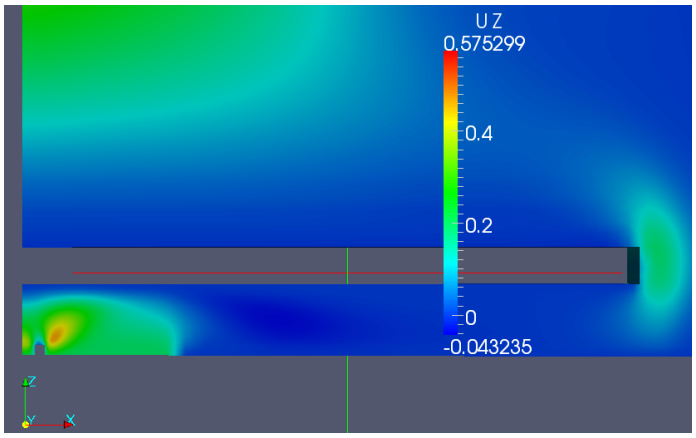

Figure 6.7: Zoom of the axial velocity profile [m/s] for $H_1 = 5.8mm$

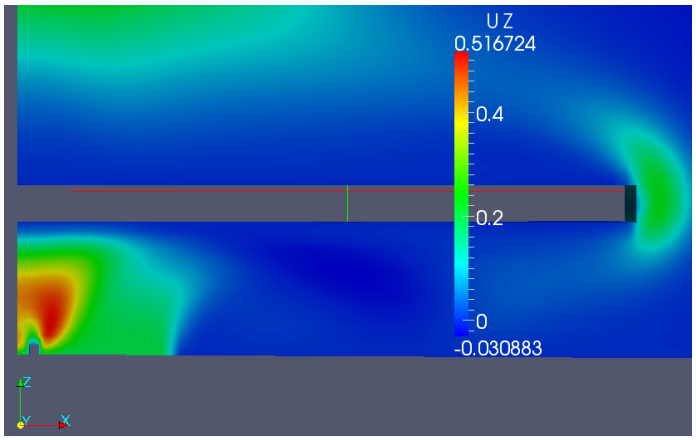

Figure 6.8: Zoom of the axial velocity profile [m/s] for $H_2 = 10.8mm$

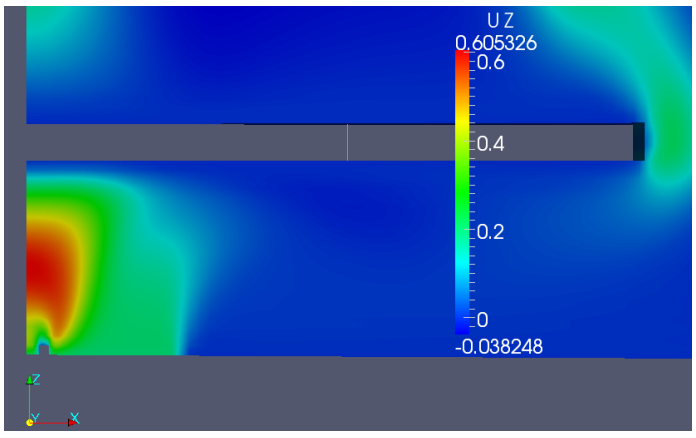

Figure 6.9: Zoom of the axial velocity profile [m/s] for $H_3 = 15.8mm$

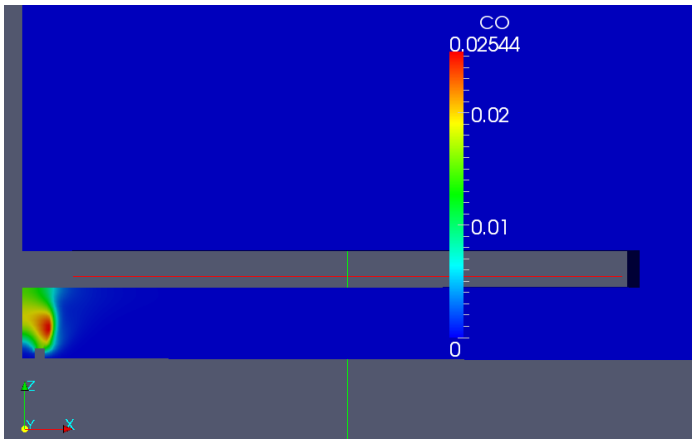

Figure 6.10: Zoom of the CO mass fraction profile for $H_1 = 5.8mm$

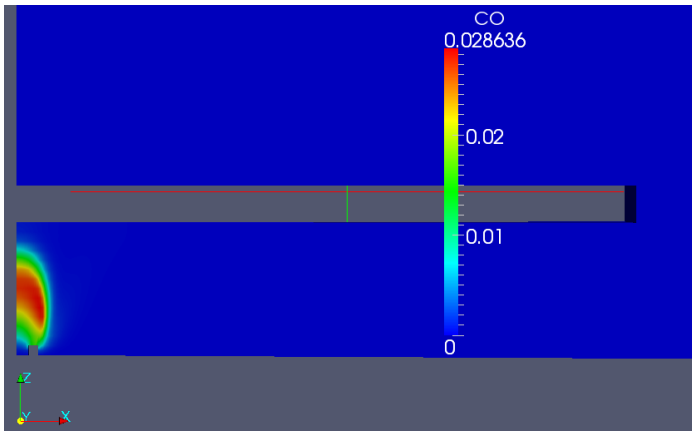

Figure 6.11: Zoom of the CO mass fraction profile for $H_2 = 10.8mm$

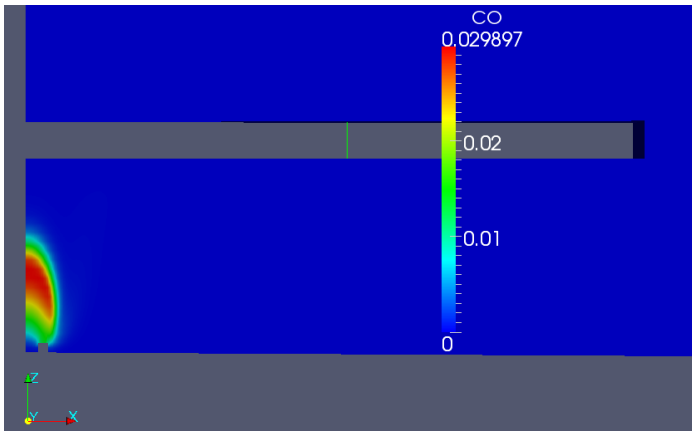

Figure 6.12: Zoom of the CO mass fraction profile for $H_3 = 15.8mm$

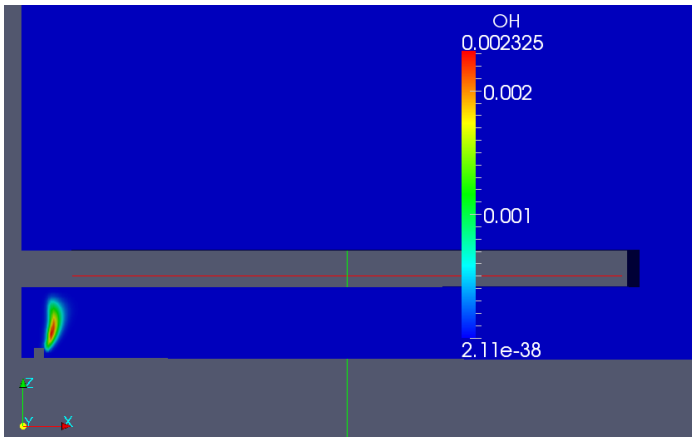

Figure 6.13: Zoom of the OH mass fraction profile for $H_1 = 5.8mm$

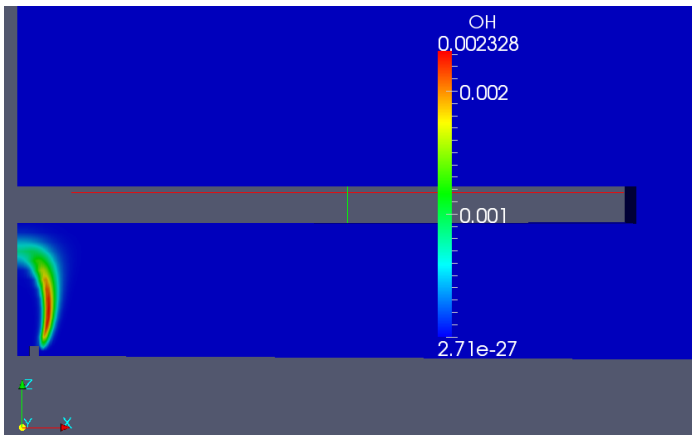

Figure 6.14: Zoom of the OH mass fraction profile for $H_2 = 10.8mm$

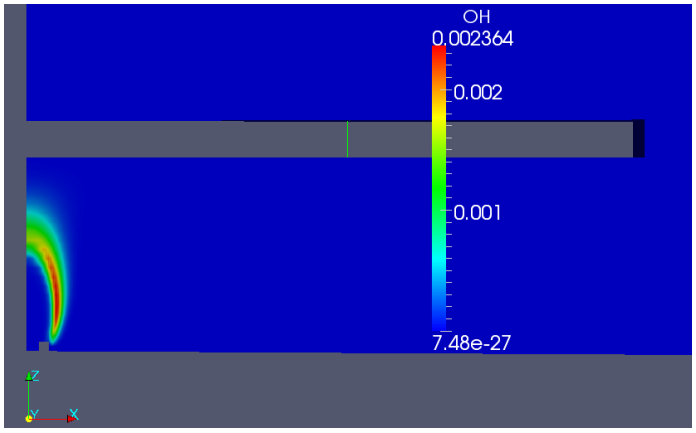

Figure 6.15: Zoom of the OH mass fraction profile for $H_3 = 15.8mm$

Chapter 7

Conclusions

The aim of this thesis was originally to investigate how electric fields affect the properties of hydrocarbon flames; in particular, the impinging coflow configuration has been considered (since this configuration is very useful to study the effects of electric fields on CO emissions, flame quenching and heat transfer to the plate itself). Substantial modeling progress towards this goal was made but the final complete simulation of electric fields acting on flames was not finalized. Nevertheless, the computations explored the various components of the simulation approach sufficiently to point the way to a complete model. At the same time, the simulations showed very good predictions of the behavior of impinging flames in general. The interaction between electric field and combustion occurs through the chemi-ionization process, which creates charged species (positive ions, negative ions and electrons) from neutral species. The contribution of the electric field has been modeled numerically by creating a new user-defined OpenFOAM solver capable to solve for fluid dynamics, chemistry and electric field; the numerical contributions of the electric field include the implementation of the Poisson Equation, of an additional body force related to the electric potential in the momentum Equation and of an additional term related by the ion drift velocity in the species Equation. Simulations obtained with OpenFOAM for laminar diffusion coflow flames (CH_4 and air) in

the impinging configuration with the plate kept at a fixed distance ($H = 5.8mm$) from the fuel and oxidizer inlets lead to the following results:

- if the reaction mechanism does not include charged species (i.e., if chemi-ionization is not modeled), the Poisson Equation is decoupled from the rest of the conservation Equations since the is not a source term; the additional terms in both species and momentum Equations are null, so the electric field does not affect the flame behavior. Simulations show an electric potential that is constant in time, as expected
- if the reaction mechanism includes charged species and the Poisson Equation is not implemented, charge generation occurs through the chemi-ionization process but there is no charge accumulation in the flame zone
- if the reaction mechanism includes charged species and the Poisson Equation is implemented, even if a zero potential is applied at both the burner exit and at the plate, charges accumulation occurs in the flame zone; the self-induced electric field affects the flame temperature, bulk velocity and species profile. In particular: the peak temperature increases (even if less than 8% with respect to the case in which electric field in not implemented in the solver), the bulk velocity is slightly affected by the contribution of the ion drift velocity, and the mass fractions of charged species increase.

The numerical results are in good agreement with those obtained from experiments [20]; in particular, the peak temperatures have an estimation error under the 10%, and the temperature profiles are very similar to those obtained with the Schlieren technique. In addition, the mass fraction of important species like CO and OH match either qualitatively and quantitatively; and the mass fractions of charged species also match either with those expected from literature and with those obtained from other numerical simulations [35].

Simulations have been performed also for the case of neutral chemistry (with no electric field implemented) with an increasing burner-to-plate distance; these results show that as the

plate moves far from the burner, it does not interfere with the reaction zone nor with the bulk velocity. Subsequently, an increase in the peak temperature and the "closure" of the tip profile of both temperature and species mass fractions has been observed; again, these results are in good agreement with experimental observations and measurements [20].

Chapter 8

Future work

It is known from literature that electric fields affect many properties of hydrocarbon flames; subsequently, they can be used to control and enhance some aspects of the combustion process, such as flame stabilization and reduction of pollutant emissions. In order to do that, it is important not only to perform experimental measures, but also to implement accurate numerical simulations; to obtain more detailed results with OpenFOAM, future wok will be focused on the following aspects:

1. introduce a non zero potential on the plate surface when a reaction mechanism including charges species is considered; this is a tough task, since chemistry is the stiff component of the problem. This means that the solver is strongly subjected to numerical instabilities induced by the interaction between chemi-ionization process and charges accumulation during the transient; in addition, a very fine mesh and boundary conditions that take into account charge recombination on the cold walls of the plate must be implemented

2. use reaction mechanisms which include excited species such as CH^* and OH^*, in order to compare the experimental results obtained from chemiluminescence

3. identification of the gradient of OH, since it is the marker of the flame location

4. use a more complicated reaction mechanism, which includes also negative ions.

Bibliography

[1] Y. Zhang and K. N. C. Bray. Characterization of impinging jet flames. *Combustion and Flame 116*, pages 671–674, 1999.

[2] G. Wortberg. Ion-concentration measurements in flat flame at atmospheric pressure. *Proceedings of the Combustion Institute 10*, pages 651–655, 1965.

[3] R .C. Brown and A. N. Eralsan. Simulation of ionic structure in lean and close-to-stoichiometric acetylene flames. *Combustion and Flame 73*, pages 1–21, 1988.

[4] M. Belhi, P. Domingo, and P. Vervisch. Direct numerical simulation of the effect of an electric field on flame stability. *Combustion and Flame 157*, pages 2286–2297, 2010.

[5] K. Yamashita, S. Karnan, and D. Dunn-Rankin. Numerical prediction of ion current from small methane jet flame. *Combustion and Flame 156*, pages 1227–1233, 2009.

[6] J. M. Goodings, D. K. Bohme, and C.-W. Ng. Detailed ion chemistry in methane-oxyden flames. *Combustion and Flame 36*, pages 45–62, 1979.

[7] J. Prager, U. Riedel, and J. Warnatz. Modeling ion chemistry and charged species diffusion in lean methane-oxygen flames. *Proceeding of the Combustion Institute 31*, pages 1129–1137, 2007.

[8] K. G. Payne and F. J. Wienberg. A preliminary investigation of field-induced ion movement in flame gases and is applications. *Proceedings of the Royal Society A 250*, pages 316–336, 1959.

[9] A. B. Fialkov. Investigations on ions in flames. *Progress in Energy and Combustion Science 23*, pages 399–528, 1997.

[10] E. M. Grenault and R. V. Wheeler. The propagation of flame in electric fields. *Journal of the Chemical Royal Society*, pages 195–199, 1931.

[11] F. J. Wienberg and F. B. Carleton. Electric field-induced flame convection in absence of gravity. *Nature 330*, pages 635–636, 1987.

[12] H. Tsuji and I. Yamaoka. Structure analysis of counterflow diffusion flames in the forward stagnation region of a porous cylinder. *Proceedings of the Combustion Institute 13*, pages 723–731, 1971.

[13] Creck Modeling Group. http://www.opensmoke.polimi.it/, 2013. laminarSMOKE: numerical modeling of laminar reacting flows.

[14] Gas Research Institute. http://combustion.berkeley.edu/drm/drm19.dat, 1994. $Gri - Mech^{TM}$.

[15] J. Hu, B. Rivin, and E. Sher. The effect of an electric field on the shape of co-flowign and candle-type methane-air flames. *Experimental Thermal and Fluid Science 21*, pages 124–133, 2000.

[16] M.J. Remie, G. Sarner, M.F.G. Cremers, A. Omrane, K.R.A.M. Schreel, M. Alden, and L.P.H. de Goey. Extended heat-transfer relation for an impinging laminar jet to a flat plate. *International Journal of Heat and Mass Transfer 51*, pages 1854–1865, 2008.

[17] J. M. Bee'r and N. A. Chigier. Impinging jet flames. *Combustion and Flame 12*, pages 575–586, 1968.

[18] R. Viskanta. Heat transfer to impinging isothermal gas and flame jets. *Experimental Thermal and Fluid Science 6*, pages 111–134, 1993.

[19] T. H. Vandermeer. *Heat transfer from impinging flame jets*. Ph.D. Thesis, Technische Universiteit Delft, 1987.

[20] Yu-Chien Chien. *Electrical aspects of impinging flames*. Ph.D. Thesis, University of California Irvine, 2014.

[21] OpenCFD Ltd (ESI Group). http://foam.sourceforge.net/docs/guides-a4/userguide.pdf, 2015. OpenFOAM User Guide.

[22] H. C. Jaggers, R. J. Bowser, and F. J. Wienberg. The effect of electric fields on burning velocity. *Combustion and Flame 19*, pages 135–136, 1972.

[23] R. Byron Bird, W. E. Stewart, and E. N. Lightoff. *Transport phenomena - Revised Second Edition*. Wiley, 2007.

[24] S. R. Turns. *An introduction to combustion: concepts and applications - Third Edition*. Mc Graw Hill, 2012.

[25] A. Cuoci, A. Frassoldati, T. Favarelli, and E. Renzi. A computational tool for the detailed kinetic modeling of laminar flames: Application to C_2H_2/CH_4 coflow flames. *Combustion and Flame 160*, pages 870–886, 2013.

[26] OpenCFD Ltd (ESI Group). https://github.com/openfoam/openfoam-2.3.x/tree/master/applications/solvers/combustion/reactingfoam, 2016.

[27] H. F. Calcote. Ion and electron profiles in flames. *Symposium (International) on Combustion 9*, pages 662–637, 1963.

[28] H. F. Calcote. Mechanism for the formation of ions in flames. *Combustion and Flame 1*, pages 385–403, 1957.

[29] T. Pedersen and R. C. Brown. Simulation of electric field effects in premixed methane flames. *Combustion and Flame 94*, pages 433–448, 1993.

[30] J. A. Green and T. M. Sudgen. Some observations on the mechanism of ionization in flames. *Symposium (International) on Combustion 9*, pages 607–624, 1963.

[31] Gas Research Institute. http://combustion.berkeley.edu/gri-mech/version30/text30.html, 1999. $Gri - Mech^{TM}$.

[32] J. Prager, U. RIedel, and J. Warnatz. Modeling ion chemistry and charged species diffusion in lean methane-oxygen flames. *Proceedings of the Combustion Institute 31*, pages 1129–1137, 2007.

[33] R. Consul, C. D. Perez-Segarra, K. Claramunt, J. Cadafalch, and A. Oliva. Detailed numerical simulation of laminar flames by a parallel multiblock algorithm using loosely coupled computers. *Combustion Theory and Modeling 7*, pages 525–544, 2003.

[34] OpenFOAM developers. https://github.com/openfoam/openfoam-2.3.x/tree/master/applications/solvers/combustion/reactingfoam, 2016. GitHub, Inc.

[35] Sunny Karnani. *Electric fiel-driven flame dynamics*. Ph.D. Thesis, University of California Irvine, 2011.

[36] S. Chander and A. Ray. Influence of burner geometry on heat transfer characteristics of methane/air flame impinging on flat surfaces. *Energy Conversion anda Management 26*, pages 2803–2837, 2005.

[37] M.J.Remie, G. Sarner, M.F.G. Cremers, A. Omrane, K.R.A.M Schreel, M. Alden, and L.P.H. de Goey. Extended heat-transfer relation for an impinging laminar flame jet to a flat plate. *International Journal of Heat and Mass Transfer 51*, pages 1854–1865, 2008.

[38] M.F.G. Cremers, M.J.Remie, K.R.A.M Schreel, and L.P.H. de Goey. Thermochemical heat release of laminar stagnation flames of fuel and oxygen. *International Journal of Heat and Mass Transfer 53*, pages 952–961, 2010.

Appendix A

Reaction mechanisms

A.1 Detail chemical kinetics including ions

Table A.1: Detailed mechanism with charged species

Reaction	A	n_T	E_a	ϵ
!CH4+2O2→ CO2+2H2O	5.20E+17	0	14906	
2O+M↔ O2+M	1.20E+17	-1	0	H2/2.40/H2O/15.40/CH4/2.00
				CO/1.75/CO2/3.60/C2H6/3.00/AR/.83/
O+H+M↔ OH+M	5.00E+17	-1	0	H2/2.00/H2O/6.00/CH4/2.00
				CO/1.50/CO2/2.00/C2H6/3.00/AR/.70/
O+H2↔ H+OH	3.87E+04	2.7	6260	
O+HO2↔ OH+O2	2.00E+13	0	0	
O+H2O2↔ OH+HO2	9.63E+06	2	4000	
O+CH↔ H+CO	5.70E+13	0	0	
O+CH2↔ H+HCO	8.00E+13	0	0	
O+CH2s↔ H2+CO	1.50E+13	0	0	
O+CH2s↔ H+HCO	1.50E+13	0	0	
O+CH3↔ H+CH2O	5.06E+13	0	0	
O+CH4↔ OH+CH3	1.02E+09	1.5	8600	
O+CO(+M)↔ CO2(+M)	1.80E+10	0	2385	H2/2.00/O2/6.00/H2O/6.00
				CH4/2.00/CO/1.50/CO2/3.50/AR/.50/

Table A.1: Continues in the following page

Table A.1: Continues from the previous page

Reaction	A	n_T	E_a	ϵ
LOW	6.02E+14	0	3000	
O+HCO↔ OH+CO	3.00E+13	0	0	
O+HCO↔ H+CO2	3.00E+13	0	0	
O+CH2O↔ OH+HCO	3.90E+13	0	3540	
O+CH2OH↔ OH+CH2O	1.00E+13	0	0	
O+CH3O↔ OH+CH2O	1.00E+13	0	0	
O+CH3OH↔ OH+CH2OH	3.88E+05	2.5	3100	
O+CH3OH↔ OH+CH3O	1.30E+05	2.5	5000	
O+C2H↔ CH+CO	5.00E+13	0	0	
O+C2H2↔ H+HCCO	1.35E+07	2	1900	
O+C2H2↔ OH+C2H	4.60E+19	-1.41	28950	
O+C2H2↔ CO+CH2	6.94E+06	2	1900	
O+C2H3↔ H+CH2CO	3.00E+13	0	0	
O+C2H4↔ CH3+HCO	1.25E+07	1.83	220	
O+C2H5↔ CH3+CH2O	2.24E+13	0	0	
O+C2H6↔ OH+C2H5	8.98E+07	1.92	5690	
O+HCCO↔ H+2CO	1.00E+14	0	0	
O+CH2CO↔ OH+HCCO	1.00E+13	0	8000	
O+CH2CO↔ CH2+CO2	1.75E+12	0	1350	
O2+CO↔ O+CO2	2.50E+12	0	47800	
O2+CH2O↔ HO2+HCO	1.00E+14	0	40000	
H+O2+M↔ HO2+M	2.80E+18	-0.86	0	O2/.00/H2O/.00/CO/.75
				CO2/1.50/C2H6/1.50/N2/.00/AR/.00/
H+2O2↔ HO2+O2	2.08E+19	-1.24	0	
H+O2+H2O↔ HO2+H2O	1.13E+19	-0.76	0	
H+O2+N2↔ HO2+N2	2.60E+19	-1.24	0	
H+O2+AR↔ HO2+AR	7.00E+17	-0.8	0	
H+O2↔ O+OH	2.65E+16	-0.6707	17041	
2H+M↔ H2+M	1.00E+18	-1	0	H2/.00/H2O/.00/CH4/2.00
				CO2/.00/C2H6/3.00/AR/.63/
2H+H2↔ 2H2	9.00E+16	-0.6	0	
2H+H2O↔ H2+H2O	6.00E+19	-1.25	0	
2H+CO2↔ H2+CO2	5.50E+20	-2	0	
H+OH+M↔ H2O+M	2.20E+22	-2	0	H2/.73/H2O/3.65/CH4/2.00
				C2H6/3.00/AR/.38/
H+HO2↔ O+H2O	3.97E+12	0	671	
H+HO2↔ O2+H2	4.48E+13	0	1068	

Table A.1: Continues in the following page

Table A.1: Continues from the previous page

Reaction	A	n_T	E_a	ϵ
H+HO2↔ 2OH	8.40E+13	0	635	
H+H2O2↔ HO2+H2	1.21E+07	2	5200	
H+H2O2↔ OH+H2O	1.00E+13	0	3600	
H+CH↔ C+H2	1.65E+14	0	0	
H+CH2(+M)↔ CH3(+M)	6.00E+14	0	0	H2/2.00/H2O/6.00/CH4/2.00
				CO/1.50/CO2/2.00/C2H6/3.00/AR/.70/
LOW	1.04E+26	-2.76	1600	
TROE	0.562	91	5836	8552
H+CH2s↔ CH+H2	3.00E+13	0	0	
H+CH3(+M)↔ CH4(+M)	1.39E+16	-0.534	536	H2/2.00/H2O/6.00/CH4/3.00
				CO/1.50/CO2/2.00/C2H6/3.00/AR/.70/
LOW	2.62E+33	-4.76	2440	
TROE	0.783	74	2941	6964
H+CH4↔ CH3+H2	6.60E+08	1.62	10840	
H+HCO(+M)↔ CH2O(+M)	1.09E+12	0.48	-260	H2/2.00/H2O/6.00/CH4/2.00
				CO/1.50/CO2/2.00/C2H6/3.00/AR/.70/
LOW	2.47E+24	-2.57	425	
TROE	0.7824	271	2755	6570
H+HCO↔ H2+CO	7.34E+13	0	0	
H+CH2O(+M)↔ CH2OH(+M)	5.40E+11	0.454	3600	H2/2.00/H2O/6.00/CH4/2.00
				CO/1.50/CO2/2.00/C2H6/3.00/
LOW	1.27E+32	-4.82	6530	
TROE	0.7187	103	1291	4160
H+CH2O(+M)↔ CH3O(+M)	5.40E+11	0.454	2600	H2/2.00/H2O/6.00/CH4/2.00
				CO/1.50/CO2/2.00/C2H6/3.00/
LOW	2.20E+30	-4.8	5560	
TROE	0.758	94	1555	4200
H+CH2O↔ HCO+H2	5.74E+07	1.9	2742	
H+CH2OH(+M)↔ CH3OH(+M)	1.06E+12	0.5	86	H2/2.00/H2O/6.00/CH4/2.00
				CO/1.50/CO2/2.00/C2H6/3.00/
LOW	4.36E+31	-4.65	5080	
TROE	0.6	100	90000	10000
H+CH2OH↔ H2+CH2O	2.00E+13	0	0	
H+CH2OH↔ OH+CH3	1.65E+11	0.65	-284	
H+CH2OH↔ CH2s+H2O	3.28E+13	-0.09	610	
H+CH3O(+M)↔ CH3OH(+M)	2.43E+12	0.515	50	H2/2.00/H2O/6.00/CH4/2.00
				CO/1.50/CO2/2.00/C2H6/3.00/

Table A.1: Continues in the following page

Table A.1: Continues from the previous page

Reaction	A	n_T	E_a	ϵ
LOW	4.66E+41	-7.44	14080	
TROE	0.7	100	90000	10000
H+CH3O↔ H+CH2OH	4.15E+07	1.63	1924	
H+CH3O↔ H2+CH2O	2.00E+13	0	0	
H+CH3O↔ OH+CH3	1.50E+12	0.5	-110	
H+CH3O↔ CH2s+H2O	2.62E+14	-0.23	1070	
H+CH3OH↔ CH2OH+H2	1.70E+07	2.1	4870	
H+CH3OH↔ CH3O+H2	4.20E+06	2.1	4870	
H+C2H(+M)↔ C2H2(+M)	1.00E+17	-1	0	H2/2.00/H2O/6.00/CH4/2.00
				CO/1.50/CO2/2.00/C2H6/3.00/
LOW	3.75E+33	-4.8	1900	
TROE	0.6464	132	1315	5566
H+C2H2(+M)↔ C2H3(+M)	5.60E+12	0	2400	H2/2.00/H2O/6.00/CH4/2.00
				CO/1.50/CO2/2.00/C2H6/3.00/
LOW	3.80E+40	-7.27	7220	
TROE	0.7507	98.5	1302	4167
H+C2H3(+M)↔ C2H4(+M)	6.08E+12	0.27	280	H2/2.00/H2O/6.00/CH4/2.00
				CO/1.50/CO2/2.00/C2H6/3.00/
LOW	1.40E+30	-3.86	3320	
TROE	0.782	207.5	2663	6095
H+C2H3↔ H2+C2H2	3.00E+13	0	0	
H+C2H4(+M)↔ C2H5(+M)	5.40E+11	0.454	1820	H2/2.00/H2O/6.00/CH4/2.00
				CO/1.50/CO2/2.00/C2H6/3.00/
LOW	6.00E+41	-7.62	6970	
TROE	0.9753	210	984	4374
H+C2H4↔ C2H3+H2	1.33E+06	2.53	12240	
H+C2H5(+M)↔ C2H6(+M)	5.21E+17	-0.99	1580	H2/2.00/H2O/6.00/CH4/2.00
				CO/1.50/CO2/2.00/C2H6/3.00/AR/.70/
LOW	1.99E+41	-7.08	6685	
TROE	0.8422	125	2219	6882
H+C2H5↔ H2+C2H4	2.00E+12	0	0	
H+C2H6↔ C2H5+H2	1.15E+08	1.9	7530	
H+HCCO↔ CH2s+CO	1.00E+14	0	0	
H+CH2CO↔ HCCO+H2	5.00E+13	0	8000	
H+CH2CO↔ CH3+CO	1.13E+13	0	3428	
H+HCCOH↔ H+CH2CO	1.00E+13	0	0	
H2+CO(+M)↔ CH2O(+M)	4.30E+07	1.5	79600	H2/2.00/H2O/6.00/CH4/2.00

Table A.1: Continues in the following page

Table A.1: Continues from the previous page

Reaction	A	n_T	E_a	ϵ
				CO/1.50/CO2/2.00/C2H6/3.00/AR/.70/
LOW	5.07E+27	-3.42	84350	
TROE	0.932	197	1540	10300
OH+H2↔ H+H2O	2.16E+08	1.51	3430	
2OH(+M)↔ H2O2(+M)	7.40E+13	-0.37	0	H2/2.00/H2O/6.00/CH4/2.00
				CO/1.50/CO2/2.00/C2H6/3.00/AR/.70/
LOW	2.30E+18	-0.9	-1700	
TROE	0.7346	94	1756	5182
2OH↔ O+H2O	3.57E+04	2.4	-2110	
OH+HO2↔ O2+H2O	1.45E+13	0	-500	
	DUPLICATE			
OH+H2O2↔ HO2+H2O	2.00E+12	0	427	
	DUPLICATE			
OH+H2O2↔ HO2+H2O	1.70E+18	0	29410	
	DUPLICATE			
OH+C↔ H+CO	5.00E+13	0	0	
OH+CH↔ H+HCO	3.00E+13	0	0	
OH+CH2↔ H+CH2O	2.00E+13	0	0	
OH+CH2↔ CH+H2O	1.13E+07	2	3000	
OH+CH2s↔ H+CH2O	3.00E+13	0	0	
OH+CH3(+M)↔ CH3OH(+M)	2.79E+18	-1.43	1330	H2/2.00/H2O/6.00/CH4/2.00
				CO/1.50/CO2/2.00/C2H6/3.00/
LOW	4.00E+36	-5.92	3140	
TROE	0.412	195	5900	6394
OH+CH3↔ CH2+H2O	5.60E+07	1.6	5420	
OH+CH3↔ CH2s+H2O	6.44E+17	-1.34	1417	
OH+CH4↔ CH3+H2O	1.00E+08	1.6	3120	
OH+CO↔ H+CO2	4.76E+07	1.228	70	
OH+HCO↔ H2O+CO	5.00E+13	0	0	
OH+CH2O↔ HCO+H2O	3.43E+09	1.18	-447	
OH+CH2OH↔ H2O+CH2O	5.00E+12	0	0	
OH+CH3O↔ H2O+CH2O	5.00E+12	0	0	
OH+CH3OH↔ CH2OH+H2O	1.44E+06	2	-840	
OH+CH3OH↔ CH3O+H2O	6.30E+06	2	1500	
OH+C2H↔ H+HCCO	2.00E+13	0	0	
OH+C2H2↔ H+CH2CO	2.18E-04	4.5	-1000	
OH+C2H2↔ H+HCCOH	5.04E+05	2.3	13500	

Table A.1: Continues in the following page

Table A.1: Continues from the previous page

Reaction	A	n_T	E_a	ϵ
OH+C2H2↔ C2H+H2O	3.37E+07	2	14000	
OH+C2H2↔ CH3+CO	4.83E-04	4	-2000	
OH+C2H3↔ H2O+C2H2	5.00E+12	0	0	
OH+C2H4↔ C2H3+H2O	3.60E+06	2	2500	
OH+C2H6↔ C2H5+H2O	3.54E+06	2.12	870	
OH+CH2CO↔ HCCO+H2O	7.50E+12	0	2000	
2HO2↔ O2+H2O2	1.30E+11	0	-1630	
	DUPLICATE			
2HO2↔ O2+H2O2	4.20E+14	0	12000	
	DUPLICATE			
HO2+CH2↔ OH+CH2O	2.00E+13	0	0	
HO2+CH3↔ O2+CH4	1.00E+12	0	0	
HO2+CH3↔ OH+CH3O	3.78E+13	0	0	
HO2+CO↔ OH+CO2	1.50E+14	0	23600	
HO2+CH2O↔ HCO+H2O2	5.60E+06	2	12000	
C+O2↔ O+CO	5.80E+13	0	576	
C+CH2↔ H+C2H	5.00E+13	0	0	
C+CH3↔ H+C2H2	5.00E+13	0	0	
CH+O2↔ O+HCO	6.71E+13	0	0	
CH+H2↔ H+CH2	1.08E+14	0	3110	
CH+H2O↔ H+CH2O	5.71E+12	0	-755	
CH+CH2↔ H+C2H2	4.00E+13	0	0	
CH+CH3↔ H+C2H3	3.00E+13	0	0	
CH+CH4↔ H+C2H4	6.00E+13	0	0	
CH+CO(+M)↔ HCCO(+M)	5.00E+13	0	0	H2/2.00/H2O/6.00/CH4/2.00
				CO/1.50/CO2/2.00/C2H6/3.00/AR/.70/
LOW	2.69E+28	-3.74	1936	
TROE	0.5757	237	1652	5069
CH+CO2↔ HCO+CO	1.90E+14	0	15792	
CH+CH2O↔ H+CH2CO	9.46E+13	0	-515	
CH+HCCO↔ CO+C2H2	5.00E+13	0	0	
CH2+O2→ OH+H+CO	5.00E+12	0	1500	
CH2+H2↔ H+CH3	5.00E+05	2	7230	
2CH2↔ H2+C2H2	1.60E+15	0	11944	
CH2+CH3↔ H+C2H4	4.00E+13	0	0	
CH2+CH4↔ 2CH3	2.46E+06	2	8270	
CH2+CO(+M)↔ CH2CO(+M)	8.10E+11	0.5	4510	H2/2.00/H2O/6.00/CH4/2.00

Table A.1: Continues in the following page

Table A.1: Continues from the previous page

Reaction	A	n_T	E_a	ϵ
				CO/1.50/CO2/2.00/C2H6/3.00/AR/.70/
LOW	2.69E+33	-5.11	7095	
TROE	0.5907	275	1226	5185
CH2+HCCO↔ C2H3+CO	3.00E+13	0	0	
CH2s+N2↔ CH2+N2	1.50E+13	0	600	
CH2s+AR↔ CH2+AR	9.00E+12	0	600	
CH2s+O2↔ H+OH+CO	2.80E+13	0	0	
CH2s+O2↔ CO+H2O	1.20E+13	0	0	
CH2s+H2↔ CH3+H	7.00E+13	0	0	
CH2s+H2O(+M)↔ CH3OH(+M)	4.82E+17	-1.16	1145	H2/2.00/H2O/6.00/CH4/2.00
				CO/1.50/CO2/2.00/C2H6/3.00/
LOW	1.88E+38	-6.36	5040	
TROE	0.6027	208	3922	10180
CH2s+H2O↔ CH2+H2O	3.00E+13	0	0	
CH2s+CH3↔ H+C2H4	1.20E+13	0	-570	
CH2s+CH4↔ 2CH3	1.60E+13	0	-570	
CH2s+CO↔ CH2+CO	9.00E+12	0	0	
CH2s+CO2↔ CH2+CO2	7.00E+12	0	0	
CH2s+CO2↔ CO+CH2O	1.40E+13	0	0	
CH2s+C2H6↔ CH3+C2H5	4.00E+13	0	-550	
CH3+O2↔ O+CH3O	3.56E+13	0	30480	
CH3+O2↔ OH+CH2O	2.31E+12	0	20315	
CH3+H2O2↔ HO2+CH4	2.45E+04	2.47	5180	
2CH3(+M)↔ C2H6(+M)	6.77E+16	-1.18	654	H2/2.00/H2O/6.00/CH4/2.00
				CO/1.50/CO2/2.00/C2H6/3.00/AR/.70/
LOW	3.40E+41	-7.03	2762	
TROE	0.619	73.2	1180	9999
2CH3↔ H+C2H5	6.84E+12	0.1	10600	
CH3+HCO↔ CH4+CO	2.65E+13	0	0	
CH3+CH2O↔ HCO+CH4	3.32E+03	2.81	5860	
CH3+CH3OH↔ CH2OH+CH4	3.00E+07	1.5	9940	
CH3+CH3OH↔ CH3O+CH4	1.00E+07	1.5	9940	
CH3+C2H4↔ C2H3+CH4	2.27E+05	2	9200	
CH3+C2H6↔ C2H5+CH4	6.14E+06	1.74	10450	
HCO+H2O↔ H+CO+H2O	1.50E+18	-1	17000	
HCO+M↔ H+CO+M	1.87E+17	-1	17000	H2/2.00/H2O/.00/CH4/2.00
				CO/1.50/CO2/2.00/C2H6/3.00/

Table A.1: Continues in the following page

Table A.1: Continues from the previous page

Reaction	A	n_T	E_a	ϵ
HCO+O2↔ HO2+CO	1.35E+13	0	400	
CH2OH+O2↔ HO2+CH2O	1.80E+13	0	900	
CH3O+O2↔ HO2+CH2O	4.28E-13	7.6	-3530	
C2H+O2↔ HCO+CO	1.00E+13	0	-755	
C2H+H2↔ H+C2H2	5.68E+10	0.9	1993	
C2H3+O2↔ HCO+CH2O	4.58E+16	-1.39	1015	
C2H4(+M)↔ H2+C2H2(+M)	8.00E+12	0.44	86770	H2/2.00/H2O/6.00/CH4/2.00
				CO/1.50/CO2/2.00/C2H6/3.00/AR/.70/
LOW	1.58E+51	-9.3	97800	
TROE	0.7345	180	1035	5417
C2H5+O2↔ HO2+C2H4	8.40E+11	0	3875	
HCCO+O2↔ OH+2CO	3.20E+12	0	854	
2HCCO↔ 2CO+C2H2	1.00E+13	0	0	
O+CH3→ H+H2+CO	3.37E+13	0	0	
O+C2H4↔ H+CH2CHO	6.70E+06	1.83	220	
O+C2H5↔ H+CH3CHO	1.10E+14	0	0	
OH+HO2↔ O2+H2O	5.00E+15	0	17330	
	DUPLICATE			
OH+CH3→ H2+CH2O	8.00E+09	0.5	-1755	
CH+H2(+M)↔ CH3(+M)	1.97E+12	0.43	-370	H2/2.00/H2O/6.00/CH4/2.00
				CO/1.50/CO2/2.00/C2H6/3.00/AR/.70/
LOW	4.82E+25	-2.8	590	
TROE	0.578	122	2535	9365
CH2+O2→ 2H+CO2	5.80E+12	0	1500	
CH2+O2↔ O+CH2O	2.40E+12	0	1500	
CH2+CH2→ 2H+C2H2	2.00E+14	0	10989	
CH2s+H2O→ H2+CH2O	6.82E+10	0.25	-935	
C2H3+O2↔ O+CH2CHO	3.03E+11	0.29	11	
C2H3+O2↔ HO2+C2H2	1.34E+06	1.61	-384	
O+CH3CHO↔ OH+CH2CHO	2.92E+12	0	1808	
O+CH3CHO→ OH+CH3+CO	2.92E+12	0	1808	
O2+CH3CHO→ HO2+CH3+CO	3.01E+13	0	39150	
H+CH3CHO↔ CH2CHO+H2	2.05E+09	1.16	2405	
H+CH3CHO→ CH3+H2+CO	2.05E+09	1.16	2405	
OH+CH3CHO→ CH3+H2O+CO	2.34E+10	0.73	-1113	
HO2+CH3CHO→ CH3+H2O2+CO	3.01E+12	0	11923	
CH3+CH3CHO→ CH3+CH4+CO	2.72E+06	1.77	5920	

Table A.1: Continues in the following page

Table A.1: Continues from the previous page

Reaction	A	n_T	E_a	ϵ
H+CH2CO(+M)↔ CH2CHO(+M)	4.87E+11	0.422	-1755	H2/2.00/H2O/6.00/CH4/2.00
				CO/1.50/CO2/2.00/C2H6/3.00/AR/.70/
LOW	1.01E+42	-7.63	3854	
TROE	0.465	201	1773	5333
O+CH2CHO→ H+CH2+CO2	1.50E+14	0	0	
O2+CH2CHO→ OH+CO+CH2O	1.81E+10	0	0	
O2+CH2CHO→ OH+2HCO	2.35E+10	0	0	
H+CH2CHO↔ CH3+HCO	2.20E+13	0	0	
H+CH2CHO↔ CH2CO+H2	1.10E+13	0	0	
OH+CH2CHO↔ H2O+CH2CO	1.20E+13	0	0	
OH+CH2CHO↔ HCO+CH2OH	3.01E+13	0	0	
CH3+C2H5(+M)↔ C3H8(+M)	9.43E+12	0	0	H2/2.00/H2O/6.00/CH4/2.00
				CO/1.50/CO2/2.00/C2H6/3.00/AR/
LOW	2.71E+74	-16.82	13065	
TROE	0.1527	291	2742	7748
O+C3H8↔ OH+C3H7	1.93E+05	2.68	3716	
H+C3H8↔ C3H7+H2	1.32E+06	2.54	6756	
OH+C3H8↔ C3H7+H2O	3.16E+07	1.8	934	
C3H7+H2O2↔ HO2+C3H8	3.78E+02	2.72	1500	
CH3+C3H8↔ C3H7+CH4	9.03E-01	3.65	7154	
CH3+C2H4(+M)↔ C3H7(+M)	2.55E+06	1.6	5700	H2/2.00/H2O/6.00/CH4/2.00
				CO/1.50/CO2/2.00/C2H6/3.00/AR/.70/
LOW	3.00E+63	-14.6	18170	
TROE	0.1894	277	8748	7891
O+C3H7↔ C2H5+CH2O	9.64E+13	0	0	
H+C3H7(+M)↔ C3H8(+M)	3.61E+13	0	0	H2/2.00/H2O/6.00/CH4/2.00
				CO/1.50/CO2/2.00/C2H6/3.00/AR/.70/
LOW	4.42E+61	-13.545	11357	
TROE	0.315	369	3285	6667
H+C3H7↔ CH3+C2H5	4.06E+06	2.19	890	
OH+C3H7↔ C2H5+CH2OH	2.41E+13	0	0	
HO2+C3H7↔ O2+C3H8	2.55E+10	0.255	-943	
HO2+C3H7→ OH+C2H5+CH2O	2.41E+13	0	0	
CH3+C3H7↔ 2C2H5	1.93E+13	-0.32	0	
CH+O↔ HCOp+E	2.51E+11	0	7.118	
HCOp+E↔ CO+H	7.40E+18	-0.68	0	

Table A.1: Continues in the following page

Table A.1: Continues from the previous page

Reaction	A	n_T	E_a	ϵ
HCOp+H2O↔ H3Op+CO	1.51E+15	0	0	
!HCOp+C2H5OH↔ H3Op+CO+C2H4	6.00E+14	0	0	
H3Op+E↔ H2O+H	2.29E+18	-0.5	0	
H3Op+E↔ OH+H+H	7.95E+21	-1.37	0	
H3Op+E↔ H2+OH	1.25E+19	-0.5	0	
H3Op+E↔ O+H2+H	6.00E+17	-0.3	0	
H3Op+C↔ HCO+H2	6.02E+12	0	0	
HCOp+HCCOH↔ C2H3O+CO	1.26E+15	-0.048	0	
HCOp+CH3↔ C2H3OP+H	7.76E+14	-0.006	0	
C2H3Op+E↔ HCCOH+H	2.29E+18	-0.5	0	
H3Op+HCCOH↔ C2H3Op+H2O	1.20E+15	0	0	
C2H3Op+E↔ CO+CH3	2.40E+17	-0.05	0	
C2H3Op+O↔ HCOp+CH2O	2.00E+14	0	0	
O2n+H2↔ H2O2+E	6.02E+14	0	0	
O2n+H↔ HO2+E	7.23E+14	0	0	
O2n+OH↔ OHn+O2	6.02E+13	0	0	
O2n+H↔ Ohn+O	1.08E+15	0	0	
OHn+O↔ HO2+E	1.20E+14	0	0	
OHn+H↔ H2O+E	1.08E+15	0	0	
OHn+C↔ HCO+E	3.00E+14	0	0	
OHn+CH↔ CH2O+E	3.00E+14	0	0	
OHn+CH3↔ CH3OH+E	6.02E+14	0	0	
CHO2n+H↔ CO2+H2+E	1.16E+14	0	0	
OHn+HCO↔ CH2On+H	2.96E+15	-0.14	-0.441	
On+C↔ CO+E	3.01E+14	0	0	
On+H2↔ OHn+H	1.99E+13	0	0	
On+CH4↔ OHn+CH3	6.02E+13	0	0	
On+H2O↔ OHn+OH	8.43E+14	0	0	
On+CH2O↔ OHn+HCO	5.60E+14	0	0	
On+CH2O↔ CHO2n+H	1.31E+15	0	0	
On+C2H6↔ C2H5+OHn	6.13E+15	-0.5	0	
On+H↔ OH+E	3.01E+14	0	0	
On+H2↔ H2O+E	4.22E+14	0	0	
On+CH↔ HCO+E	3.01E+14	0	0	
On+CH2↔ CH2O+E	3.01E+14	0	0	
On+CO↔ CO2+E	3.91E+14	0	0	

Table A.1: Continues in the following page

Table A.1: Continues from the previous page

Reaction	A	n_T	E_a	ϵ
On+O↔ O2+E	8.43E+13	0	0	
On+C2H2↔ HCCOH+E	7.23E+14	0	0	
On+H2O↔ H2O2+E	3.61E+11	0	0	
O2n+O↔ On+O2	1.99E+14	0	0	

Table A.1: Concluded from the previous page

A.2 Methane 3-step mechanism

Table A.2: Skeletal mechanism with no charged species

Reaction	A	n_T	E_a	ϵ
CH4+O2→ CO+2H2O	2.00E+15	0	35000	FORD/CH4/0.9/
				FORD/O2/1.1/
CO+O2→ CO2	2.00E+09	0	12000	FORD/CO/1
				FORD/O2/0.5
CO2→ CO+O2	8.11E+10	0	77200	FORD/CO2/1

A.3 Reduced mechanism based on GRI 1.2

Table A.3: Reduced mechanism with no charged species

Reaction	A	n_T	E_a	ϵ
O+H+M↔ OH+M	5.00E+17	-1	0	H2/2.00/ H2O/6.00/ CH4/2.00
				CO/1.50/ CO2/2.00/ C2H6/3.00 AR/0.70
O+H2↔ H+OH	5.00E+04	2.67	6290	
O+HO2↔ OH+O2	2.00E+13	0	0	
O+CH2↔ H+HCO	8.00E+13	0	0	

Table A.3: Continues in the following page

Table A.3: Continues from the previous page

Reaction	A	n_T	E_a	ϵ
O+CH2s↔ H+HCO	1.50E+13	0	0	
O+CH3↔ H+CH2O	8.43E+13	0	0	
O+CH4↔ OH+CH3	1.02E+09	1.5	8600	
O+CO+M↔ CO2+M	6.02E+14	0	3000	H2/2.00/ H2O/6.00/CH4/2.00
				CO/1.50/CO2/3.50/C2H6/3.00/AR/0.50
O+HCO↔ OH+CO	3.00E+13	0	0	
O+HCO↔ H+CO2	3.00E+13	0	0	
O+CH2O↔ OH+HCO	3.90E+13	0	3540	
O+C2H4↔ CH3+HCO	1.92E+07	1.83	220	
O+C2H5↔ CH3+CH2O	1.32E+14	0	0	
O+C2H6↔ OH+C2H5	8.98E+07	1.92	5690	
O2+CO↔ O+CO2	2.50E+12	0	47800	
O2+CH2O↔ HO2+HCO	1.00E+14	0	40000	
H+O2+M↔ HO2+M	2.80E+18	-0.86	0	O2/0.00/ H2O/0.00/ CO/0.75
				CO2/1.50/C2H6/1.50/N2/0.00/AR/0.00
H+2O2↔ HO2+O2	3.00E+20	-1.72	0	
H+O2+H2O↔ HO2+H2O	9.38E+18	-0.76	0	
H+O2+N2↔ HO2+N2	3.75E+20	-1.72	0	
H+O2+AR↔ HO2+AR	7.00E+17	-0.8	0	
H+O2↔ O+OH	8.30E+13	0	14413	
2H+M↔ H2+M	1.00E+18	-1	0	H2/0.00/H2O/0.00/CH4/2.00
				CO2/0.00/C2H6/3.00/AR/0.63
2H+H2↔ 2H2	9.00E+16	-0.6	0	
2H+H2O↔ H2+H2O	6.00E+19	-1.25	0	
2H+CO2↔ H2+CO2	5.50E+20	-2	0	
H+OH+M↔ H2O+M	2.20E+22	-2	0	H2/0.73/H2O/3.65/CH4/2.00
				C2H6/3.00/ AR/0.38
H+HO2↔ O2+H2	2.80E+13	0	1068	
H+HO2↔ 2OH	1.34E+14	0	635	
H+CH2(+M)↔ CH3(+M)	2.50E+16	-0.8	0	H2/2.00/H2O/6.00/CH4/2.00
				CO/1.50/CO2/2.00/C2H6/3.00/AR/0.70
LOW	3.20E+27	-3.14	1230	
TROE	0.68	78	1995	5590
H+CH3(+M)↔ CH4(+M)	1.27E+16	-0.63	383	H2/2.00/H2O/6.00/CH4/2.00
				CO/1.50/CO2/2.00/C2H6/3.00/ AR/0.70
LOW	2.48E+33	-4.76	2440	
TROE	0.783	74	2941	6964

Table A.3: Continues in the following page

Table A.3: Continues from the previous page

Reaction	A	n_T	E_a	ϵ
H+CH4↔ CH3+H2	6.60E+08	1.62	10840	
H+HCO(+M)↔ CH2O(+M)	1.09E+12	0.48	-260	H2/2.00/H2O/6.00/CH4/2.00
				CO/1.50/CO2/2.00/C2H6/3.00/AR/0.70
LOW	1.35E+24	-2.57	1425	
TROE	0.7824	271	2755	6570
H+HCO↔ H2+CO	7.34E+13	0	0	
H+CH2O(+M)↔ CH3O(+M)	5.40E+11	0.454	2600	H2/2.00/H2O/6.00/CH4/2.00
				CO/1.50/CO2/2.00/C2H6/3.00
LOW	2.20E+30	-4.8	5560	
TROE	0.758	94	1555	4200
H+CH2O↔ HCO+H2	2.30E+10	1.05	3275	
H+CH3O↔ OH+CH3	3.20E+13	0	0	
H+C2H4(+M)↔ C2H5(+M)	1.08E+12	0.454	1820	H2/2.00/H2O/6.00/CH4/2.00
				CO/1.50/CO2/2.00/C2H6/3.00/AR/0.70
LOW	1.20E+42	-7.62	6970	
TROE	0.9753	210	984	4374
H+C2H5(+M)↔ C2H6(+M)	5.21E+17	-0.99	1580	H2/2.00/H2O/6.00/CH4/2.00
				CO/1.50/CO2/2.00/ C2H6/3.00/AR/0.70
LOW	1.99E+41	-7.08	6685	
TROE	0.8422	125	2219	6882
H+C2H6↔ C2H5+H2	1.15E+08	1.9	7530	
H2+CO(+M)↔ CH2O(+M)	4.30E+07	1.5	79600	H2/2.00/H2O/6.00/CH4/2.00
				CO/1.50/CO2/2.00/C2H6/3.00/AR/0.70
LOW	5.07E+27	-3.42	84350	
TROE	0.932	197	1540	10300
OH+H2↔ H+H2O	2.16E+08	1.51	3430	
2OH↔ O+H2O	3.57E+04	2.4	-2110	
OH+HO2↔ O2+H2O	2.90E+13	0	-500	
OH+CH2↔ H+CH2O	2.00E+13	0	0	
OH+CH2s↔ H+CH2O	3.00E+13	0	0	
OH+CH3↔ CH2+H2O	5.60E+07	1.6	5420	
OH+CH3↔ CH2s+H2O	2.50E+13	0	0	
OH+CH4↔ CH3+H2O	1.00E+08	1.6	3120	
OH+CO↔ H+CO2	4.76E+07	1.228	70	
OH+HCO↔ H2O+CO	5.00E+13	0	0	
OH+CH2O↔ HCO+H2O	3.43E+09	1.18	-447	
OH+C2H6↔ C2H5+H2O	3.54E+06	2.12	870	

Table A.3: Continues in the following page

Table A.3: Continues from the previous page

Reaction	A	n_T	E_a	ϵ
HO2+CH2↔ OH+CH2O	2.00E+13	0	0	
HO2+CH3↔ O2+CH4	1.00E+12	0	0	
HO2+CH3↔ OH+CH3O	2.00E+13	0	0	
HO2+CO↔ OH+CO2	1.50E+14	0	23600	
CH2+O2↔ OH+HCO	1.32E+13	0	1500	
CH2+H2↔ H+CH3	5.00E+05	2	7230	
CH2+CH3↔ H+C2H4	4.00E+13	0	0	
CH2+CH4↔ 2CH3	2.46E+06	2	8270	
CH2s+N2↔ CH2+N2	1.50E+13	0	600	
CH2s+AR↔ CH2+AR	9.00E+12	0	600	
CH2s+O2↔ H+OH+CO	2.80E+13	0	0	
CH2s+O2↔ CO+H2O	1.20E+13	0	0	
CH2s+H2↔ CH3+H	7.00E+13	0	0	
CH2s+H2O↔ CH2+H2O	3.00E+13	0	0	
CH2s+CH3↔ H+C2H4	1.20E+13	0	-570	
CH2s+CH4↔ 2CH3	1.60E+13	0	-570	
CH2s+CO↔ CH2+CO	9.00E+12	0	0	
CH2s+CO2↔ CH2+CO2	7.00E+12	0	0	
CH2s+CO2↔ CO+CH2O	1.40E+13	0	0	
CH3+O2↔ O+CH3O	2.68E+13	0	28800	
CH3+O2↔ OH+CH2O	3.60E+10	0	8940	
2CH3(+M)↔ C2H6(+M)	2.12E+16	-0.97	620	H2/2.00/H2O/6.00/CH4/2.00
				CO/1.50/ CO2/2.00/C2H6/3.00/AR/0.70
LOW	1.77E+50	-9.67	6220	
TROE	0.5325	151	1038	4970
2CH3↔ H+C2H5	4.99E+12	0.1	10600	
CH3+HCO↔ CH4+CO	2.65E+13	0	0	
CH3+CH2O↔ HCO+CH4	3.32E+03	2.81	5860	
CH3+C2H6↔ C2H5+CH4	6.14E+06	1.74	10450	
HCO+H2O↔ H+CO+H2O	2.24E+18	-1	17000	
HCO+M↔ H+CO+M	1.87E+17	-1	17000	H2/2.00/H2O/0.00/CH4/2.00
				CO/1.50/CO2/2.00/C2H6/3.00
HCO+O2↔ HO2+CO	7.60E+12	0	400	
CH3O+O2↔ HO2+CH2O	4.28E-13	7.6	-3530	
C2H5+O2↔ HO2+C2H4	8.40E+11	0	3875	

Table A.3: Concluded from the previous page

A.4 Reduced ions mechanism

Table A.4: Reduced mechanism with charged species

Reaction	A	n_T	E_a	ϵ
CH4↔ CH3+H	4.23E+15	.000	108.69E+3	
CH4+OH↔ CH3+H2O	2.00E+14	.000	8.41E+3	
CH4+O↔ CH3+OH	3.48E+13	.000	8.38E+3	
CH4+H↔ CH3+H2	4.35E+14	.000	13.74E+3	
CH3+O2↔ CH2O+OH	5.29E+11	.000	1.70E+3	
CH2O+OH↔ CO+H2O+H	5.87E+14	.000	4.88E+3	
CO+OH→CO2+H	1.30E+12	.000	1.53E+3	
CO2+H→CO+OH	1.45E+14	.000	23.76E+3	
O2+H→OH+O	2.24E+14	.000	16.80E+3	
OH+O→O2+H	1.71E+13	.000	0.87E+3	
O+H2→OH+H	1.74E+13	.000	9.45E+3	
OH+H→O+H2	7.70E+12	.000	7.58E+3	
O+H2O→2OH	5.75E+13	.000	18.10E+3	
2OH→O+H2O	5.38E+12	.000	1.05E+3	
OH+H2→H2O+H	2.19E+13	.000	5.15E+3	
H2O+H→H2+OH	8.41E+13	.000	20.10E+3	
H+OH+M↔ H2O+M	2.00E+19	-1.000	.00	H2/ .73/ H2O/3.65/ CH4/2.00/
O+O+M↔ O2+M	8.90E+14	-0.500	.00	H2/ 2.40/ H2O/15.40/ CH4/ 2.00
				CO/ 1.75/ CO2/ 3.60/
H+H+M↔ H2+M	1.00E+18	-1.000	.00	H2/ .00/ H2O/ .00/ CH4/2.00/ CO2/ .00/
CH3+O↔ CH+H2O	2.80E+08	.000	.00	
CH+O↔ HCO^++E	5.75E+11	.000	6.00E+3	
HCO^++H2O↔ CO+$H3O^+$	5.02E+17	.000	24.00E+3	
$H3O^+$+E↔ H2O+H	1.44E+17	.000	.00	
CH+O2↔ CO+OH	6.00E+10	.000	.00	
O+N2→NO+N	1.36E+14	.000	75.40E+3	
NO+N→O+N2	3.10E+13	.000	0.33E+3	
N+O2→NO+O	6.43E+09	1.000	6.25E+3	
NO+O→N+O2	1.55E+09	1.000	38.64E+3	
NO+O+M↔ NO2+M	1.05E+15	.000	-1.87E+3	H2/2.00/ H2O/6.00/ CH4/2.00
				CO/1.50/ CO2/2.00/
NO2+O↔ NO+O2	2.10E+12	.000	.00	
NO2+H↔ NO+OH	3.00E+14	.000	.00	